AN APPROACH TO FINITE-ELEMENT
MODELLING OF THE MIDDLE EAR

by

Susan M. Funnell

A thesis submitted to the Faculty of Graduate Studies and
Research in partial fulfillment of the requirements
for the degree of Master of Engineering

Department of Electrical Engineering
McGill University
Montréal, Canada
July, 1989

ABSTRACT

A method has been developed for modelling the cat middle eaɪ usɪng structural finɪte-element analysis. One aim of thɪs research ɪs to model the changing ossicular axis of rotatɪon. Anatomical information ɪs input to the computer by digitizɪng outlines of structuɪes of ɪnteɪest from serial-section slides. The resultɪng three-dimensɪonal volume is discretized ɪnto tetrahedral elements usɪng a previously developed mesh generator developed to mesh ɪrregularly shaped objects. Further development of this generator was done to allow ɪt to handle more complex objects. Preliminary static models of a test structure and of a simple lɪgament ɪndɪcate that the modelling scheme developed is capable of modelling the complex structures in the mɪddle ear. Further improvements requɪred in the mesh generator, such as the need for a more robust two-dimensɪonal contour triangulation algorɪthm, are ɪdentɪfied. The proposed direction of future work on the middle-eaɪ model ɪs descrɪbed.

RÉSUMÉ

Une méthode de modélisation de l'oreille moyenne du chat a été développée en utilisant la méthode des éléments f·nis. Un des buts de cette recherche est de modeler les changements de l'axe de rotation des osselets. Comme données anatomiques on utilise, en f?rme numérique, les contours des tranches en série des structures pertinentes. En utilisant une méthode de maillage pour des objets de forme irrégulière qu'on a développée auparavant, le volume résultant est divisé en des éléments tétraédriques. On a développé plus loin cette méthode pour permettre de traiter des objets plus complexes. Des modèles statiques préliminaires, d'une structure d'essai et d'un ligament simple, indiquent que la méthode est capable de modeler les structures complexes de l'oreille moyenne. On identifie aussi des améliorations nécessaires à cette méthode, comme un algorithme plus robuste pour trianguler des contours bi-dimensionnels. On propose la direction à suivre pour des travaux futurs sur ce modèle de l'oreille moyenne.

ACKNOWLEDGEMENTS

I would like to thank my advisor, Dr. W.R.J. Funnell (no relation), who inspired this work, for the help he has given me in preparing this thesis and for the answers he supplied to the many, many questions that arose during the course of this work. He has helped me gain skills that will be invaluable in future research efforts.

The BioMedical Engineering Unit has been an enjoyable place to work and I would like to thank the staff and students here for making it a productive and informative place to be. I'd especially like to thank my lab mate, Jenny Day, for her many discussions on finite elements, philosophy, foreign film..... and other topics.

Finally, I am indebted to my parents, Margaret and Owen Funnell, for instilling in me the idea that I could succeed at anything I try and to my husband, Paul Van Esbroeck, for his love and humour in helping me to persevere.

TABLE OF CONTENTS

CHAPTER 4   THE FINITE-ELEMENT METHOD

CHAPTER 5   ANATOMICAL DATA DESCRIPTION, INPUT AND MANIPULATION

CHAPTER 6   MESH GENERATION FROM SERIAL SECTIONS

CHAPTER 7   PRELIMINARY MODEL TESTS AND RESULTS

CHAPTER 8   CONCLUSIONS AND FUTURE DEVELOPMENTS

LIST OF FIGURES

CHAPTER 1

INTRODUCTION

1.1 OBJECTIVES

It is becoming increasingly clear that the mechanical behaviour of the middle ear is more complex than previously thought. Traditionally, the middle ear has been thought of as a lever system whose axis of rotation remains in a relatively fixed position. Recent evidence indicates that this axis of rotation changes with frequency in a complicated manner.

Finite-element analysis is a method well suited to the detailed analysis of complicated mechanical systems. This thesis describes preliminary work on the design and implementation of a finite-element model of the middle-ear ossicles and important soft tissuer. By combining this model with a previously developed finite-element model of the eardrum (Funnell et al., 1987), a quantitative understanding of the mechanical behaviour of the middle ear should be obtained.

There are a number of reasons why a better quantitative understanding of the mechanical behaviour of the middle ear is required. Much research is currently being focussed on high-frequency hearing loss in humans. Research in this area is hindered by the difficulty of characterizing the high-frequency input to the cochlea. This input is strongly affected by the middle ear, but currently available models of the middle ear do not provide much insight into the mechanical operation of this structure at high frequencies. The finite-element model should help to address this problem.

A finite-element middle-ear model should help in the design and

choice of techniques for middle-ear surgery and should aid in the clinical evaluation of middle-ear and inner-ear function. It should help also in the design and fitting of hearing aids. The research involved in developing this model is important in advancing finite-element analysis techniques for biological structures in general.

1.2 THESIS OUTLINE

This thesis describes work done in developing and testing tools needed to construct a structural finite-element model of the middle ear. Preliminary work on this model will be presented. The tools described in this thesis will eventually be used to model the dynamic behaviour of the middle ear as a whole.

Chapter 2 is a review of the anatomy of the middle ear. Chapter 3 discusses experimental observations on the structure and function of the middle ear. It describes currently available models of the middle ear and a brief discussion of the material properties of structures in the middle ear is included. Finally, it outlines the computer-based finite-element model being developed during the course of this research. Chapter 4 explains the finite-element method and briefly describes finite-element packages available for structural analysis, including the package modified and used for this model.

Serial-section histological slides are used as the anatomical basis for the model of the ossicles and important soft tissues. Chapter 5 describes the histological data used and outlines the system used to input this data to the computer and to redisplay it. Chapter 6 describes various mesh-generation techniques used to define finite-element meshes. In particular it describes a series of three-dimensional mesh-generation computer programs (Boubez, 1986b) that were tested, debugged, enhanced

and automated during the course of this research. The resulting master program is used to create meshes of middle-ear structures based on the data input from the histological slides.

Chapter 7 describes preliminary results of a static finite-element analysis of a test structure and of a simple ligament model. Finally, Chapter 8 outlines conclusions drawn from this preliminary work and describes future work needed to complete the modelling of the static and dynamic behaviour of the middle ear.

CHAPTER 2

REVIEW OF MIDDLE-EAR ANATOMY

2.1 INTRODUCTION

The middle ear serves as an impedance-matching transformer. It transforms the acoustic sound pressure in front of the tympanic membrane, or eardrum, into perilymph fluid pressure in the cochlea, or inner ear. The cochlea converts the mechanical energy transmitted by the middle ear to neural activity capable of being analysed by higher processing centers of the central nervous system. Direct acoustical stimulation of the cochlea would be ineffective because of the high impedance of perilymph fluid as compared to air.

2.2 THE HUMAN MIDDLE EAR

2.2.1 Introduction

To understand how the middle ear acts as a transformer, a review of the anatomy of important structures in and around the middle ear is necessary. The human ear is illustrated in Figure 2.1. The middle-ear cavity is of complex form and consists of three parts. The main part of the cavity is the tympanum which lies behind the eardrum. Above and extending backward and laterally is the epitympanum. Still farther backward and laterally is the mastoid antrum (not shown in the figure) which is connected to numerous and irregularly placed air cells. These air-filled cavities are connected to the outside world via the Eustachian tube. The cavities contain the ossicles, a series of three bones: the malleus, the incus and the stapes. Two windows exist between the middle ear and the inner ear, the round window and the oval window.

epitympanum

incus

malleus

oval window

stapes

cochlea

ear canal

eardrum

Eustachian tube

round window

tympanum
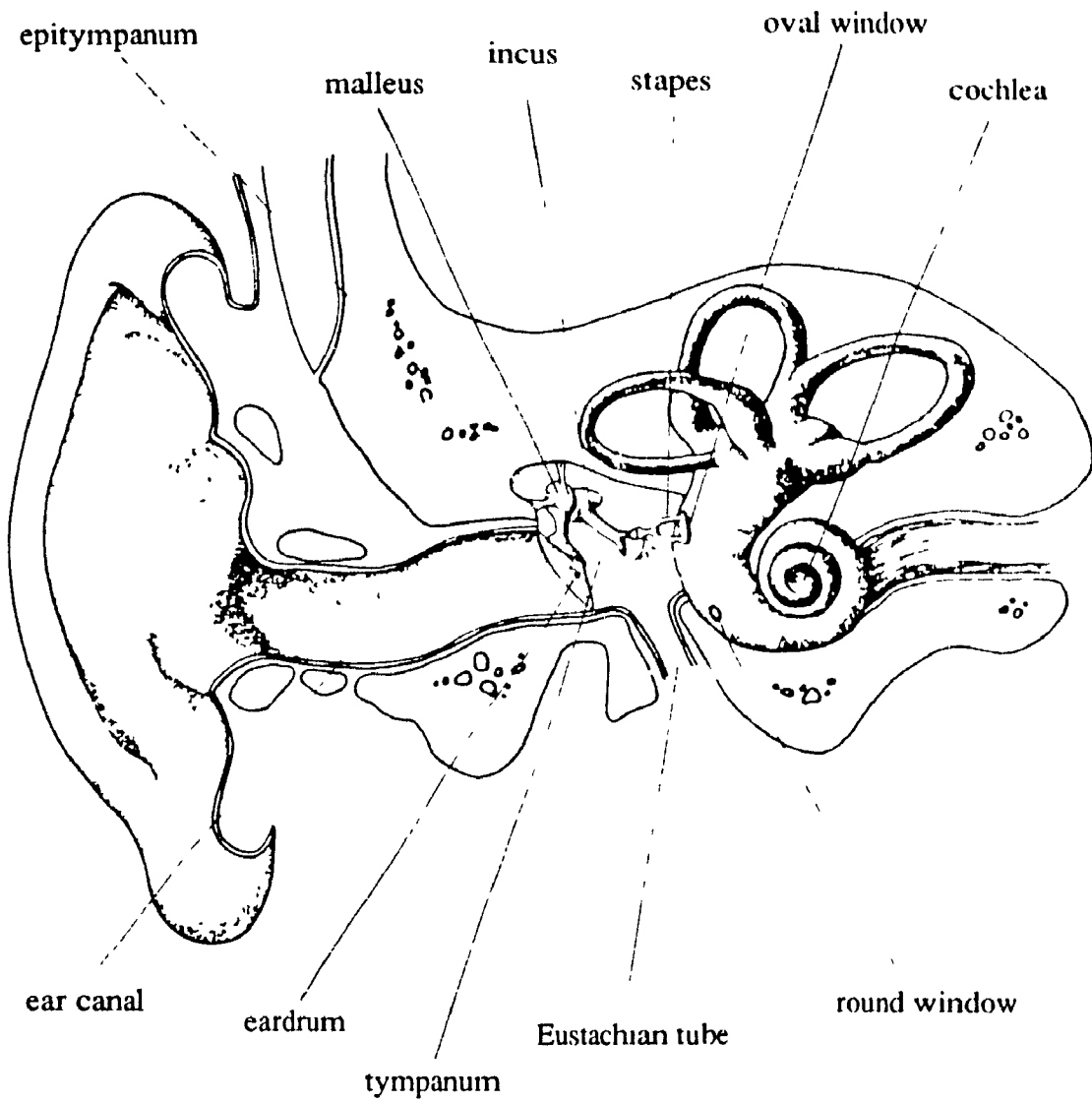
FIGURE 2.1: THE HUMAN EAR
on the right side, seen from the front.
(After Lindsay and Norman, 1977)

An annular ligament connects the footplate of the stapes to the oval window.

2.2.2 The Eardrum

The eardrum is approximately 0.1 mm thick and lies obliquely in the ear canal as shown in Figure 2.2. It is held firmly in a little groove in a bony ring formed by the walls of the canal except in a region at the upper border where the ring is incomplete, called the notch of Rivinus. The eardrum has a conical shape whose deepest point, the umbo, points toward the middle ear. The sides of this cone are convex outward.

The eardrum contains the manubrium or handle of the malleus. The manubrium is embedded in the eardrum along the radius of the eardrum, and runs from the notch of Rivinus to the umbo. The manubrium-eardrum interaction is complicated and quite dependent on the structure and function of the eardrum. Funnell and Laszlo (1982) give a thorough review of eardrum structure and function.

The typical mammalian eardrum consists of two main areas, the pars tensa and the pars flaccida. The pars tensa, a very thin sheet of connective tissue, is surrounded by a thick fibrous annular ligament that anchors it to the wall of the ear canal around most of its circumference. (This annular ligament should not be confused with the annular ligament connecting the footplate of the stapes to the oval window.) The section of the annular ligament not anchored to the bone is connected to the more elastic pars flaccida, which is at the superior part of the drum. The manubrium is embedded in the pars tensa.

The eardrum is composed of three layers. Within the middle layer are four sublayers, two of which form the main structural components of the eardrum. The innermost of the two layers is composed of circular

superior malleolar ligament

lateral malleolar ligament

notch of Rivinus

head of malleus

incus

annular
ligament

stapes

anterior malleolar
ligament

manubrium

umbo

eardrum
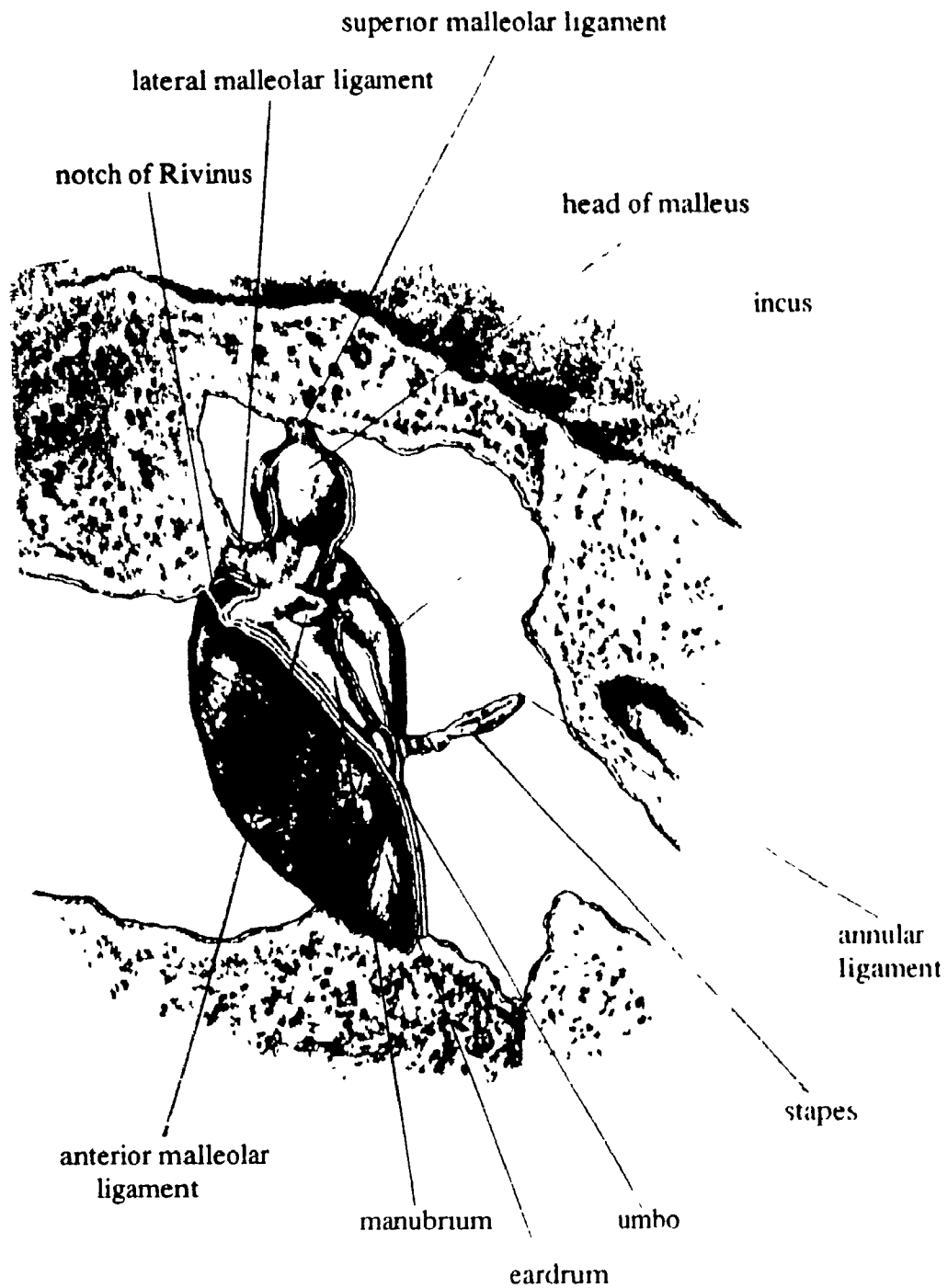
FIGURE 2.2: THE HUMAN MIDDLE EAR
on the right side, seen from the front.
(After Deaver, 1926)

fibres while the outermost is composed of radial fibres. These fibre layers consist of parallel arrays of fibres in a meager matrix of ground substance.

2.2.3 The Ossicular Chain

The head of the malleus articulates with the incus and the incus articulates with the stapes, a stirrup-shaped bone. This ossicular chain is suspended in the middle-ear cavities by a number of ligaments and muscles (Figures 2.2-2.3). In the human there are four ligaments. The first is the anterior malleolar ligament, connecting the anterior process of the malleus to the anterior wall of the middle ear. The second ligament is the lateral malleolar ligament, joining the lateral portion of the neck of the malleus to the edge of the notch of Rivinus. The third ligament is the posterior incudal ligament, connecting the short process of the incus to the posterior wall of the epitympanum. It is extremely thick and is divided into lateral and medial bundles. The lateral bundle is thicker and stronger than the medial one. The fourth ligament is the annular ligament connecting the footplate of the stapes to the oval window. According to Kobayhashi (1954b), the so-called superior malleolar ligament is merely a fold of mucous membrane.

In the human, as in most mammals, there are two muscles as illustrated in Figure 2.3. The body of the tensor tympani muscle lies in a canal that runs above the Eustachian tube. The muscle fibres are attached at the anterior end to the canal walls and run posteriorly to insert into the tensor tympani tendon. This tendon is attached to the upper part of the manubrium of the malleus. The stapedius muscle lies in an almost vertical canal posterior to the tympanic cavity. The muscle fibres are attached at one end to the bony walls of the canal and at the

4

medial bundle

lateral bundle

tensor tympani muscle

posterior incudal ligament

stapedius muscle

Eustachian tube
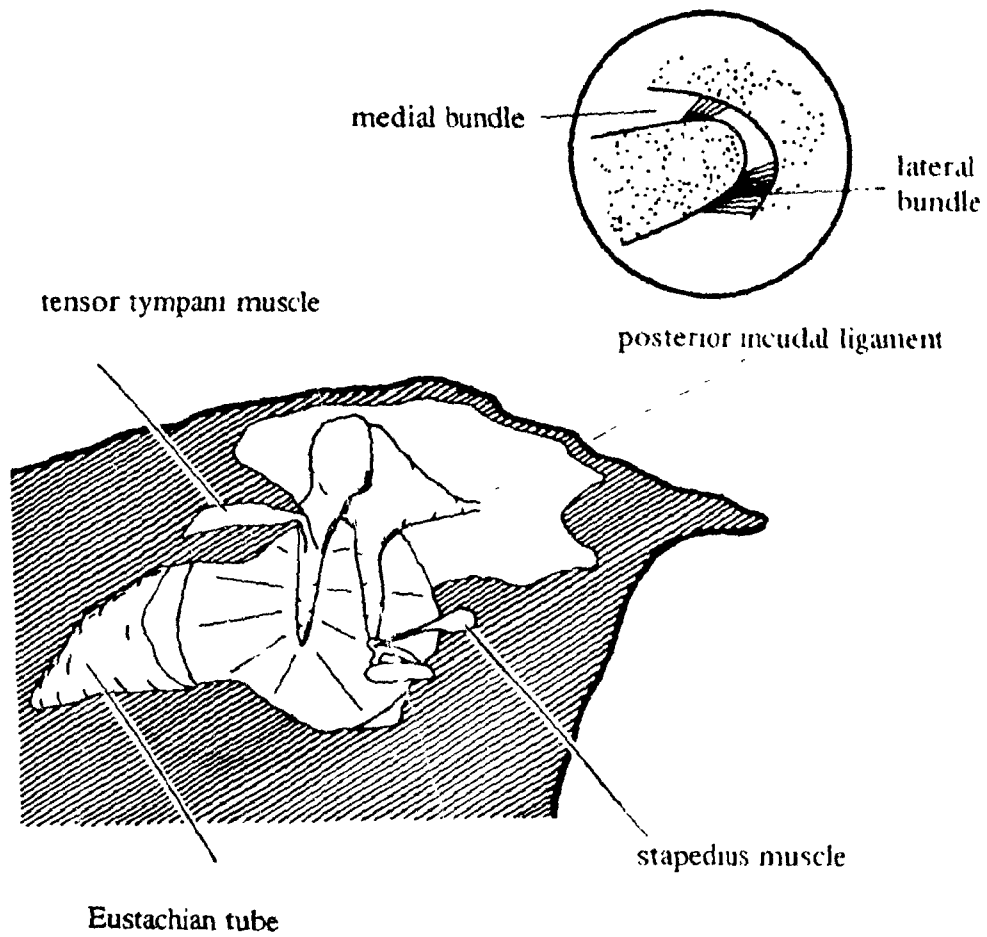
FIGURE 2.3: THE HUMAN MIDDLE EAR
on the right side, seen from within.
(After Funnell, 1972)

other end to the stapedius tendon. This tendon is attached at the posterior aspect of the neck of the stapes. Both muscles are composed of numerous short fibres grouped in parallel. This *pennate* type of muscle provides much tension and little displacement. Upon contraction both muscles exert tension lateral to the course of the ossicular chain. These muscles are involved in the middle-ear reflex (Wever & Lawrence, 1954).

2.2.4 The Cochlea

The cochlea or inner ear is a spiral-shaped passage in the temporal bone lying medial to the middle ear as illustrated in Figure 2.1. It is divided lengthwise into three fluid-filled tubes. The first tube, the scala vestibuli, is in contact with the oval window via the fluid-filled vestibule of the cochlea. The floor of the scala vestibuli is Reissner's membrane which borders on the second fluid-filled tube, the cochlear duct. The floor of the cochlear duct is the basilar membrane which borders on the third fluid-filled tube, the scala tympani. The scala tympani is in contact with the second opening to the middle ear, the membrane-covered round window.

Vibration of the stapedial footplate in the oval window creates a wave of pressure in the scala vestibuli. This wave propagates along the scala vestibuli to its apical end and back through the scala tympani to the round window. As the wave propagates, most of its energy is dissipated directly through Reissner's membrane to the cochlear duct and in turn through the basilar membrane. The vibration pattern of the basilar membrane determines the resulting neural activity mentioned in the introduction to this chapter.

2.3 THE CAT MIDDLE EAR

The model developed in the course of this research is of a cat middle ear, because experimental data on the cat middle ear are more abundant than are data on the human middle ear. The use of cats, instead of humans, in experimental work has the advantage that measurements may be taken in vivo, instead of in cadavers. Thus, these measurements are not as susceptible to degenerative effects. Also, the middle ear of the cat permits a relatively easy access to the eardrum and middle-ear cavities. It should be noted that the modelling procedure used here for the cat could easily be used to model a human middle ear.

The overall anatomy of the cat middle ear is similar to that of the human but there are numerous differences in detail. Figure 2.4 shows a schematic representation of both the cat and human ossicles and cavities. The epitympanum in the cat is considerably smaller than in human and there is no antrum. The tympanum is considerably larger in the cat and is divided into two cavities, the ectotympanum (sometimes referred to as the bulla cavity) and the entotympanum (sometimes referred to as the middle-ear cavity). These cavities are separated by a bony septum and only a small opening or foramen is left between them.

The three ossicles of the cat are similar to those of the human. The manubrium is similarly connected to the eardrum, as is the stapes to the oval window. There are two muscles, the stapedius and tensor tympani, acting in much the same manner as in the human. In the cat, only the posterior incudal ligament and the annular ligament at the stapes have true ligamental structure. According to Kobayashi (1954a), the anterior, lateral and superior malleolar ligaments are either folds of mucous membrane or absent completely. In the cat, as in the human, the posterior incudal ligament is extremely thick and is divided into a

0 ___ 5 mm

epitympanum

posterior incudal ligament

mastoid antrum

epitympanum

entotympanum

ectotympanum

tympanum

CAT
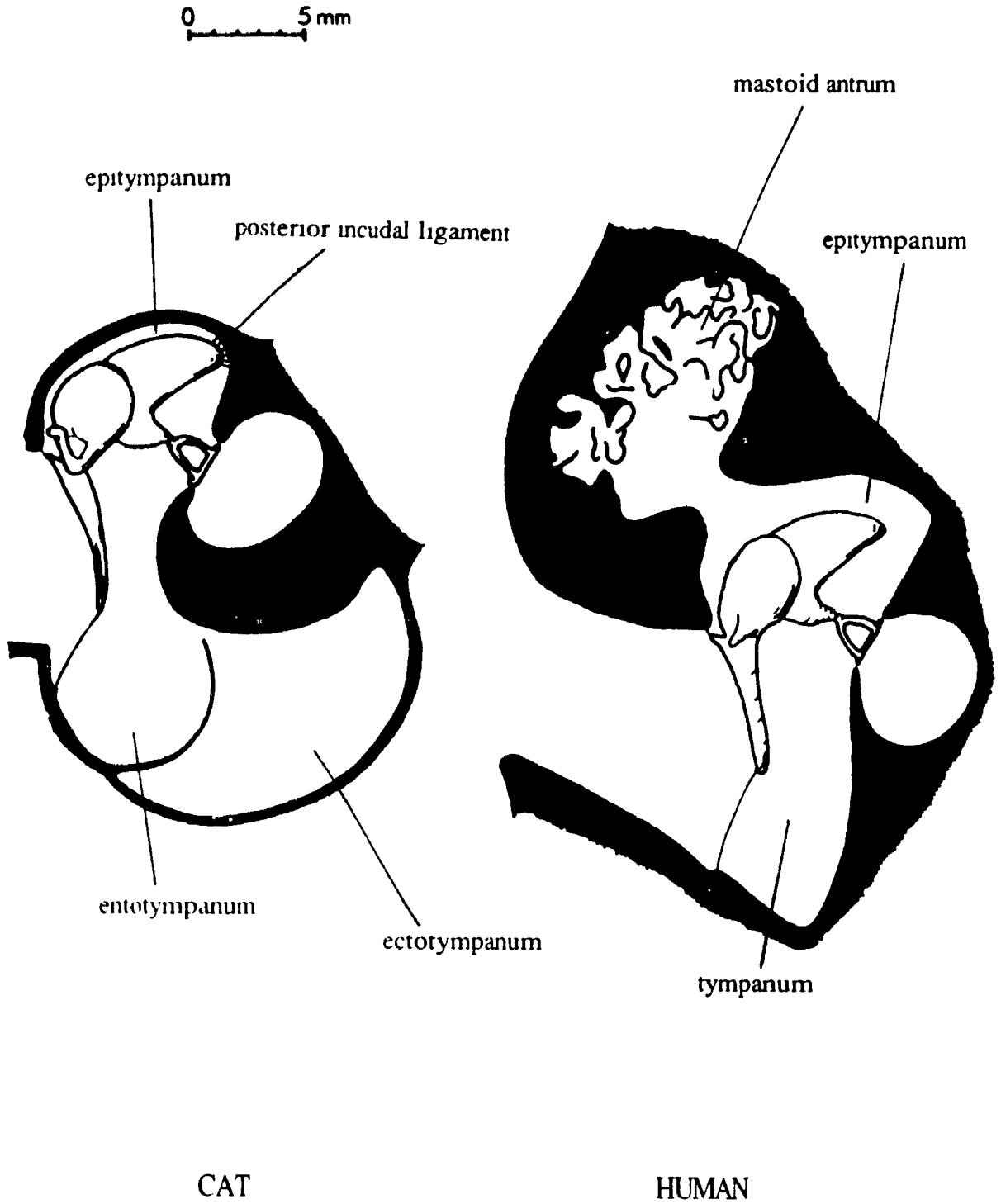
HUMAN

FIGURE 2.4: THE OSSICLES AND CAVITIES OF THE CAT AND THE HUMAN
Schematic representation
(After Funnell, 1972)

thicker and stronger lateral bundle, and a thinner and weaker medial bundle.

2.4 CONCLUSION

The eardrum and the bones and soft tissues of the middle ear are important in understanding the transformer action of the middle ear. This transformer action will be discussed in the next chapter. Previously developed mathematical models of middle-ear function will be described, and the motivation for developing a finite-element model will be discussed.

CHAPTER 3

EXPERIMENTAL OBSERVATIONS ON AND MODELS OF MIDDLE-EAR FUNCTION

3.1 INTRODUCTION

This chapter describes some experimental observations on the transformer action of the middle ear, and also describes a number of models of the middle ear that have been developed to model this action. The motivation for developing a finite-element model of the middle-ear ossicles and important soft tissues will be discussed. A brief discussion of the material properties of structures in the middle ear is included. Finally, the outline of a proposed finite-element middle-ear model will be presented.

3.2 THE MIDDLE-EAR TRANSFORMER

3.2.1 Primary Transformer Action

One method of transformer action (Helmholtz, 1869) depends on the areal ratio of the eardrum to the oval window. Most of the force of the air pressure at the eardrum is transmitted to the oval window via the footplate of the stapes. Due to the smaller area of the oval window, pressure is increased. This areal ratio depends not on the actual membrane areas but rather on the *effective* areas of the two membranes. The effective area of a membrane is the area a rigid piston would need to have, in order to displace a volume of air equal to the volume of air actually displaced when the membrane is deformed, for some *average* membrane displacement. These effective areas are highly dependent on the vibration pattern in the middle ear and on the particular shape of the eardrum. Wever and Lawrence (1954) estimate that the effective area

ratio is approximately 24.3 in the cat and 14.0 in the human.

3.2.2 Lever Action of the Ossicular Chain

A second method for securing a mechanical advantage in the middle ear is the lever action of the ossicular chain. Because of the complicated geometry and method of suspension of this chain, the physical basis of this lever action is hard to determine.

Wever and Lawrence (1954) postulated an ossicular lever system for the cat. This postulated system was based on experiments that they performed on anesthetized cats. These experiments involved driving points on the manubrium and on the incus with a constant-displacement driver at audio frequencies and observing the cochlear potential at the round-window membrane. The magnitudes of these cochlear potentials were assumed to be proportional to the amplitude of the resulting stapes motion. They performed a series of four experiments to determine the probable axis of rotation of the ossicular chain.

The purpose of the first series of experiments was to determine if a lever system did exist and if so in which direction the effective force arm of the system ran. Various points along the manubrium, from its tip to its base, were stimulated. The resulting cochlear potentials increased as the point of stimulation moved closer to the base of the manubrium. The pattern of these points indicated where the force arm was and that its fulcrum was near the base of the manubrium.

The second series of experiments involved driving a point on the tip of the manubrium alternately with one at the end of the long process of the incus. The resulting potentials were consistently higher when stimulating the incus, for all frequencies tested between 100 Hz and 10 kHz. For frequencies between 100 Hz and 1 kHz the mean ratio of

potentials resulting from incus stimulation to those resulting from manubrial stimulation (averaged over three cats) was 2.5. This value represents the ossicular lever ratio in the cat.

The third series of experiments was performed to determine the locus of the fulcrum of the incus. As the point of stimulation of the incus approaches the fulcrum of the incus the resulting potentials should approach infinity. (In fact they were observed to become highly irregular at this point.)

The last series of experiments indicated the probable position of the axis of rotation of the ossicular chain. Once the incudal lever arm had been roughly identified, from the third series of experiments, the distance of a number of manubrial driving points from the axis of rotation could be calculated. This distance is equal to the length of the incudal lever arm, times the ratio of the potential resulting from driving the incus, over that resulting from driving the manubrium. Knowing a number of these distances, the probable ossicular axis of rotation could be determined. Wever and Lawrence postulated the axis to run from a point on the short process of the incus (from the posterior incudal ligament) to a point on the anterior process of the malleus (at the anterior malleolar ligament) as shown in Figure 3.1.

A number of previous researchers had postulated an axis of rotation for the human middle ear similar to that proposed by Wever and Lawrence for the cat (i.e. running approximately from the posterior incudal ligament to the anterior malleolar ligament). Dahmann (1929, 1930 as described by Wever and Lawrence) formulated a system by observing angular deflections of light from small mirrors set up within the human middle ear. He located the main vibratory axis of the ossicular system by noting that a mirror on a rotational axis produces no deflection of a
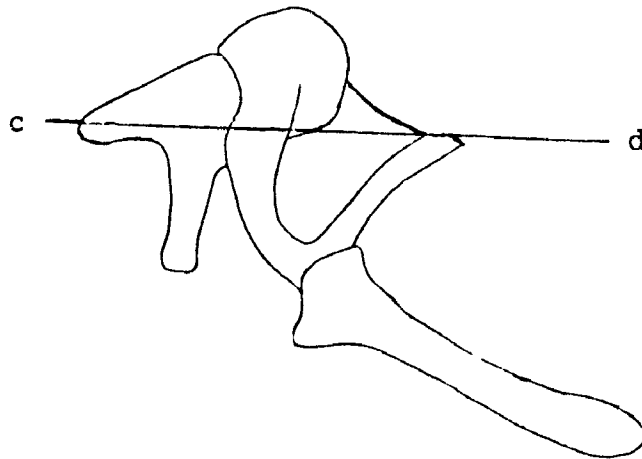
FIGURE 3.1: PROBABLE OSSICULAR AXIS OF ROTATION OF THE CAT
according to Wever and Lawrence.
The figure is in the plane of the annular ligament of the eardrum.
Line *cd* (oriented 34 degrees above this plane) is the probable
ossicular axis of rotation. (After Wever and Lawrence, 1954)

light beam along the line of the axis but only in a plane perpendicular to the axis. His calculated lever ratio is 1.31:1. Békésy (1941) deduced a similar position of the axis of rotation by noting that the cutting of the posterior incudal ligament and the anterior malleolar ligament caused no change in the vibratory amplitude of the stapes when driven by high-frequency sound introduced at the ear canal. He assumed the line joining these ligaments coincided with the center of gravity of the ossicles themselves and thus, by reason of distribution of their masses alone, they rotated about this axis.

Other researchers have postulated somewhat different lever systems. Based on his morphological and functional studies of the middle ear, Helmholtz postulated that the human ossicular chain formed a single lever system with a lever ratio of 1.5. Fumagalli (1949) based his middle-ear lever system on extensive morphological studies of various animals, including man. He proposed two vibratory axes, one with a lever ratio of 1.3:1 for low tones (similar to that proposed by Dahmann) and one with a ratio of 10:1, for higher frequencies. Stuhlman (1937) studied a large-scale model of human ossicles he had made after observing human middle ears. He came up with three different lever ratios, depending on whether the joint between the malleus and incus was fixed (1.27:1) and, if it were not, depending on whether the vibratory motion of the eardrum-ossicular chain was inward (2:1) or outward (1:1). The lever systems mentioned in this paragraph were determined at large displacements and thus possibly outside the normal operating range of the middle ear.

More recent researchers have formulated middle-ear models (Onchi, Møller, Zwislocki, Peake and Guinan, Lynch) and have agreed with the position of the ossicular axis of rotation proposed by Wever and

Lawrence, at least for lower frequencies. Their models will be described later in this chapter.

3.2.3 Eardrum Curvature

A third method of transformer action, proposed by Helmholtz, depends on the particular curvature of the eardrum. The radial fibres of the drum are anchored firmly at one end to the edge of the bony tympanic ring and at the other to the manubrium. The middle section is relatively free to move in response to sound pressure. Sound waves hitting this free section were thought to be transformed to smaller amplitude, higher pressure vibrations at the manubrium tip by the lever action of the eardrum itself as illustrated in Figure 3.2. This lever ratio would be highly dependent on the amount of curvature in the radial fibres.

Using a capacitive probe, Békésy (1941) made measurements of human cadaver eardrum vibration patterns. The one figure published with his results indicated that the central portion of the drum experienced no bending in the direction at right angles to the manubrium and indicated the eardrum vibrated as a whole. This contradicted Helmholtz's hypothesis. However, later measurements of vibration patterns by Khanna and Tonndorf (1972) indicated displacements were greatest partway between the manubrium and the annular ligament and were greatest in the posterior segment of the drum, indicating Helmholtz's hypothesis might be correct. It is apparent that an accurate representation of eardrum shape and mechanical characteristics is required to determine what lever action, if any, exists in this structure.
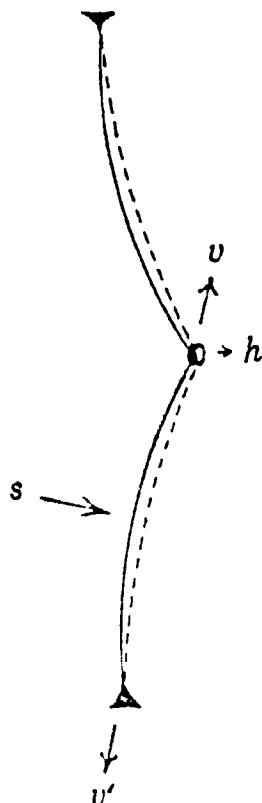
FIGURE 3.2: LEVER ACTION OF THE EARDRUM
The eardrum is shown in cross section. A sound pressure s applied to the
radial fibers of the eardrum is transformed into relatively large forces
v and v' at the ends of the fibers. The force v has a horizontal
component h which tends to move the center of the eardrum inward.
(From Wever and Lawrence, 1954)

3.3 LUMPED PARAMETER MODELS

3.3.1 Introduction

The aim of a good middle-ear model is to determine the precise nature of the middle-ear transformer, especially its dependence on frequency. Mathematical models of the middle ear have been used for many years to model its transfer characteristics. All models of the ossicular chain, and most models of the eardrum, have been lumped-parameter models, usually cast in the form of mechano-acoustical circuits or equivalent electrical circuits. Lumped models attempt to lump certain characteristics of a system in large discrete circuit elements. These circuits may then be analysed using ordinary differential equations.

A mathematical equivalence may be formulated between acoustical, electrical and mechanical circuits. All these circuits have three generic quantities; quantity a is the drop across an element, quantity b is the flow through an element, and quantity c is the magnitude of an element. As long as the product of the drop across an element a and the flow through an element b has the units of energy per unit time an analogy may be drawn (Beranek, 1954).

In most middle-ear circuit models the following analogies, summarized in Figure 3.3, are drawn. The flow through an element a is electrical current, mechanical velocity or acoustical volume velocity. The drop across an element b is electrical voltage, mechanical force or acoustical pressure. Electrical capacitors, mechanical springs and acoustical cavities are equivalent elements. Electrical inductors, mechanical masses and acoustical tubes are also equivalent elements. Electrical resistors, mechanical dashpots and acoustical meshes are a third set of equivalent elements. These elements have magnitude c. It should be noted that a number of circuit models include transformers as
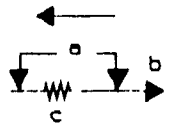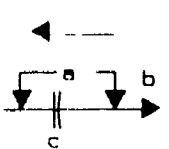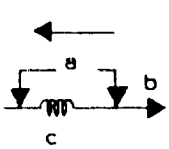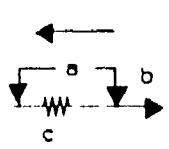
Element	Electrical	Mechanical	Acoustical
a	e(voltage)	f(force)	p(pressure)
b	i(current)	u(velocity)	U(volume velocity)
	$c = R_E$ resistance	$c = R_M$ resistance	$c = R_A$ resistance
	$c = C_E$ capacitance	$c = C_M$ compliance	$c = C_A$ compliance
	$c = L$ inductance	$c = M_M$ mass (inertia)	$c = M_A$ mass (inertia)
	$c = Z_E = e/i$ impedance	$c = Z_M = f/u$ impedance	$c = Z_A = p/U$ impedance

FIGURE 3.3: TABLE OF EQUIVALENCES BETWEEN ELECTRICAL,
MECHANICAL AND ACOUSTICAL CIRCUITS
(After Beranek, 1954)

an element to represent the interface between different modes (i.e a transition between electrical, mechanical or acoustical circuits) or to represent a lever action. These elements may be avoided by absorbing their transformer ratios into the values of other circuit elements.

3.3.2 Examples of Lumped Parameter Models

Guinan and Peake (1967) observed ossicular motion in the anesthetized cat visually with stroboscopic illumination. They measured stapes displacement in response to tones of known sound pressure. These experiments were performed on ears with tympanic cavities open but a correction was made for this, so the transfer function of the middle ear with cavities intact could be calculated. They determined a linear range of up to 130 dB in response to tones of less than 2000 Hz and 140 dB for tones below 3350 Hz. Observations on human cadavers indicate that there is a large rocking motion at the stapes, but the cat stapes was predominantly piston-like in motion. For frequencies below 3000 Hz, the ossicles were seen to move as one rigid body. Above that however the displacements of the incus and the stapes lagged behind those of the malleus, possibly due to flexing of the incudomalleolar joint. They concluded that the ossicular 'lever ratio' in the cat was frequency dependent, but for frequencies below 3000 kHz it was constant and equal to two. Below 7000 Hz it was determined to be approximately constant and equal to two.

The circuit model derived from the experiments performed (Peake & Guinan, 1967) is illustrated as an electrical circuit in Figure 3.4. All circuit illustrations of middle-ear models presented in this chapter will be in terms of electrical circuits for consistency. In this model the pressure at the lateral end of the ear canal is reduced by the first
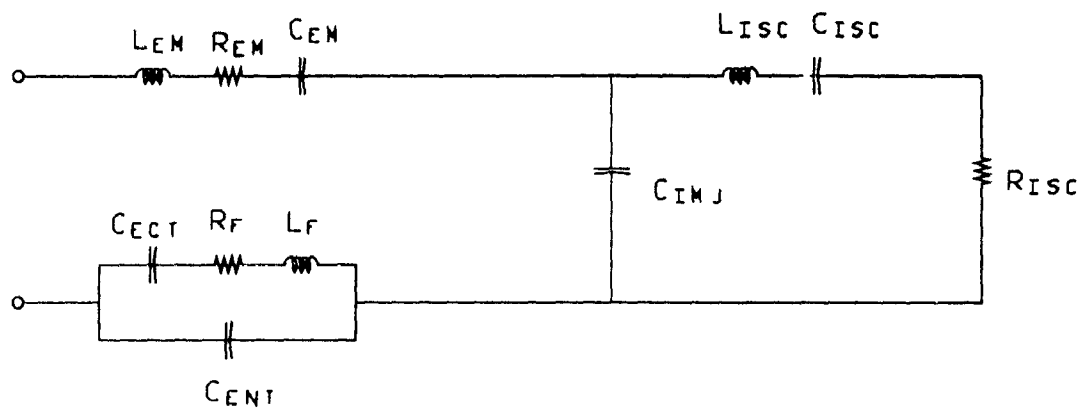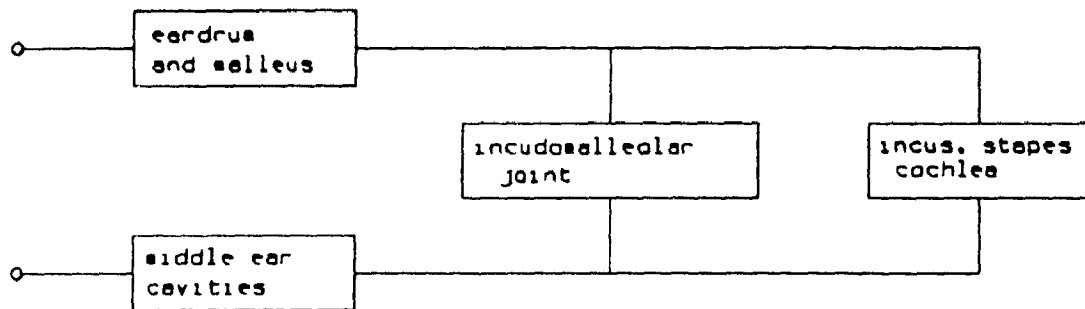
Subscript Key:

EM: eardrum and malleus
IMJ: incudomalleolar joint
ISC: incus, stapes and cochlea
ECT: ectotympanum
F: foramen
ENT: entotympanum

FIGURE 3.4: CAT MIDDLE-EAR MODEL (After Peake and Guinan, 1967)

complex, which consists of the eardrum and malleus. The complex is modelled by an inertia (L_{EM}), a resistance (R_{LM}) and a compliance (C_{FM}). The incudomalleolar joint is not assumed to be rigid in this model. Some of the volume velocity in the middle ear is lost to the cochlea (energy is shunted past the cochlea) through the compliance (C_{IM1}) of this joint. The incus/stapes/cochlea complex is represented by a compliance (C_{ISC}), a resistance (R_{ISC}) and an inertia (L_{ISC}). The pressure in the middle-ear cavities is modelled by the acoustic mass (L_F) and resistance (R_F) of the foramen connecting the entotympanum and ectotympanum, the acoustical compliance of the air in the ectotympanum (C_{ECT}) and the acoustical compliance of the air in the entotympanum (C_{ENT}).

From observations on cadavers, Onchi (1961) proposed a circuit model of the human middle ear. By measuring the impedance at the eardrum for the normal ear and for the experimentally modified ear he determined model parameters to fit his equations. His model is illustrated in Figure 3.5. It differs from the cat model of Peake and Guinan because it includes the effect of the human antrum and mastoid cells rather than the effects of the ectotympanum and entotympanum. This model also differs from that of Peake and Guinan in that the eardrum is modelled as two parts. Some of the energy at the eardrum is shunted past the ossicular chain through the compliance associated with the ligamentous connection of the middle portion of the eardrum and the malleus (C_{IM}). The other eardrum compliance in the model (C_I) represents the compliance between the middle zone of the eardrum and the bony wall where it is rigidly clamped. In this model the incudomalleolar joint is modelled as rigid and the incudostapedial joint is modelled as non-rigid, by an associated compliance.
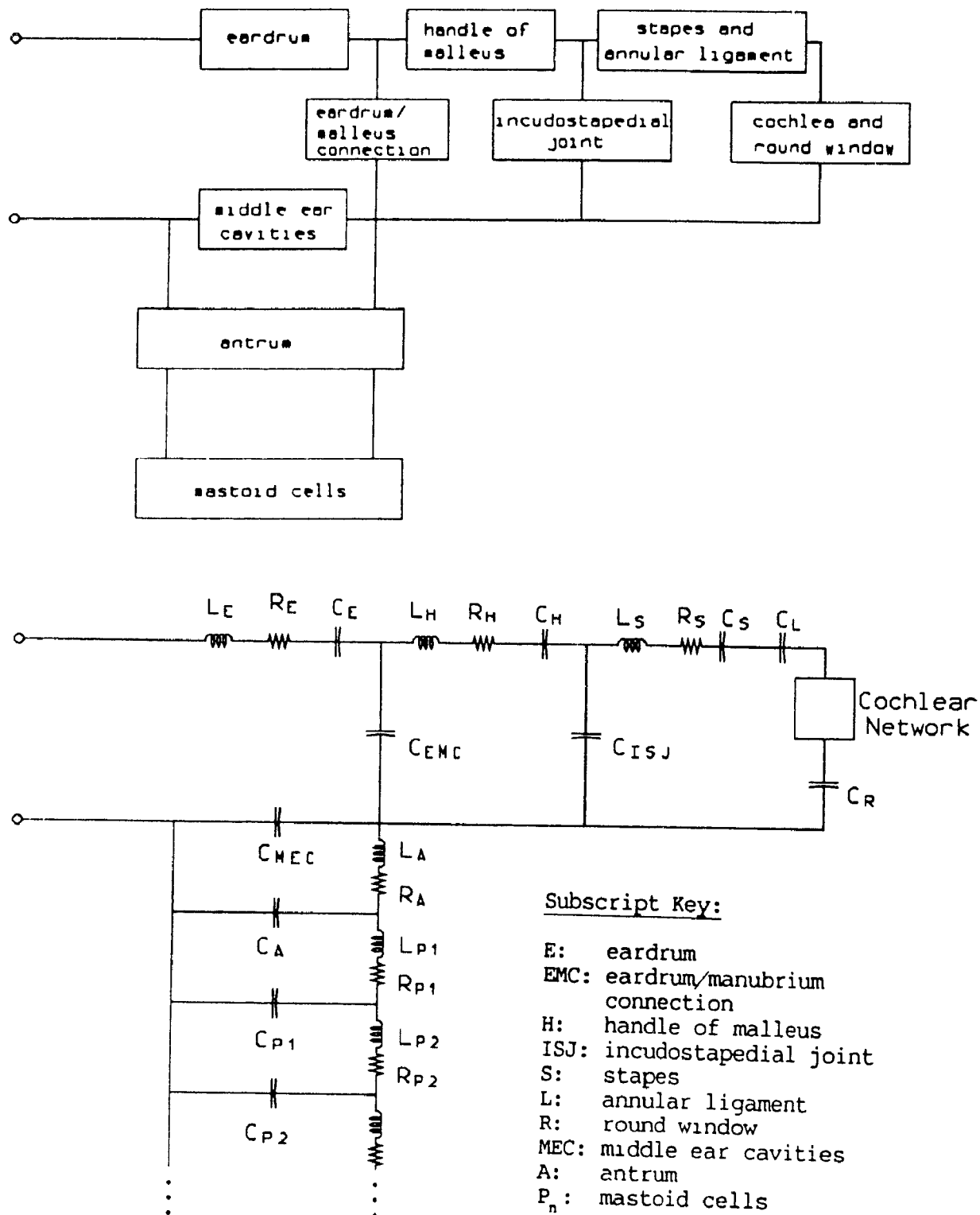
FIGURE 3.5: HUMAN MIDDLE-EAR MODEL (After Onchi, 1961)

Møller (1961) proposed a circuit model of the middle ear by taking acoustic impedance measurements from live humans. By taking measurements for different clinical situations he could determine the effects of certain functional parts of the middle ear. For instance, measurements were taken during stapedius muscle contraction, representing the middle ear with stapes blocked. Good agreement between model and impedance measurements was found from 200 to 1800 Hz. His model is illustrated in Figure 3.6. It does not include the effects of the middle-ear cavities. In this model energy is shunted past the ossicular chain by the impedance of the eardrum and past the cochlea by both the non-rigid incudostapedial joint and the non-rigid incudomalleolar joint.

Zwislocki (1962) constructed a circuit model of the normal human ear based on the functional anatomy of the middle ear. Parameter values were derived from impedance measurements of normal and pathological ears and from anatomical data. His model was valid for the range of 100 to 2000 Hz. Above that his data were scarce and inconclusive. His model is illustrated in Figure 3.7. Energy is shunted past the cochlea by two separately vibrating sections of the eardrum. Energy is also shunted past the cochlea by the non-rigid incudostapedial joint. This model includes the effects of the middle-ear cavities, the antrum and the mastoid cells.

A model of the cat middle ear by Lynch (1981) is illustrated in Figure 3.8 and is similar to the model of Peake and Guinan. This model differs from that of Peake and Guinan in that it includes an uncoupled portion of the eardrum. The components of the impedance of the middle-ear cavities, Z_{mec}, were modelled using four elements, as in the model of Peake and Guinan, and the value of Z_{mec} agreed well with measurements
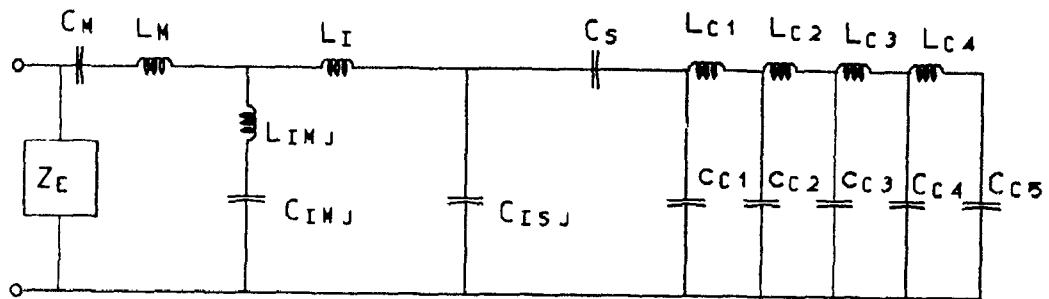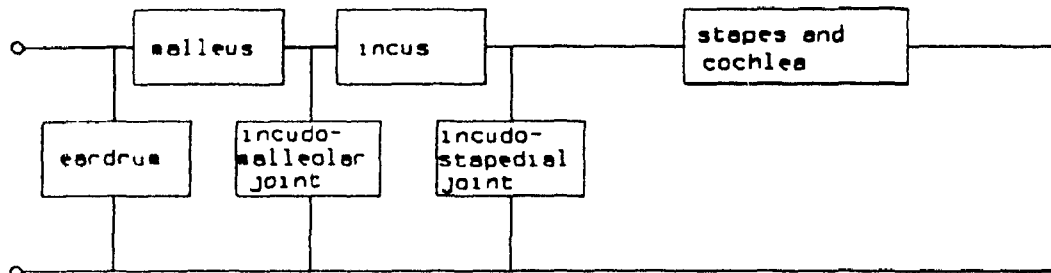
Subscript Key:

E: eardrum
M: malleus
IMJ: incudomalleolar joint
I: incus
ISJ: incudostapedial joint
S: stapes
C: cochlea

FIGURE 3.6: HUMAN MIDDLE-EAR MODEL (After Møller, 1961)
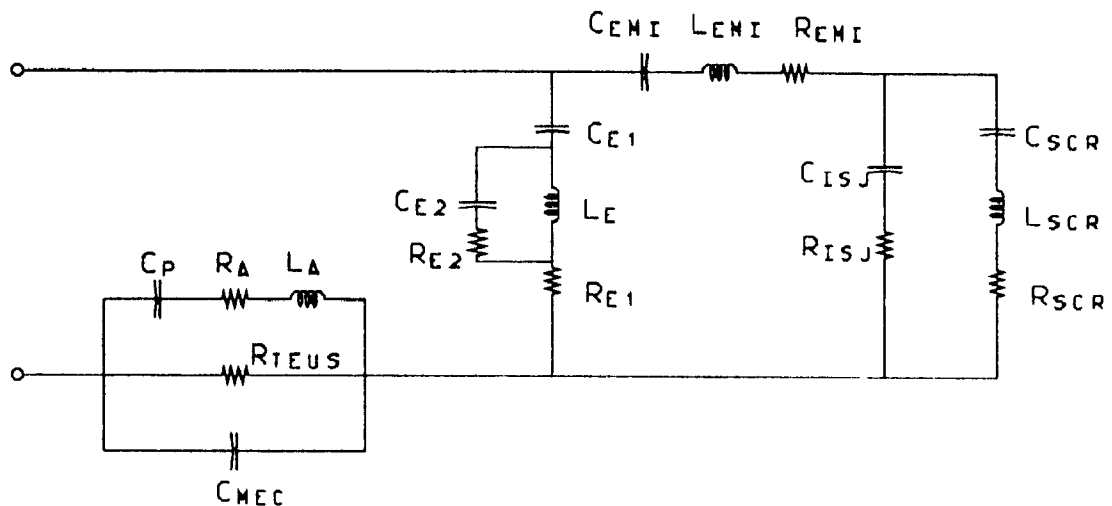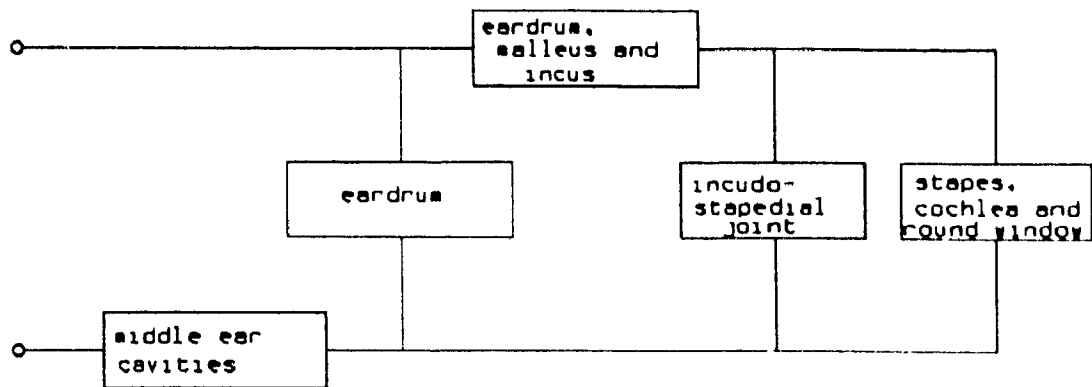
Subscript Key:

E: eardrum
EMI: eardrum, malleus and incus
ISJ: incudostapedial joint
SCR: stapes, cochlea and round window
A: passage between tympanic cavity and antrum
P: antrum and mastoid cells
TEUS: tympanic cavity and Eustachian tube
MEC: middle ear cavities

FIGURE 3.7: HUMAN MIDDLE-EAR MODEL (After Zwislocki, 1962)

FIGURE 3.8: CAT MIDDLE-EAR MODEL (After Lynch, 1981)

between 10 Hz and 10 kHz. Measurements of the admittance at the eardrum were made for various experimental adjustments of the ossicular chain to determine effects of certain elements in the impedance of the ossicular chain, Z_{oc}. The complete interpretation of these results into specific anatomically identifiable circuit elements is not included in the circuit diagram of Figure 3.8.

One of the experimental adjustments involved removing the cochlear 'load' by interrupting the incudostapedial joint. This had a large effect on the eardrum input impedance between 800 Hz and 2.8 kHz. Z_{oc} was largely influenced by the cochlear load over this range but elsewhere it was influenced more by the ossicular chain and the eardrum. Both Z_{mec} and Z_{oc} were mainly resistive between 2.1 and 3.0 kHz and thus a transformer ratio was calculated for this range of frequency by taking the ratio of a previously measured cochlear impedance and the eardrum impedance. The value of 52 calculated implicitly included the areal-ratio lever action and the ossicular lever action. The portion of the eardrum not coupled to the malleus affected Z_{oc} above 4 kHz but was unimportant below 1 kHz. Lynch found the low-frequency value of Z_{oc} to be dependent on the annular ligament of the stapes and the eardrum compliance. By mass loading the ossicles it was found that inertial effects had a small but noticeable effect on Z_{oc} in the 2 kHz to 3 kHz region.

Included in the circuit diagram of Figure 3.8 are elements based on a model by Lynch et al., 1982. They determined the acoustic impedance of the cochlea, and of the combined stapes and cochlea. They did this by measuring the complex amplitudes of the sound pressure at the stapes, the stapes velocity, and the sound pressure in the vestibule, and by determining experimentally how modifications of certain structures

influenced the impedance. They found that for the range 5 Hz to 5 kHz
the impedances were mostly resistive but were dependent on the basilar
membrane and cochlear fluid. At frequencies below 3 kHz the stapes-
cochlea impedance was greater than the cochlear impedance and was
controlled by the stiffness of the annular ligament. For frequencies
below 30 Hz, the impedance of the cochlea was assumed, from Nedzelnitsky
(1980), to be determined by the stiffness of the round window. This
assumption was supported by measurements of the impedance of the stapes
and cochlea for a series of cochlear manipulations.

The action of the eardrum in transmitting vibrations to the malleus
is obviously complicated. To try to model this, Shaw proposed an
eardrum model consisting of two 'zones' (Shaw 1977, Shaw & Stinson 1983)
or three 'zones' (Shaw & Stinson, 1986). In the two-zone model one zone
modelled the freely vibrating portion of the eardrum. The other zone
modelled the portion of the eardrum tightly coupled to the malleus. In
the three-zone model, the freely vibrating zone of the two-zone model
was subdivided into anterior and posterior zones of the eardrum. The
zones in these models were modelled as rigid pistons each coupled
together by a frequency-dependent mechanical impedance. At lower
frequencies the impedance represented the stiffness of the membrane
between the zones. At higher frequencies it represented the internal
damping of the membrane.

Vlaming (1987) proposed a middle-ear model with either a two- or
three-zone drum model. In his three-zone model, one zone contained the
malleus, the second zone represented the posterior portion of the drum
and the third represented the anterior portion. The anterior and
posterior zones were each coupled to the malleus zone but not to each
other.

All of the above lumped-parameter models represent the mechanical or acoustical behaviour of relatively large anatomical structures or combinations of structures by a combination of idealized circuit elements or more directly by a set of ordinary differential equations. These model parameters are not necessarily closely tied to physical or anatomical data. For example, the models previously mentioned involve the assumed axis of rotation of structures in the middle eai. If this axis is incorrect then relating parameter values to anatomical structures will give misleading results. If the axis of rotation changes with frequency then parameter values are frequency dependent and the mathematical formalism of the ideal circuit element is destroyed.

Recent experiments (Gundersen et al. 1976, Gyo et al. 1987, Brenkman et al. 1987, Decraemer et al. 1989) indicate that this axis of rotation is not necessarily fixed and can vary considerably with frequency. Decraemer et al. used a homodyne interferometer on cats with closed bulla to measure the relative vibration amplitude and phase between two points on the manubrium. Assuming the malleus is rigid and rotates around a certain fixed axis, the relative vibration amplitude of all points on the malleus may be calculated. The amplitude ratio was calculated for a point near the umbo and a point partway between the umbo and the lateral process of the malleus. Assuming an ossicular axis of rotation running approximately from the anterior malleolar ligament to the posterior incudal ligament (i.e. similar to that shown in Figure 3.1), the ratio was calculated to be 0.81.

For low frequencies the observed value was 0.85. Between 100 Hz and 10 kHz the observed value varied between 0.85 and 1 and then dropped down to 0.45 as the frequency increased past 10 kHz. The relative phase response of the two points varied also. These results are not consistent

with a simple rotation of the malleus and suggest that the mode of malleus vibration varies with frequency. It is also possible that the manubrium is not rigid.

3.4 OTHER EARDRUM MODELS

Some of the problems associated with lumped-parameter models of the eardrum have been addressed in a finite-element model of the cat eardrum presented by Funnell (1975). Instead of having two or three zones as did the models of Vlaming, and of Shaw and Stinson, this model may be interpreted as having N zones, where N is the number of finite elements. The coupling of these zones is accomplished implicitly in the finite-element analysis. Thin, so-called shell finite elements model the detailed geometry of the eardrum as illustrated in Figure 3.9. Material properties were estimated from the literature. Parameter fitting did not occur and the model could be independently verified from vibratory and impedance measurements. Although finite-element analysis is computationally more expensive than is lumped-parameter modelling, it is useful to complement and possibly guide lumped models. This finite-element model was the first to present an eardrum model using the geometry and details of mechanical properties of it and surrounding structures.

Vibration patterns calculated from a static (low-frequency) finite-element model (Funnell & Laszlo, 1978) agreed well with experimentally observed results (Khanna, 1970). Important characteristics of the model were found to be the material stiffness and thickness, and the curvature, conical shape and anisotropy of the eardrum. Boundary conditions and the Poisson's ratio (the ratio of lateral strain to longitudinal strain) of the eardrum material were found not to be so
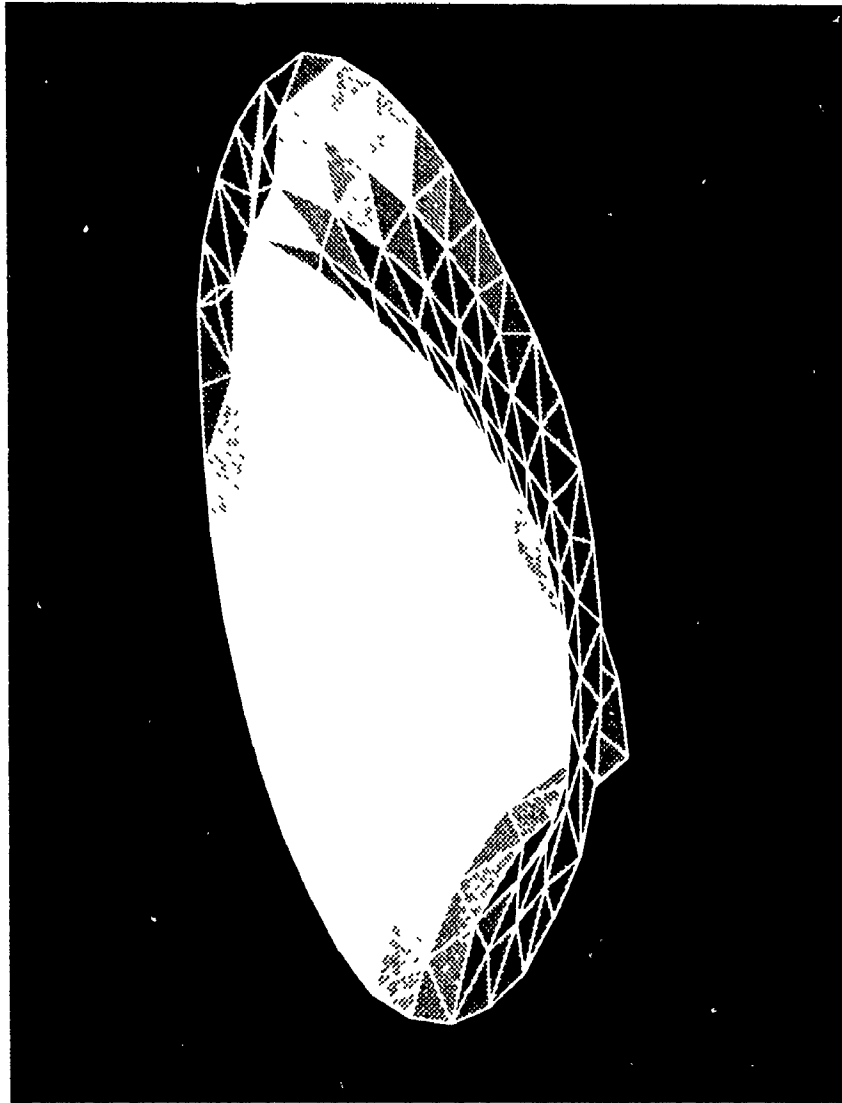
FIGURE 3.9: FINITE-ELEMENT MODEL OF THE CAT EARDRUM
The geometry of the cat eardrum is modelled by Funnell using
shell elements. The umbo protrudes medially and is
seen at the bottom right portion of the figure.

important.

Inertial effects were then included in the model (Funnell, 1983). The natural frequencies and mode shapes of the eardrum agreed reasonably well with experimental results (Khanna & Tonndorf, 1972). Results suggested that the conical shape and possibly the curvature of the eardrum extend its frequency range. Ossicular parameters seemed to have little effect on the natural frequencies and mode shapes of the eardrum.

Finally, the effects on the eardrum of damping were studied (Funnell et al., 1987). The experimental data needed to estimate the damping are scarce, especially at high frequencies, so a range of values was used. A mass-proportional damping coefficient of 1.5×10^3 s^{-1} and a stiffness proportional term of zero agreed fairly well with experimental evidence cited. In this model, the frequency response of the eardrum away from the manubrium showed sharp variations. For points on the manubrium the variations were smoother, even when there was no ossicular loading, indicating that spatial integration over the eardrum occurred at the manubrium. This is consistent with the experimental work of Decraemer et al. (1989).

Another eardrum model that overcomes certain problems with lumped parameter models was proposed by Rabbitt and Holmes (1986). They proposed an analytic model based extensively on physical characteristics of the membrane, especially on the anisotropic nature of the eardrum. Bending, shear and extensional stiffness equations are used to describe structural damping, transverse inertia and membrane restoring forces. This approach complements the finite-element analysis approach. It is simpler computationally, but the accuracy of the geometric and material assumptions of this model are critical to its success. Every assumption

and approximation made affects the subsequent problem formulation. It is more difficult to change the assumptions in this model than in a finite-element model where element material properties may be altered easily and successive mesh refinements may be used.

3.5 MOTIVATION FOR A FINITE-ELEMENT MIDDLE-EAR MODEL

The models of Rabbitt and Holmes and of Funnell et al. require a detailed model of the ossicular chain and cochlea. For the model of Rabbitt and Holmes, at high frequencies the parameters selected to represent the ossicular chain corresponded to a rotational axis of the malleus which did not agree well with the low-frequency axis determined experimentally.

The dynamic behaviour of the ossicular axis of rotation appears of great importance in understanding how the middle ear functions. Present models of the eardrum model the ossicular axis of rotation as fixed. Due to the mechanical coupling between the eardrum and the malleus, part of the force acting on the eardrum is transmitted to the malleus. This coupling has yet to be adequately modelled.

Finite-element analysis is a method that could model both the manubrium/eardrum interaction and the resulting motion of the ossicular axis of rotation, especially at high frequencies where other models seem to break down. As was demonstrated in the finite-element eardrum model, the detailed mechanical behaviour of a complicated mechanical system can be modelled using this method. A model of the ossicles and important soft tissues in the middle ear, together with the existing eardrum model, would implicitly model the lever action, determining properties such as the effective area of the eardrum.

Modelling of the distributed interaction of the annular ligament

and cochlea could also be accomplished with this technique. Recent research suggests that raised perilymph pressure changes the way the eardrum responds to contractions of the stapes muscles, probably due to a change in stapes position. A lumped model of the stapes and its ligament and muscle has been developed (Tweed, 1985). It was unsuccessful under certain conditions, suggesting that another approach may be helpful. In the cochlear model mentioned earlier (Lynch et al., 1982) evidence indicated that the mechanically important parts of the annular ligament may not be uniformly distributed, and that they may not necessarily occupy the annular space. The finite-element method may be useful in analysing this situation.

3.6 MATERIAL PROPERTIES

3.6.1 Introduction

Before further discussion of a middle-ear finite-element model, characterization of the material properties of the middle-ear connective tissues and ossicles is required. This information is needed in order to describe the stress-strain relationships of the finite elements. The following is a brief discussion of these properties.

3.6.2 Connective Tissues

3.6.2.1 Introduction

Connective tissues are composed of fibres which are in turn composed of collagen, elastin and other proteins. The mechanical responses of these tissues are generally loading-path and rate dependent. This non-conservative characteristic of these tissues complicates modelling beyond the normal problems of nonlinear elastic theory.

Few experimental data are available for material properties of soft tissues, especially for structures in the middle ear. When data are available, they must be considered carefully as to how they were collected and thus to their limitations. For instance, when material property data are collected from excised specimens, degenerative effects must be carefully assessed. When considering data collected in vivo, the effects of biochemical responses in the body must be considered.

The material parameters initially used to model the posterior incudal ligament are very simplistic, but will later be refined. The following is a brief discussion of linearity, homogeneity and isotropy of material properties in the middle ear.

3.6.2.2 Linearity

Material linearity exists in a problem if, for the range of displacements considered, the material exhibits a linear stress-strain relationship (i.e., the displacements in a problem must be small enough so that the material remains within its linear stress-strain range). Geometric linearity exists if, for the range of displacements considered, the effects of changing load and boundary conditions are considered insignificant.

Although little direct evidence is available, the posterior incudal ligament (and later other middle-ear soft tissues) is modelled using both material and geometric linearity. Various experiments on the rat middle ear indicate linearity of the umbo displacement at various frequencies. Vlaming (1987) demonstrates linearity of umbo displacement at several frequencies up to 8960 Hz for sound pressure levels between 30 and 110 dB SPL. This situation is illustrated in Figure 3.10. As mentioned earlier, Guinan and Peake (1967) also determined a linear
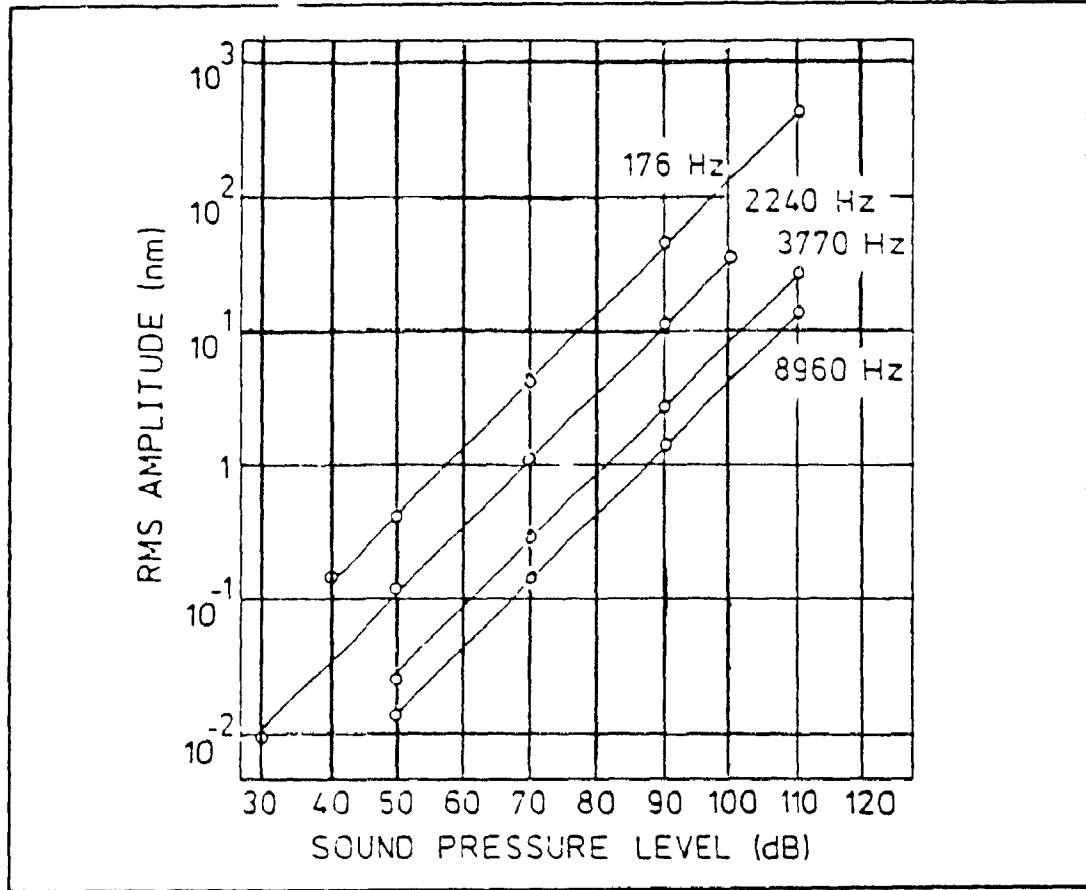
FIGURE 3.10: LINEARITY OF UMBO DISPLACEMENT
at several frequencies for sound pressure levels
between 30 and 110 dB SPL. (From Vlaming, 1987)

range of up to 130 dB in response to tones of less than 2000 Hz and 140 dB for tones of less than 3350 Hz.

3.6.2.3 Homogeneity and Isotropy

Because of their oriented nature and varying composition, the material properties of connective tissues are in general neither isotropic nor homogeneous. Both inhomogeneity and anisotropy can be modelled in linear finite-element analysis. Inhomogeneity is modelled by defining different material properties for each element. Anisotropy is modelled by using appropriate stress-strain relationships for each element (see section 4.3.4). In the initial finite-element analysis of the connective tissues in the middle ear, both homogeneity and isotropy are assumed.

3.6.3 Modelling Parameters

Because so little experimental evidence is available for the middle ear the material properties of the structures of interest have been estimated indirectly. Funnell (1975) estimates the posterior incudal ligament to have a modulus of elasticity of 2×10^7 N/m$'$ and a Poisson's ratio of 0.3 based on material properties measured for the eardrum.

The middle-ear ossicles are generally assumed to be completely rigid. Due to the scope of this thesis, modelling of the ossicles will not be done here. However, in the future, the ossicles will initially be modelled as rigid. This may be an incorrect assumption in light of the experiments by Decraemer et al., 1989, which indicate possible bending of the manubrium. As the middle-ear modelling proceeds, the question of bending will be addressed.

3.7 DESCRIPTION AND SCOPE OF THE MIDDLE-EAR MODEL

The first step in modelling the middle ear should be the development of a static (low-frequency) model of the important soft tissues. These soft tissues should then be integrated with the ossicles and a static analysis should be performed on the integrated complex. This static model would include effects of ligaments whose stiffness appears significant at low frequencies, such as the posterior incudal ligament, the anterior malleolar ligament and the annular ligament. The passive effects of the middle-ear muscles can be ignored in a static model as they are thought to have little effect at low frequencies (Funnell, 1972).

Next a model determining the natural frequencies and mode shapes of the middle ear should be attempted, and finally a model simulating the damped frequency response should be developed.

In order to develop a static model of the middle ear a modelling scheme must be developed. The methodology used here is as follows. First, the geometric parameters of the model are gathered by digitizing outlines of structures of interest from histological slides. Chapter 5 describes the data input and manipulation scheme developed and used. The next step in the modelling scheme is to generate finite-element meshes of structures of interest from three-dimensional surface reconstructions of the digitized contours. Chapter 6 describes the mesh generation scheme developed and used to do this.

The final step in the modelling scheme is the finite-element analysis of important structures in the middle ear, and the assembly of these structures to form the integrated middle-ear model. Due to the limited scope of this thesis, only an initial static analysis of the lateral bundle of the posterior incudal ligament is performed. Chapter 7

describes this analysis. Comments on the modelling procedure and future work required for the middle-ear model will be discussed in Chapter 8.

Before examining in detail the modelling method developed and used in the course of this research, an understanding of finite-element analysis is required. The next chapter explains the finite element method.

CHAPTER 4

THE FINITE-ELEMENT METHOD

4.1 INTRODUCTION

Solving problems in structural mechanics involves determining the distribution of stresses and/or displacements throughout a structure. In order to determine the system of stresses and displacements, the governing differential equations of the problem that preserve equilibrium, differential element continuity, and constitutive (stress-strain) requirements must be established. Unfortunately it is difficult to determine equations that adequately represent a physical problem for all but the simplest problems, since complications in geometry, loading and material properties must be considered. When analysing two or three-dimensional problems these governing equations contain partial differentials, further complicating the problem.

This chapter describes how the determination and solution of governing equations in a continuum may proceed in general. In particular it describes the displacement-based finite-element method. This method involves dividing the physical system to be analysed into a mesh of two or three-dimensional subregions or elements and finding a solution over each of these elements that is very much simpler than that required over the entire region. The mechanical behaviour of each element is analysed and the result of the analysis is a matrix equation relating the behaviour of the element to applied forces. The matrix equations are functions of the shape and material properties of the elements. These matrix equations can be combined into a global matrix equation describing the behaviour of the entire structure. In this manner the

response of the structure to applied loads can be expressed in terms of displacements at the edges of any or all elements. The finite-element method is particularly useful in complicated systems where the governing equations over the entire region are difficult to find.

4.2 DETERMINATION OF THE GOVERNING EQUATIONS OF A PROBLEM

In continuous systems, a number of different approaches may be used to determine the system of governing differential equations. In the direct or differential formulation of a problem, the equilibrium, continuity and constitutive requirements of a typical differential element are established in terms of the state variables, leading to a system of differential equations in those variables. In general these equations must be supplemented by differential equations that impose constraints on the variables. Also the boundary conditions (geometric and force boundary conditions for structural mechanics) and the initial conditions (for dynamic problems) must be stated.

Another approach used to establish the governing differential equations of a problem is the variational approach. In this approach the principle of minimum potential energy is, in general, employed. To do this one must calculate the total potential energy of a system, Π. For structural problems, the potential energy includes the strain energy (SE) and the force energy (FE). The actual configuration of a deformed elastic continuum yields a minimum value of this potential energy (Π= SE + FE). By invoking the stationarity of Π ($\delta\Pi=0$), this minimum is determined and thus the governing equations of the system may be derived. This procedure works not only for problems in structural mechanics but for any problem where the functional Π can be determined, e.g. heat flow, acoustical, or electrical field problems. It should be

mentioned that there are areas where a functional may not be known, or may not exist, as in some types of flow in fluid mechanics. Alternate methods such as the weighted residual methods must then be used (Reddy, 1984).

If the variational form of a problem exists, an approximate solution for the dependent variable, U, can be formulated by creating a trial solution function that minimizes the functional $\Pi(U)$. The approximate trial function $\tilde{U}$ must satisfy the boundary conditions and contain arbitrary constants that can be adjusted. For instance, the form of the trial function may be

$$\tilde{U}(X)= \sum_i c_i \phi_i (X) \tag{4.1}$$

where ϕ_i are linearly independent basis functions and c_i are constants to be determined. Substituting this into the functional $\Pi(U)$ and setting $\partial \Pi_a (\tilde{U})/\partial c_i =0$, ($\Pi_a$ is the approximation of the Π because $\tilde{U}(X)$ is only an approximation), one will end up with n differential equations in n unknowns. Thus the approximate displacements may be determined. This method was proposed by Rayleigh and generalized by Ritz (Grandin, 1986).

Another approach used to determine the governing equations of a system, which can be shown to be equivalent to the above variational approach (Bathe, 1982), is the one usually employed in the analysis of a linear elastic continuum. It involves the principle of virtual displacements. A bit of explanation is needed before stating this principle. There are many geometric configurations a body can undertake that satisfy the geometric constraints. Possible configurations lie in the neighbourhood of the true configuration that satisfies equilibrium. The small, compatible displacements that correspond to these possible configurations are termed virtual displacements. During these

displacements the forces are fixed at their equilibrium values. The principle of virtual work states that the total internal virtual work (the work resulting from the true stresses going through virtual strains) is equal to the total external virtual work (corresponding to the actual forces going through the assumed displacements). This may be stated mathematically as follows.

$$\int_V \bar{\varepsilon}^T \tau \, dV = \int_V \bar{U}^{B^T} f^B \, dV + \int_S \bar{U}^{S^T} f^S \, dS + \sum_i \bar{U}^{i^T} F^i \qquad (4.2)$$

where $\bar{\varepsilon}$ is the vector of virtual strains. (The reader should recall that the transpose of ε, $\varepsilon^T = [\varepsilon_{xx} \ \varepsilon_{yy} \ \varepsilon_{zz} \ \gamma_{xy} \ \gamma_{yz} \ \gamma_{zx}]$,

where $\varepsilon_{xx} = \dfrac{\partial U}{\partial X}$, $\varepsilon_{yy} = \dfrac{\partial V}{\partial Y}$, $\varepsilon_{zz} = \dfrac{\partial W}{\partial Z}$,

$$\gamma_{xy} = \frac{\partial U}{\partial Y} + \frac{\partial V}{\partial X}, \quad \gamma_{yz} = \frac{\partial V}{\partial Z} + \frac{\partial W}{\partial Y}, \quad \gamma_{zx} = \frac{\partial W}{\partial X} + \frac{\partial U}{\partial Z}.)$$

τ is the vector of actual stresses, $\tau^T = [\tau_{xx} \ \tau_{yy} \ \tau_{zz} \ \tau_{xy} \ \tau_{yz} \ \tau_{zx}]$. The vectors f^B, f^S and F^i are the surface traction vector, the body force vector and the concentrated force vector respectively. $\bar{U}^B$, $\bar{U}^S$ and $\bar{U}^i$ are the vectors of virtual displacements of the body from an unloaded configuration in a UVW Cartesian coordinate system, corresponding to the forces mentioned above. $(\bar{U}^T = [\bar{U} \ \bar{V} \ \bar{W}].)$

This equation provides the basis for generating finite-element equations that govern the response of the system.

4.3 THE FINITE-ELEMENT METHOD

4.3.1 Introduction

It is difficult to model an entire continuum by one assumed set of basis functions. The displacement-based finite-element method involves

dividing the physical system to be analysed into a mesh of discrete elements and using much simpler basis functions for each element. The elements are joined together mathematically by forcing shared nodes, created on the edges of two-dimensional elements or on the faces of three-dimensional elements, to have identical displacements. Appropriate degrees of freedom are constrained by forcing the displacements of certain nodes or their derivatives to be zero. One of the most critical points in finite-element analysis is that the behaviour of the element must be accurately modelled by the set of basis functions.

In general elements should also be compatible, which means no gaps or overlaps should exist between elements in a continuum. This requirement is not absolute, however. Finite-element analysis tends to overestimate the stiffness of a structure, and overlaps and gaps tend to 'soften' a structure. Thus sometimes incompatible elements are actually preferred (Cook, 1981).

4.3.2 Derivation of System Matrix Equations

The governing equation for a continuum may be written as the sum of integrations over all finite elements from (4.2):

$$\sum_i \int_{(e)} \bar{\epsilon}^{(e)^T} \tau^{(e)} dV^{(e)} = \sum_e \int_{(e)_V} \bar{U}^{B(e)^T} f^{B(e)} dV^{(e)}$$

$$+ \sum_e \int_{(e)_S} \bar{U}^{(e)^T} f^{(e)} dS^{(e)}$$

$$+ \sum_i \bar{U}^{i^T} F^i \tag{4.3}$$

where the superscript e refers to elements 1,2....n and n is the number

of finite elements. The superscript I refers to the nodes of the element assemblage.

In the finite-element method the displacements of points within an element, measured in a local coordinate system, are functions of the displacements of the structural nodal points, measured in a global coordinate system, and may be interpolated from them as follows:

$$u^{(e)}(x,y,z)=H^{(e)}(x,y,z)\hat{U} \qquad (4.4)$$

where $\hat{U}$ is a vector of global nodal displacements and $H^{(e)}$ is an element displacement interpolation matrix. (Note here that $H^{(e)}$ implicitly includes a transformation from a global to a local coordinate system). Although $\hat{U}$ contains all global nodal displacements, the strains and displacements within an element depend only on displacements at the nodes of that element.

The corresponding element strains may then be derived. They are

$$\epsilon^{(e)}(x,y,z)= B^{(e)}(x,y,z)\hat{U} \qquad (4.5)$$

where $B^{(e)}$ is the strain-displacement matrix of an element calculated by differentiating and combining appropriate rows of $H^{(e)}$.

Element stress-strain relationships may be described in terms of the element stress-strain matrix $C^{(e)}$, which describes the material properties of the element, and the initial stress in the element, $\tau^{I(e)}$.

$$\tau^{(e)} = C^{(e)}\epsilon^{(e)} + \tau^{I(e)}. \qquad (4.6)$$

Using (4.4), (4.5) and (4.6), equation (4.3) may be rewritten

$$\overset{r}{U^T}\left[\ \sum_e \int_{V_{(e)}} \mathbf{B^{(e)}}^T \mathbf{C^{(e)}} \mathbf{B^{(e)}} dV^{(e)}\right]\hat{U} = \overset{x}{U^T}\left[\ \{\ \sum_e \int_{V_{(e)}} \mathbf{H^{B(e)}}^T \mathbf{f^{B(e)}} dV^{(e)}\}\right.$$

$$+ \{\ \sum_e \int_{S_{(e)}} \mathbf{H^{S(e)}}^T \mathbf{f^{S(e)}} dS^{(e)}\} \qquad (4.7)$$

$$\left. -\{\ \sum_e \int_{V_{(e)}} \mathbf{B^{(e)}}^T \mathbf{\tau^{I(e)}} dV^{(e)}\}\ +\ \mathbf{F}\right]$$

where $\overset{x}{\mathbf{U}}$ are the virtual nodal displacements and **F** is a vector of externally applied forces at the nodes of the element assemblage. By imposing unit virtual displacements in turn at all nodes, $\overset{x}{\mathbf{U}}$ becomes the identity matrix **I**. (This may be done because imposing a virtual displacement at one node is assumed not to affect the force distribution at all others.) Thus (4.7) may be restated in matrix form as

$$\hat{\mathbf{KU}} = \mathbf{R} \qquad\qquad (4.8)$$

where $\mathbf{K} = \sum_e \mathbf{K^{(e)}}, \qquad \mathbf{K^{(e)}} = \int_{V_{(e)}} \mathbf{B^{(e)}}^T \mathbf{C^{(e)}} \mathbf{B^{(e)}} dV^{(e)}$

and **R** is the load vector which includes the effects of the element body forces $\mathbf{R^B}$, surface forces $\mathbf{R^S}$, concentrated nodal forces $\mathbf{R^1}$ and element initial stresses $\mathbf{R^1}$.

This is a statement of the static equilibrium. In the equilibrium considerations, the applied force may vary with time. Thus the displacements also vary with time. If loads are applied rapidly, inertial forces are significant. Also, energy is dissipated in vibration and thus velocity-dependent damping forces must be included. By

incorporating these effects into the governing equations, a matrix equation describing a dynamic system may be derived. It is

$$M\ddot{U} + D\dot{U} + K\hat{U} = R \tag{4.9}$$

where **M** is a matrix containing inertial terms and **D** is a matrix containing damping coefficients. The symbols ($\cdot$) and ($\cdot\cdot$) indicate first and second derivatives respectively.

This thesis deals only with static analysis in the middle ear. Static analysis will in effect model the low-frequency behaviour of the middle ear below 1 Khz where inertial and damping effects are negligible. However, as with the eardrum model of Funnell, the ultimate aim of this research is to solve (4.9) to determine the high-frequency dynamic response of the middle ear.

4.3.3 Choice of Local and Natural Coordinate Systems

Typically, when working with finite elements, three types of coordinate system must be considered. The first is the global coordinate system which is the frame of reference for the entire continuum. Its coordinate axes have dimensions of length. The second system is the local coordinate system. Its orientation is determined with respect to the individual element and may be different from that of the global system. Its dimensions and units are usually the same as for the global system. The third system is the natural coordinate system. It consists of dimensionless coordinates that identify positions in an element without regard to size and shape. The local and natural coordinate systems exist for convenience in developing element relations, e.g. performing integrations as in (4.8). The choice of which

of these systems to use determines how the displacement assumptions are formulated.

When working with a local xyz Cartesian system, the displacements may be interpolated using generalized coordinates as follows:

$$u(x,y,z) = \alpha_1 + \alpha_2 x + \alpha_3 y + \alpha_4 z + \alpha_5 x^2 \ldots \qquad (4.10)$$

$$v(x,y,z) = \beta_1 + \beta_2 x + \beta_3 y + \beta_4 z + \beta_5 x^2 \ldots \qquad (4.11)$$

$$w(x,y,z) = \gamma_1 + \gamma_2 x + \gamma_3 y + \gamma_4 z + \gamma_5 x^2 \ldots \qquad (4.12)$$

where α_i , β_i and γ_i are the generalized coordinates, and polynomials in x, y and z are the basis functions. There must be one basis function for each degree of freedom in the element. The generalized coordinates here turn out to be combinations of the element nodal point displacements.

The motivation for using the natural coordinate system is that the element displacements may be interpolated directly in terms of the element nodal point displacements as follows:

$$u(x,y,z) = \sum_i h_i(r,s,t)u_i \qquad (4.13)$$

$$v(x,y,z) = \sum_i h_i(r,s,t)v_i \qquad (4.14)$$

$$w(x,y,z) = \sum_i h_i(r,s,t)w_i \qquad (4.15)$$

where h_i are the basis functions (here assumed identical in each dimension); u_i , v_i , w_i are the element nodal displacements in the x, y and z directions; and r, s and t are the natural dimensionless coordinates. Using this formulation, the element geometry is interpolated in the same way as are the displacements, as follows:

$$x = \sum_i h_i x_i \qquad (4.16)$$

$$y = \sum_{i} h_i y_i \qquad (4.17)$$

$$z = \sum_{i} h_i z_i \qquad (4.18)$$

Use of this formulation has the advantage that the element basis functions are easily constructed, by inspection, and the elements can easily have curved boundaries.

Figure 4.1 illustrates the natural coordinate system for a eight-node brick element and for a four-node tetrahedral element. The basis functions for these linear elements can be built by inspection by noting that the value of function h_i is unity at node i and zero at all other nodes. The basis functions for the brick, in terms of natural coordinates, are

$$h_1 = (1+r)(1-s)(1-t)/8$$

$$h_2 = (1+r)(1+s)(1-t)/8$$

$$h_3 = (1-r)(1+s)(1-t)/8$$

$$h_4 = (1-r)(1-s)(1-t)/8 \qquad (4.19)$$

$$h_5 = (1+r)(1-s)(1+t)/8$$

$$h_6 = (1+r)(1+s)(1+t)/8$$

$$h_7 = (1-r)(1+s)(1+t)/8$$

$$h_8 = (1-r)(1-s)(1+t)/8.$$

The natural coordinates L1, L2, L3 and L4 for the tetrahedron are the ratios of volumes of tetrahedra. To determine coordinate L1 of point P, a tetrahedron is drawn with apex at point P and whose base is opposite node 1 as shown in Figure 4.1. Coordinate L1 is the ratio of the resulting interior tetrahedron (P-2-3-4) to the volume of the entire

Eight-node Brick

(r, s, t)
1(1,-1,-1)
2(1, 1,-1)
3(-1, 1,-1)
4(-1,-1,-1)
5(1,-1, 1)
6(1, 1, 1)
7(-1, 1, 1)
8(-1,-1, 1)
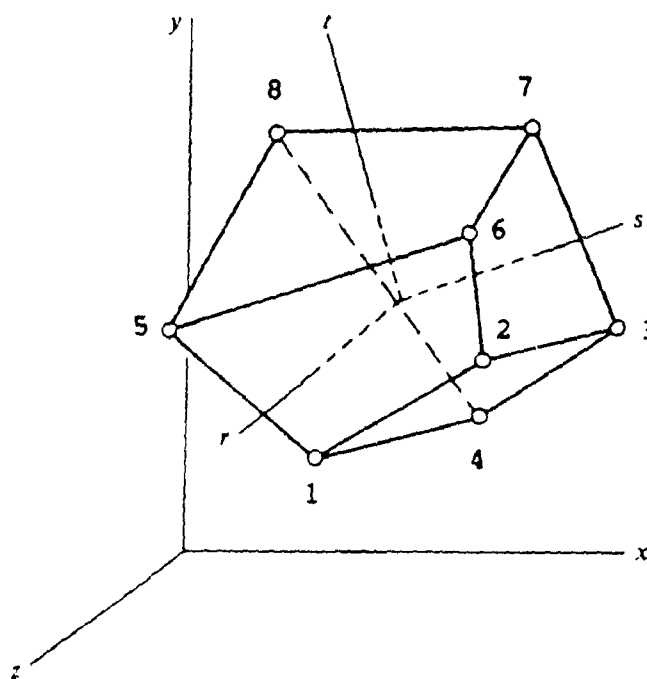
Four-node Tetrahedron

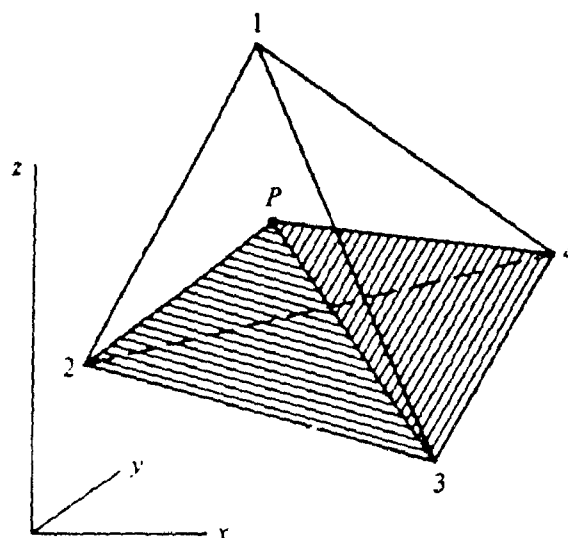| (r,s,t) |
|---------|
| 1(0,0,0) |
| 2(1,0,0) |
| 3(0,1,0) |
| 4(0,0,1) |

FIGURE 4.1: THE NATURAL COORDINATE SYSTEM
for the eight-node brick and the four-node tetrahedron.
(See text for explanation.)
(After Grandin, 1986)

tetrahedron. Coordinates L2, L3 and L4 are similarly determined. Only three of these coordinates are independent. Letting r=L2, s=L3 and t=L4, the basis functions for the four-node tetrahedron are

$$h_1 = 1-r-s-t$$
$$h_2 = r$$
$$h_3 = s$$
$$h_4 = t.$$

(4.20)

4.3.4 Building the Element Stiffness Matrices

To solve (4.8) for $\hat{U}$, the element stiffness matrices $K^{(e)}$ must be constructed. Once they are constructed, the entire structural stiffness matrix K and load vector R are then built.

To construct the element stiffness matrix, the local strain displacement matrix $B^{(e)}$ must be calculated using (4.13) to (4.15) such that

$$\varepsilon^{(e)}(x,y,z) = B^{(e)}(r,s,t)\hat{u}$$

(4.21)

where $\hat{u}$ is the vector of element nodal displacements. The strain-displacement matrix $B^{(e)}$ here is expressed in terms of the natural coordinate system. (Note that in equation (4.5) $B^{(e)}$ was expressed in a local coordinate system and implicitly included a transformation from global to local coordinates.) This matrix is determined by taking derivatives of the displacement interpolation functions h_i, with respect to the local Cartesian system, to build the strain matrix $\varepsilon^{(e)}$. $B^{(e)}$ is then determined by inspection. However the displacement interpolation functions h_i are stated in terms of the natural system. The relationship

between the x, y and z derivatives and the r, s and t derivatives must be found by the transformation

$$\frac{\partial}{\partial x} = J^{-1} \frac{\partial}{\partial r}$$ (4.22)

where **J** is the transformation matrix from local to natural coordinates.

The next step in building the element stiffness matrix $K^{(e)}$ is to determine the element constitutive matrix $C^{(e)}$ relating stress to strain. This matrix describes the elastic properties of the material in question and may describe a *linear* isotropic or anisotropic material. (The linear equilibrium equation (KU=R) was derived assuming small virtual displacements. The fact that the displacements are small has entered into the evaluation of the stiffness matrices $K^{(e)}$ and the load matrix **R** because all integrations have been performed over the original volumes of the finite elements and the strain displacement matrix $B^{(e)}$ is assumed constant and independent of element displacements.) The matrix $C^{(e)}$ for an element with isotropic material properties is

$$C^{(e)} = \frac{E}{(1 + \nu)(1 - 2\nu)} \begin{bmatrix} 1-\nu & \nu & \nu & 0 & 0 & 0 \\ \nu & 1-\nu & \nu & 0 & 0 & 0 \\ \nu & \nu & 1-\nu & 0 & 0 & 0 \\ 0 & 0 & 0 & \tfrac{1}{2}-\nu & 0 & 0 \\ 0 & 0 & 0 & 0 & \tfrac{1}{2}-\nu & 0 \\ 0 & 0 & 0 & 0 & 0 & \tfrac{1}{2}-\nu \end{bmatrix},$$ (4.23)

where E is the material modulus of elasticity and ν is Poisson's ratio. The modulus of elasticity is the rate of change of tensile or compressive stress with respect to tensile or compressive strain.

Equation 4.23 describes an isotropic material. However, a fully populated 6 x 6 $C^{(e)}$ matrix would define a general anisotropic material which possesses different properties in different directions. Special cases between the extremes of total anisotropy and total isotropy exist and can be modelled by defining entries in $C^{(e)}$ accordingly. Inhomogeneity may be modelled by defining different $C^{(e)}$ matrices for different elements.

Once $B^{(e)}$ and $C^{(e)}$ are determined the integration in (4.8) may proceed. Because the volume integration takes place in the natural system, the volume differential must be expressed in natural coordinates.

Calculation of the integrals describing the load vectors R^b, R^t and R^s proceed in a similar manner as for K. R^t may be built directly. The integrations described are usually performed on computer. For a brick element, these integrations must be done by one of a number of numerical techniques such as Newton-Cotes and Gauss quadrature. For a four-node tetrahedron (with linear displacement assumptions along each edge) the element stiffness matrix integration is exact. It is

$$K^{(e)} = B^{(e)^T} C^{(e)} B^{(e)} \int_{V(e)} dV \qquad (4.24)$$

$$\text{where} \int_{V(e)} dV = \frac{|J^{(e)}|}{6}$$

$|J^{(e)}|$ is the determinant of the Jacobian transformation of the element from the local to the natural system. $B^{(e)}$ happens to be constant throughout the element.

This integration of the element stiffness matrix produces an $n \times n$ element stiffness matrix where n is the number of degrees of freedom in

the element. Element load vectors of dimension n are produced.

4.3.5 Building the System Stiffness Matrix

Construction of the system stiffness matrix is now straightforward. To illustrate how this proceeds, a matrix for a two element system, illustrated in Figure 4.2, will be constructed. For simplicity, the elements used are triangular elements with one degree of freedom per node. The two-element assembly has a global numbering scheme as shown in the figure. The local numbering of the elements is 1-2-3 for the first element and 2-4-3 for the second element. The stiffness matrix for the first element is

$$\begin{bmatrix} k1_{11} & k1_{12} & k1_{13} \\ k1_{21} & k1_{22} & k1_{23} \\ k1_{31} & k1_{32} & k1_{33} \end{bmatrix} \begin{bmatrix} u_1 \\ u_2 \\ u_3 \end{bmatrix} = \begin{bmatrix} f_1 \\ f_2 \\ f_3 \end{bmatrix} \tag{4.25}$$

and for the second one it is

$$\begin{bmatrix} k2_{11} & k2_{12} & k2_{13} \\ k2_{21} & k2_{22} & k2_{23} \\ k2_{31} & k2_{32} & k2_{33} \end{bmatrix} \begin{bmatrix} u_2 \\ u_4 \\ u_3 \end{bmatrix} = \begin{bmatrix} g_2 \\ g_4 \\ g_3 \end{bmatrix} . \tag{4.26}$$

The system matrix is

$$\begin{bmatrix} k1_{11} & k1_{12} & k1_{13} & 0 \\ k1_{21} & k1_{22}+k2_{11} & k1_{23}+k2_{12} & k2_{13} \\ k1_{31} & k1_{32}+k2_{21} & k1_{33}+k2_{22} & k2_{23} \\ 0 & k2_{31} & k2_{32} & k2_{33} \end{bmatrix} \begin{bmatrix} u_1 \\ u_2 \\ u_3 \\ u_4 \end{bmatrix} = \begin{bmatrix} f_1 \\ f_2 + g_2 \\ f_3 + g_3 \\ g_4 \end{bmatrix} . \tag{4.27}$$

The boundary conditions are specified by constraining the appropriate degrees of freedom to their prescribed values. For instance u_2 may be constrained to be fixed as follows.
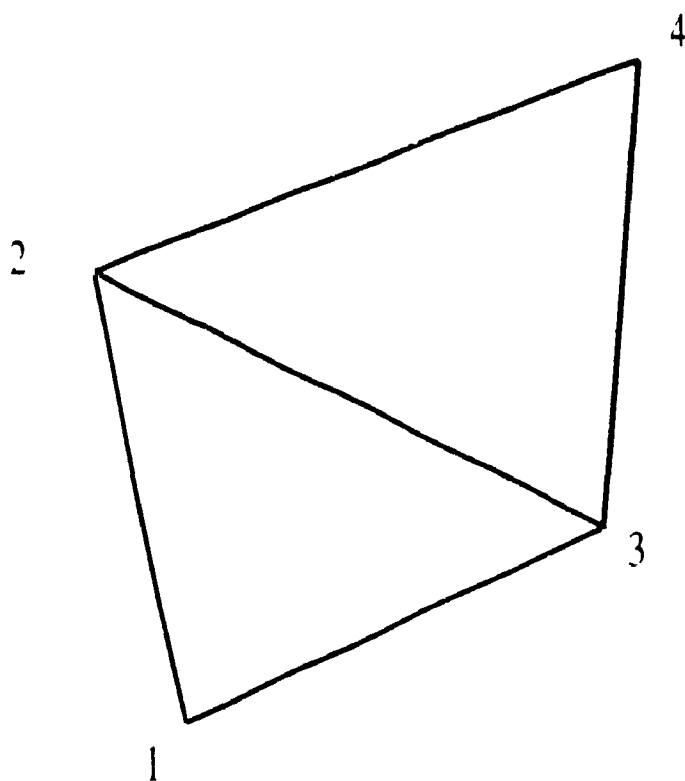
FIGURE 4.2: SIMPLE TWO—ELEMENT SYSTEM
Two triangular elements are coupled at nodes 2 and 3.

$$
\begin{bmatrix}
k1_{11} & k1_{12} & k1_{13} & 0 \\
0 & 1 & 0 & 0 \\
k1_{11} & k1_{12}+k2_{11} & k1_{13}+k2_{12} & k2_{13} \\
0 & k2_{21} & k2_{22} & k2_{23}
\end{bmatrix}
\begin{bmatrix}
u_1 \\ u_2 \\ u_3 \\ u_4
\end{bmatrix}
=
\begin{bmatrix}
f_1 \\ 0 \\ f_3 + g_3 \\ g_4
\end{bmatrix}
\qquad (4.28)
$$

The solution of the system matrix will yield the actual nodal displacements. (Once the displacements have been calculated, the stress field may also be calculated from (4.6).)

4.3.6 Convergence

It can be shown from minimum energy considerations (Bathe, 1982) that in finite-element analysis the strain energy of a structure is always underestimated, providing that the elements in the mesh of that structure are complete and compatible.

In order for an element to be complete its interpolation functions must be able to represent rigid body modes and constant strain states. Rigid body modes are those displacement modes where no stresses are developed in the structure (e.g., pure translation). Constant strain states must be able to be represented because in the limit of infinitesimally small elements the strain in the element must approach a constant value so that any complex variation in strain may be represented. As mentioned earlier, in order for elements to be compatible the displacements between elements must be continuous (i.e., no gaps or overlaps can develop).

Both the brick and tetrahedral elements mentioned earlier are complete and compatible if the basis functions of (4.19) and (4.20) are assumed. Thus the strain energy in a mesh composed of these elements will be underestimated. Displacements therefore will also be

underestimated. Consequently the mesh will be too stiff. As the size of the elements in a mesh of these elements decreases, the displacement interpolations of (4.13) to (4.15) will be more able to represent complex strain states and will be more able to accurately represent the true strain energy in the idealized continuum. As this occurs, the calculated displacements will increase towards the true displacements. This convergence will be monotonic provided that every finer mesh used is a subset of a previous coarser mesh. If this is not the case the displacements will increase towards the true displacements but not necessarily monotonically.

4.3.7 Finite-Element Packages

Many finite-element packages exist to handle both linear and nonlinear analysis (Brebbia, 1985). The most popular commercial finite element package available today is generally accepted to be MSC/NASTRAN. It is a large-scale general-purpose digital computer program whose capabilities include static and dynamic analysis of structural problems with material and/or geometric linearity or nonlinearity. Its element library includes more than fifty elements. Tetrahedral elements are available as are various pre- and post-processing packages to help the user generate meshes and inspect results.

The finite-element package used in this analysis is SAP IV, a program for the static and dynamic analysis of linear systems (Bathe et al., 1974). It was used because it was readily available, was inexpensive, and has been used and modified for several years in this middle-ear research (Funnell, 1978).

4.3.8 Choice of Elements

There are many element types besides the brick or the tetrahedron available for finite element analysis. These two elements are general three-dimensional elements that could theoretically be used in any structural analysis. However, by taking advantage of certain characteristics of a given structure, elements may be used which are less general but also less complicated. For example, when analysing the eardrum, Funnell took advantage of the fact that the eardrum is a curved shell structure. (Its dimensions in the eardrum thickness direction are much smaller than in the other two directions.) One of the simplifications this leads to for instance is that the stress through the thickness is zero.

The mesh generation scheme used in this analysis produces tetrahedral elements with nodes defined at each vertex. This mesh generator was used for a number of reasons, to be explained in Chapter 6. The linear basis functions of (4.20) may be used to perform the analysis of these meshes of tetrahedral elements.

Unfortunately, the finite-element package available for this research did not include code for a tetrahedral element. There are two ways to proceed given this problem. It is possible to 'convert' the brick element to a tetrahedral element by assigning certain nodes of the element the same spatial coordinates. This process is illustrated in Figure 4.3. The resulting collapsed-brick tetrahedral element uses the basis functions of the brick (4.19). The second possibility is to write code for a true tetrahedral element.

Both the collapsed-brick tetrahedral element and the true tetrahedral element give equivalent results in the linear case. However new code for the true tetrahedral element is used in the finite-element
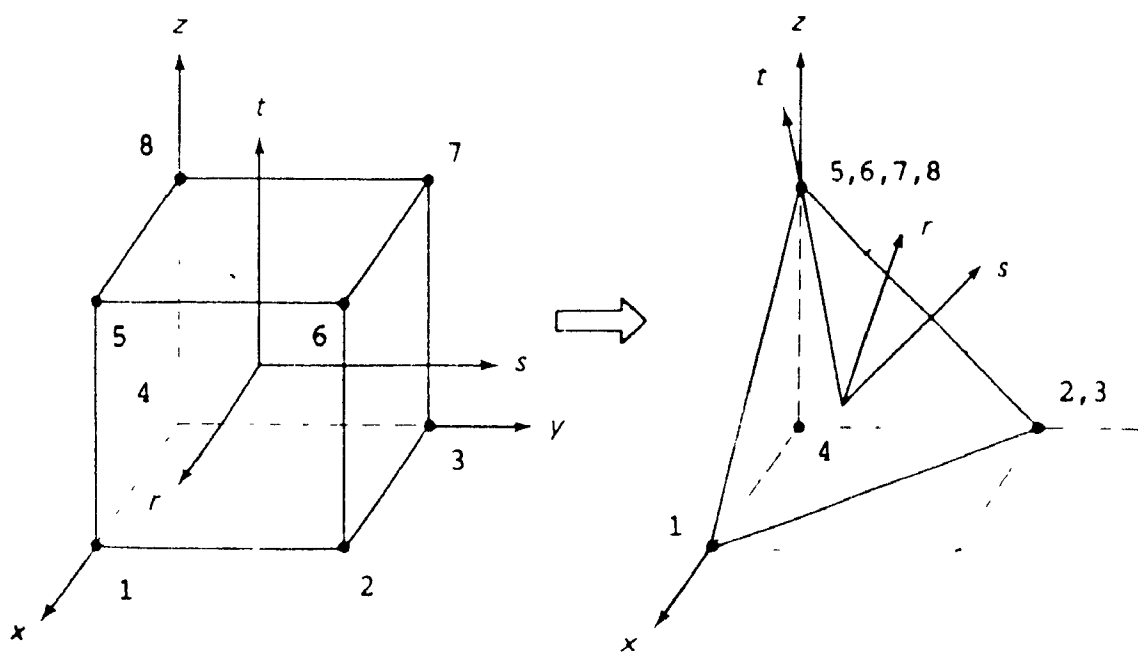
FIGURE 4.3: COLLAPSING AN EIGHT-NODE BRICK ELEMENT
The eight-node brick element is converted to a four-node tetrahedron
by assigning certain nodes of the brick the same global
coordinates. (After Bathe, 1982)

analyses of Chapter 7, to save unnecessary calculations.

It should be noted that the SAP code itself had to be modified to handle the collapsed-brick tetrahedral element. Sometimes element interpolation functions may be used that do not satisfy the requirements of compatibility. In the case of the brick element described in this chapter, extra basis functions may be added to the interpolation functions. Because these basis functions are not associated with any nodal degrees of freedom, incompatibilities may arise. However, if these displacement functions are known beforehand to represent the displacements of the brick they can be allowed. For example, if the brick is approximately rectangular, extra quadratic basis functions can allow a constant bending moment. These extra basis functions tend to make the element less stiff, which in turn tends to speed up the convergence of a solution. SAP code includes these extra basis functions or 'incompatible modes' because it assumes that the brick elements used are not extremely distorted. Because the collapsed-brick tetrahedral elements are extremely distorted these incompatible modes had to be deleted from the code.

4.4 SPECIAL CONSIDERATIONS FOR PHYSIOLOGICAL SYSTEMS

The study of the relationships between the geometry, material properties and loading history of a body is needed in order to solve any problem in structural mechanics. Finite-element analysis in man-made systems provides a satisfactory solution to the detailed mechanics of complicated structures because usually these relationships can be adequately established. When dealing with biological systems, however, these relationships are much less clear. Thus, the accuracy and validity of any finite-element analysis must be objectively established before

its results can be used.

Many of the difficulties in analysing anatomical structures come from the geometric complexity, the inhomogeneous material property distribution and uncertainties about the in vivo loading conditions. In addition, even in a simplified physiological finite-element analysis the three-dimensional nature of a problem, often required to model complicated geometries, may tax the computer power available. Even it an extremely accurate structural analysis could be done, the effects of biochemical responses present in physiological systems may further complicate matters.

The model of the middle ear being developed is a relatively simple one. Experimental evidence on loading conditions and material properties in the middle ear, and indeed in most physiological systems, is scarce. It is apparent that if a simplified finite-element analysis is to be performed on a physiological system, its purpose is not to provide definitive quantitative results but rather it is to provide a quantitative basis for more study of the same problem in an evolving fashion.

CHAPTER 5

ANATOMICAL DATA DESCRIPTION, INPUT AND MANIPULATION

5.1 INTRODUCTION

In order to view in detail mammalian anatomy, a number of techniques may be employed. A specimen may be investigated post mortem. This is often done by sectioning the structure of interest, staining the sections and mounting the sections on glass slides for later viewing, usually under a microscope. More recent techniques involve imaging the structure of interest non-invasively, often in vivo. Medical imaging techniques include conventional X-rays, computed X-ray tomography (CT), position emission tomography (PET) and magnetic resonance imaging (MRI). Both imaging and sectioning techniques produce two-dimensional cross-sectional representations of structures of interest, but present non-invasive imaging techniques produce representations of fairly low resolution. One of the problems of data acquisition of structures of interest in the middle ear is that the structures are extremely small. The middle-ear cavity volume in the cat is approximately 2 cm^3. Present medical imaging techniques cannot provide the resolution necessary to allow one to extract the outlines of structures accurately.

The first step in defining the present finite-element model of the middle ear is the input of two-dimensional anatomical data to the computer. Using the mesh generation scheme described in the next chapter, contours of structures of interest from these two-dimensional slides or images may be used as a basis for producing three-dimensional finite-element meshes. The present chapter describes a data input and manipulation scheme used to process two-dimensional contours to produce

three-dimensional surface definitions required for finite-element analysis. It also briefly describes display software used to view these three-dimensional surface definitions and later the resulting finite element meshes. The software described in this chapter is an outgrowth of developments spanning many years (Chawla et al. 1982, Funnell & Phelan, 1981).

5.2 HISTOLOGICAL MATERIAL

The histological material used as a basis for the middle ear model consists of 250 serial section slides from a left cat ear obtained from Dr. S.M. Khanna of Columbia University in 1982. The 2-kg cat had been used for an ultrasound experiment (Basek, 1970). Prior to sectioning, the ear was decalcified and embedded in plastic. The sections were cut at 50μm intervals in a plane approximately parallel to the legs (crura) of the stapes and every second section was stained and mounted.

Figure 5.1 is a photograph of one of the slides. In this slide structures of interest include the lateral and medial bundles of the posterior incudal ligament, the eardrum and connective tissues, the malleus and incus, and the tensor tympani muscle.

5.3 CONTOUR IDENTIFICATION

Contours may be extracted from two-dimensional representations either by manual tracing of outlines or by automatic edge detection image-processing techniques. Edge-detection techniques involve looking for sharp intensity variations in an image and extracting these variations to produce edges. These techniques could be used for contour identification from images of histological slides. However for the complicated structure in the middle ear, this would not be a simple

FIGURE 5.1: PHOTOGRAPH OF A HISTOLOGICAL SLIDE
of the left middle ear of the cat, shown approximately
6.3 x magnification. Structures of interest are identified
in the digitized version of this slide shown in Figure 5.2.

task. For simplicity, the method used in the course of this research to extract contours is to manually trace the outlines from magnified projections of histological slides.

5.4 DATA INPUT AND MANIPULATION

5.4.1 Introduction

A program (DIG), is used for the data input and manipulation. This program was developed in this lab and was used to produce a file containing the three-dimensional surface point definitions of structures in the middle ear.

5.4.2 Tracing and Alignment

Each histological slide of interest was placed in a holder under a light source. The image of the slide was projected through a lens, of approximate magnification 19, downward onto a digitizer surface. The digitizer, a Numonics Graphic calculator, is an electro-optical device. The contours of structures of interest were then digitized onto computer. The errors involved in tracing the contours are considered to be insignificant compared to cat-to-cat anatomical variations. Figure 5.2 is a digitized version of some of the structures on the slide of Figure 5.1. Contours are divided into classes by colour for easy distinction (i.e. muscles, ligaments, bones).

Contours are indexed and any or all contours on any or all slides may be redisplayed at any time. Contours may be rotated, expanded or shrunk for better viewing and to allow for contour alignment. Because no absolute alignment reference exists in the histological material the contours on consecutive slide must be aligned in a physically reasonable way. This is done interactively by marking corresponding landmarks on
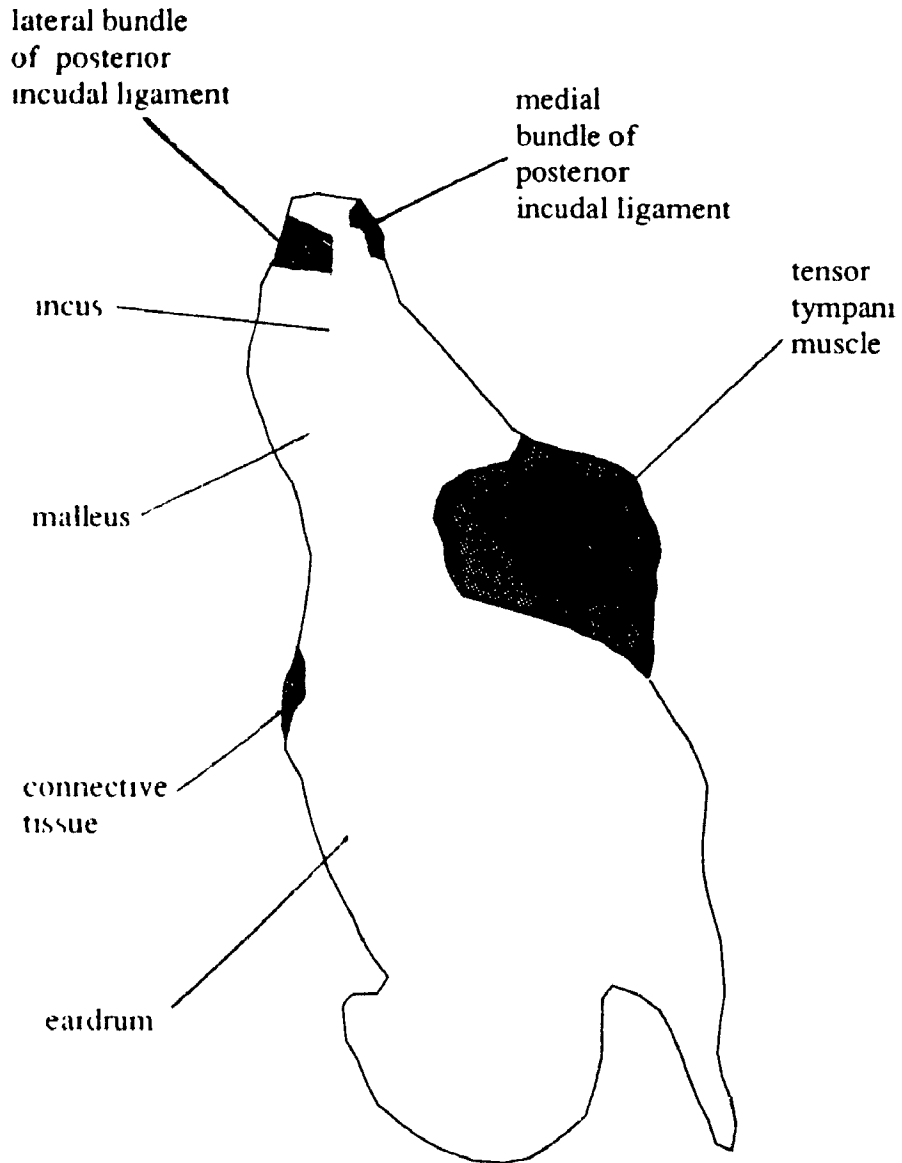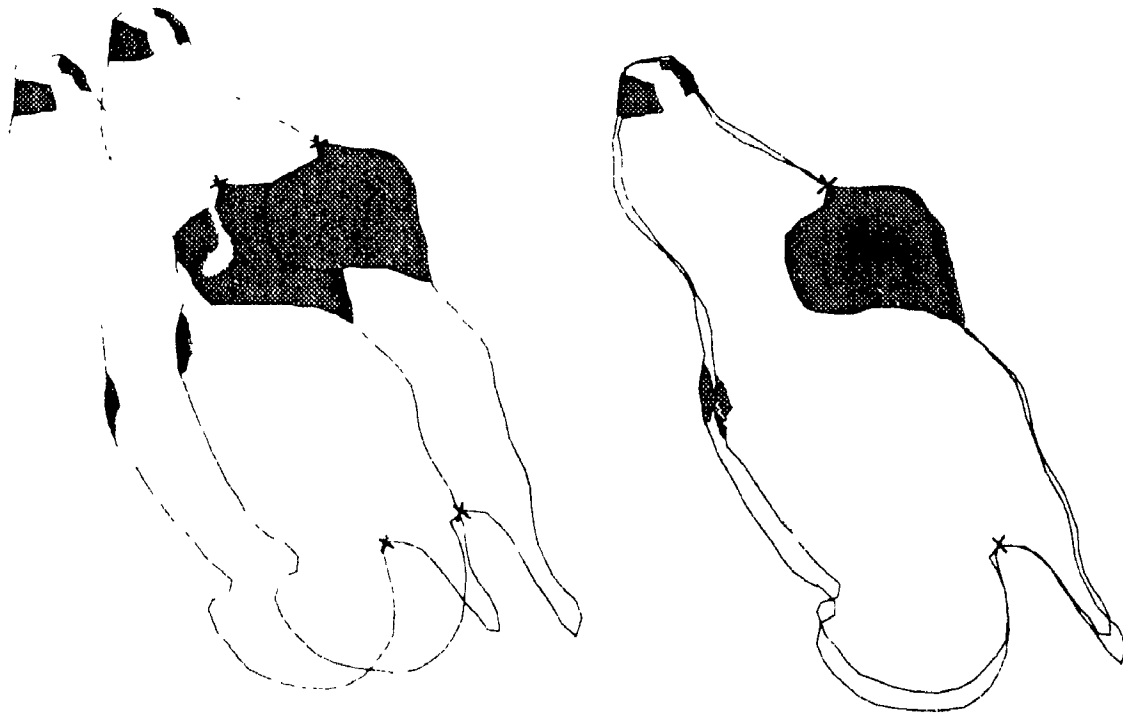
lateral bundle
of posterior
incudal ligament

medial
bundle of
posterior
incudal ligament

tensor
tympani
muscle

incus

malleus

connective
tissue

eardrum

FIGURE 5.2: DIGITIZED CONTOUR
showing outlines of some important structures
on the slide illustrated in Figure 5.1.

consecutive slides and aligning accordingly. Figure 5.3a illustrates two unaligned marked contours and Figure 5.3b illustrates the contours after alignment. Obviously the accuracy of the geometric representation of structures in the middle ear depends on the alignment of contours. Ideally histological material containing an alignment reference should be used, but unfortunately that is not yet available for the middle ear.

Contours are entered in segments. Sections of contours that are shared between two distinct structures (e.g. between the posterior incudal ligament and the incus, or between the ligament and the middle-ear wall) are marked as such. Thus, in the surface-point definition files, sections of a structure shared with other structures are easily identifiable. This is done so that after mesh generation, shared nodes on meshes of these connected structures may be identified for integration with other structures, or constrained as required. (E.g. the section of the lateral bundle of the posterior incudal ligament attached to the middle ear wall must be constrained not to move in the finite-element analysis. Also, shared nodes between the incus and the posterior incudal ligament must not be duplicated in a finite-element analysis of the integrated middle-ear model.)

5.4.3 Extraction and Display

Once all slides containing a structure of interest have been aligned, that structure may be extracted from the digitized data using a simple command. For example, all sections containing contours of the lateral bundle of the posterior incudal ligament may be extracted. The result is a file containing the three-dimensional surface point definition of the object. Figure 5.4 is a display of all contours of the lateral bundle of the posterior incudal ligament after alignment.

(a)   (b)

FIGURE 5.3: DIGITIZED CONTOURS
a) before and b) after alignment.
Contours are aligned by marking corresponding landmarks on
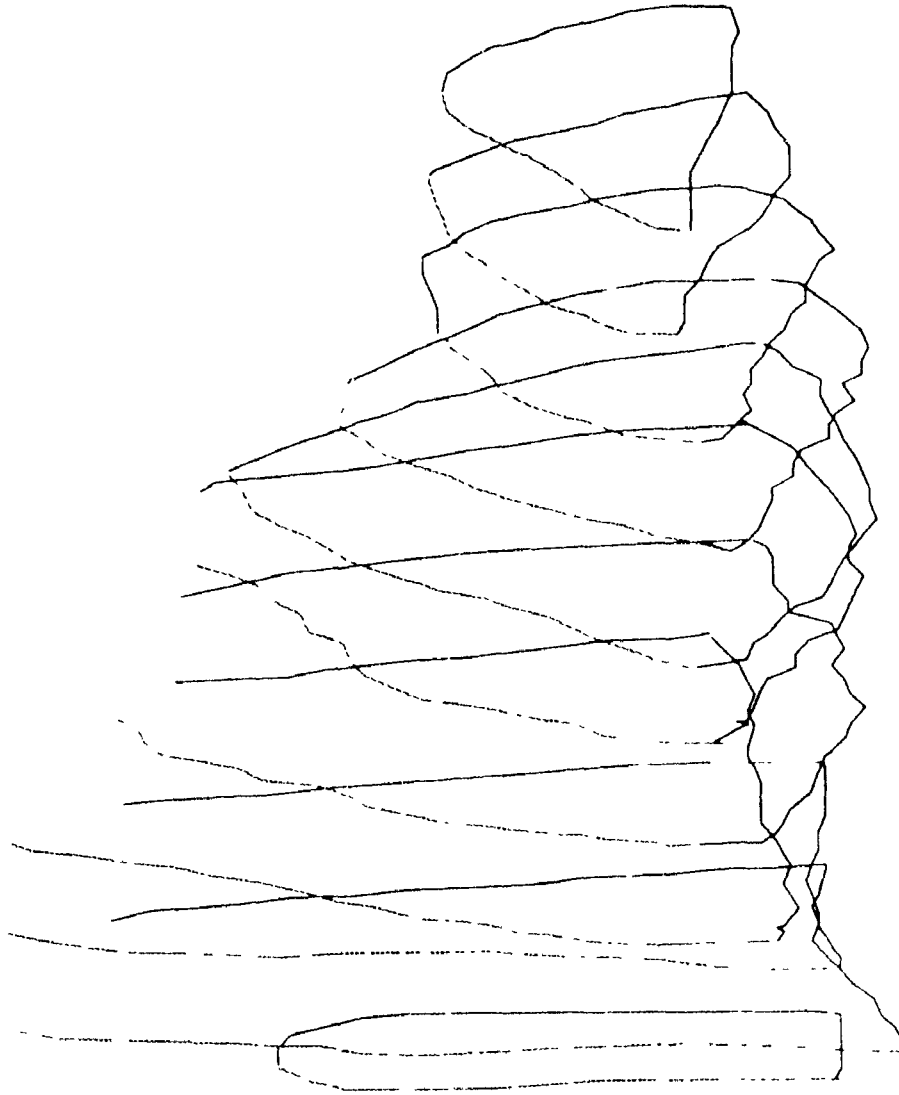consecutive slides and aligning accordingly.

FIGURE 5.4: DIGITIZED CONTOURS
OF THE LATERAL BUNDLE OF THE POSTERIOR INCUDAL LIGAMENT.
The incus/ligament boundary is at the left of the figure. The
middle-ear wall/ligament boundary is at the right of the figure.

The surface-point definition files may be processed using a surface-reconstruction program, TR3, developed in this lab. This program works by triangulating between boundary nodes on consecutive digitized contours (Funnell 1984a, 1984b). Thus the surface of structures of interest may be reconstructed.

Another program developed in this lab, SMF, has the ability to display triangular-face representations of middle-ear structures from either surface triangulations produced by TR3 or from triangular-face representations of the final tetrahedral meshes produced by the mesh generation scheme described in the next chapter. Thus surface reconstructions or meshes of middle-ear structures can be easily displayed and examined. The program has the ability to rotate these triangular face representations so that a structure of interest may examined from many perspectives. Structures can be displayed with shading in a desired colour scheme on a VAXStation or other graphics display. A 'cut' may be made through an object and faces in front of that cut may be removed. These reconstructions may also be displayed in black and white on a hard copy. Figure 5.5 is a three-dimensional surface reconstruction of contours of the lateral bundle of the posterior incudal ligament, the incus and the malleus produced using the program TR3 and displayed using the program SMF. Hard copies of displays or meshes produced by SMF will be presented Chapters 6 and 7.

Once the surface-point definition files have been defined, the next phase of modelling may proceed. The next chapter describes the mesh generation scheme used to transform these surface reconstruction files into a finite-element mesh.
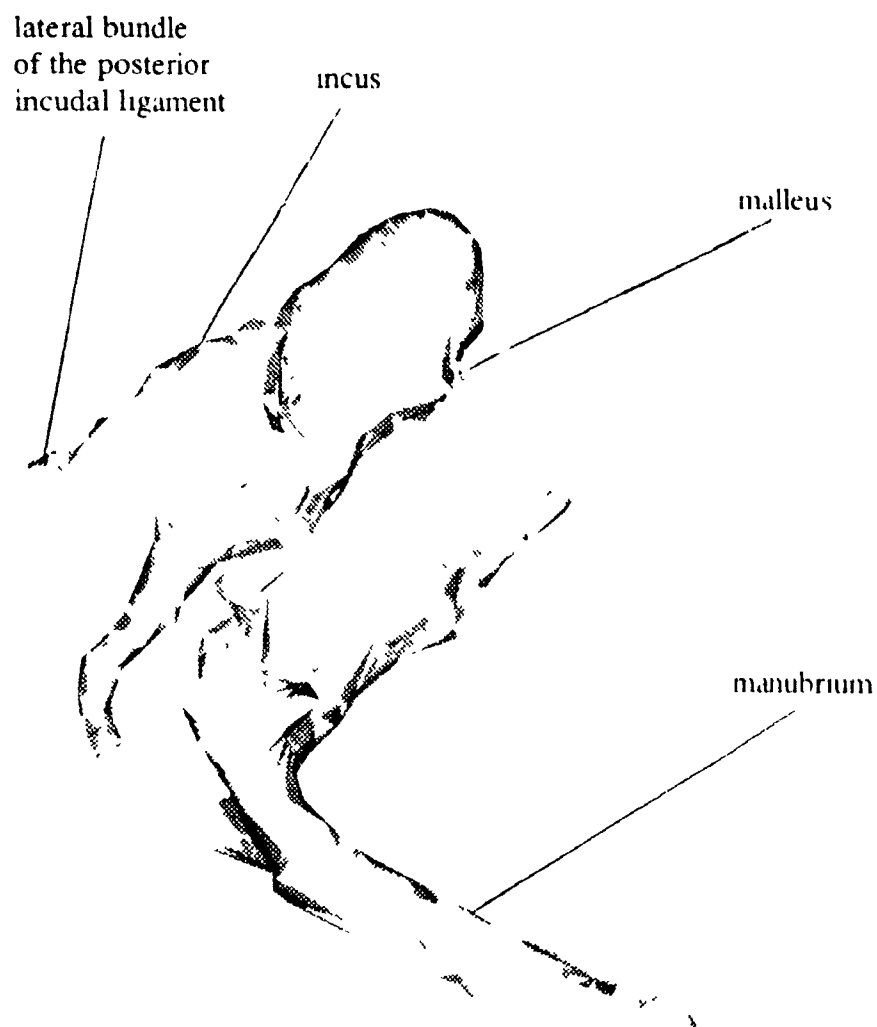
lateral bundle
of the posterior
incudal ligament

incus

malleus

manubrium

FIGURE 5.5: THREE-DIMENSIONAL SURFACE RECONSTRUCTION
of contours of the incus, the malleus and the lateral
bundle of the posterior incudal ligament, produced using
the surface-reconstruction program TR3 and displayed
using the display program SMF.

CHAPTER 6

MESH GENERATION FROM SERIAL SECTIONS

6.1 INTRODUCTION

One of the largest problems in any finite-element modelling scheme is that of mesh generation. Two-dimensional mesh generation of irregular contours is not trivial. The task of creating a mesh of three-dimensional elements is definitely not a simple one.

Many different approaches to three-dimensional mesh generation have been taken (Boubez, 1985, 1986a, 1986b). In interactive techniques, the computer helps to visualize the mesh as it is being created and graphic input devices help to define coordinates. This task is time-consuming and, due to the two-dimensional nature of most graphic devices, is particularly difficult in three-dimensional analysis.

Interpolation mapping techniques involve laying down similar meshes on consecutive two-dimensional contours. These contours all have the same number of nodes and corresponding nodes on consecutive contours are joined by interpolation. Deformation mapping techniques involve generating a regular mesh and deforming it to fit the object. These methods work well for regular geometries. However, since the same number of nodes is generated for each cross section, for irregular geometries nodes become crowded in smaller cross-sections, resulting in an excessive number of narrowly shaped elements. When irregularly shaped cross sections are encountered, bad interpolations are common in interpolation methods, and in deformation methods it may be difficult to find proper mapping functions.

Filling techniques involve defining nodes within an object and

filling the object with elements by generating tetrahedra to surround the nodes. This generation is difficult for irregular shapes. Because a convex hull of the nodes is generated, this method requires much work to handle holes and concavities.

6.2 TOPOLOGICAL METHODS

Topological methods are better suited to meshing irregular contours. They involve cutting tetrahedra away from an object using a library of topological operators. First the surface of the object must be triangulated. A list of faces, edges and vertices, together with information defining their relationships, describes this triangulation.

Most topological methods involve using two main topological operators which each act on an object by removing a tetrahedron. As a tetrahedron is cut away, the edge, vertex and face list must be updated to describe the new shape of the mesh. This is done repeatedly until the list describes only one tetrahedron.

Topological methods are relatively slow as compared to other three-dimensional meshing techniques. However they can generally produce consistent meshes for irregularly shaped objects. A number of topological methods have been developed (Ewing et al. 1970, Mantyla & Kagawa 1983, Woo & Thomasma 1984, Wordenweber 1984).

The mesh generation technique used to create meshes for the middle ear will be one designed and initially developed by Bouhez (1986b). This generator was developed specifically with anatomical structures in mind. Serial histological sections are commonly used to study anatomical structures in the life sciences and thus are an obvious tool to be exploited when describing the geometry of such structures. A mesh generation technique which can build meshes from serial section data

would have applications in many areas in the life sciences and elsewhere.

This mesh generator originally consisted of a series of programs capable of reading specific serial section data and generating a mesh of tetrahedral elements from a slice of an 'irregularly' shaped object. A slice of an object is that part of an object defined by two consecutive two-dimensional contours. This generator was tested by Boubez on fairly simple irregular shapes, using relatively low mesh resolutions, and had never been used for any finite-element analysis.

A major portion of the work done for this master's thesis involved continued development and testing of this generator. This work involved streamlining and debugging it, adding and improving graphical displays to help the user monitor its progress, testing and enhancing it to enable it to be used for more general irregularly shaped multi-sliced objects, and automating it into one master program. This chapter describes the philosophy behind the generator and outlines some of the additional work performed on it.

## 6.3 THE MESH GENERATOR

6.3.1 Philosophy

The philosophy behind the mesh generator is described in detail in Boubez (1986b). The following section summarizes this description.

Two dimensional closed contours input from each histological slide are triangulated as follows. Equidistant nodes are created on the contour, spaced according to the mesh resolution required. The contour is superimposed on a grid of equilateral triangles and all internal grid nodes that are positioned at least a certain minimum distance from the contour boundary are kept, forming a regular two-dimensional core of

triangles as shown in Figure 6.1a. Internal grid nodes that are too close to the contour boundary are discarded so as to avoid small elements in the outer ring in the subsequent triangulation of that ring. The triangulation is performed by joining nodes on the core boundary to nodes on the contour boundary as illustrated in Figure 6.1b. The triangulation algorithm identifies all external edges on the inner core of triangles by inspecting a list of edges making up the internal core triangles and discarding those that occur twice. The nodes on this boundary are numbered in increasing order in a counterclockwise direction. All edges on the external boundary are also identified and numbered in a counterclockwise direction. The first step in the triangulation is to join the two initial nodes on the inner and outer boundary. These nodes are the larger nodes shown in Figure 6.1b. The next line of the triangulation is the shortest line that can be drawn from either of the first two nodes to the second node on the opposite boundary. The algorithm proceeds around the two-dimensional ring until the triangulation is complete. This triangulation is done for each two-dimensional contour of the structure of interest.

Next, consecutive two-dimensional contours are overlaid. Corresponding nodes on overlapping two-dimensional cores are joined as shown in Figure 6.1c and the resulting three-dimensional core of right-angled prisms, illustrated in Figure 6.2, is shredded into tetrahedra using a lookup table. The remaining areas of each two-dimensional contour are used to generate a ring.
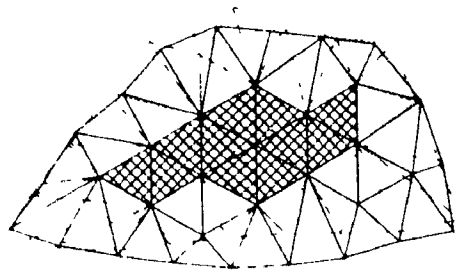
The outer and inner edges of this ring are triangulated as shown in Figure 6.2. The main work of the mesh generator is to mesh this ring of each slice of the structure until the entire structural mesh is created. It meshes a ring by repeatedly cutting away tetrahedra until
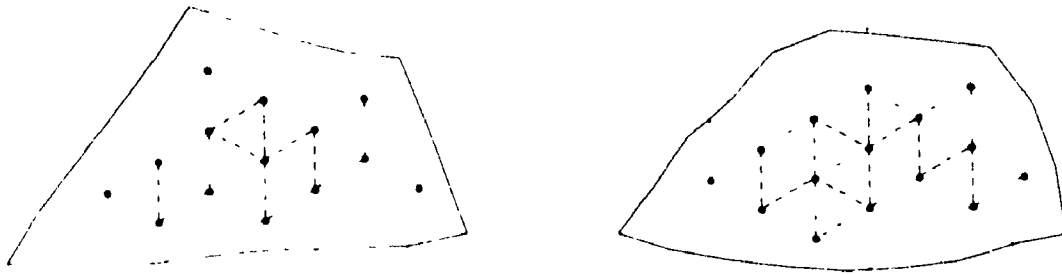
a) Two-dimensional cores of triangles.
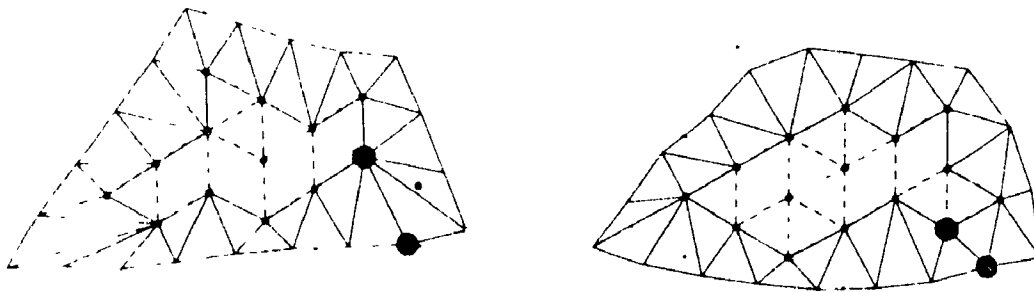
b) Full triangulation of two-dimensional contours.

c) Resulting overlap of two-dimensional cores.

FIGURE 6.1: TWO-DIMENSIONAL CORE AND RING TRIANGULATIONS
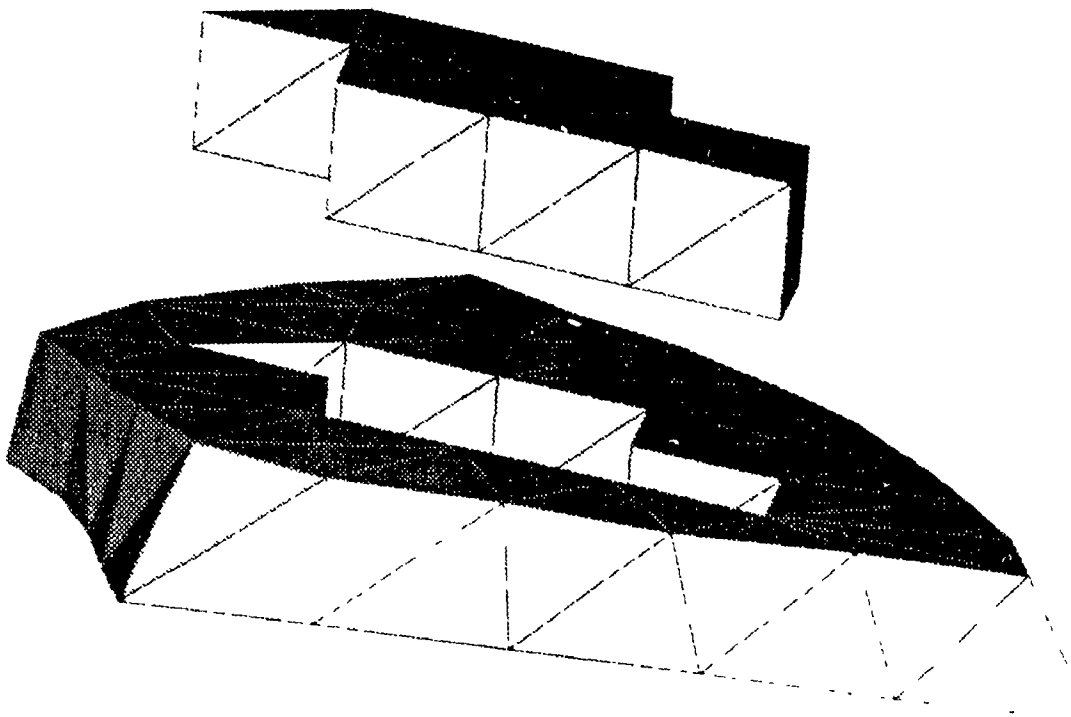AND RESULTING CORE OVERLAP.

FIGURE 6.2: THREE-DIMENSIONAL CORE AND RING
of two consecutive two-dimensional contours of the lateral
bundle of the posterior incudal ligament.

only one tetrahedron is left. As mentioned, this cutting away is done by deleting appropriate edges, faces and vertices from the list describing the structure until the list describes only one tetrahedron. The meshed structure built up is described by a list of tetrahedra. Each tetrahedron is described by twelve nodal coordinates grouped in threes, each group representing one face of the tetrahedron. This descriptive format is used by the display program SMF (see section 5.4.3) to display any stage of the mesh generation procedure.

The meshing is done using four operators. The first two operators are the two cutting operators referred to earlier (see section 6.2) and are illustrated in Figure 6.3a and 6.3b. The vertex operator T1 locates a trivalent convex vertex and removes the tetrahedron attached to it in one cut. Usually the T1 operator is used repeatedly until no suitable vertex can be found (i.e. all tetrahedra protruding from the ring are cut off). Next the edge operator T2 is used. A starting edge number is given to it and it proceeds through the list of edges in the ring until it locates a convex edge. It removes the tetrahedron attached to this edge in two cuts. The vertex operator T1 is then reused to cut off protruding tetrahedra. If after a number of cuts neither T1 or T2 can be used, a third operator, the topological cut operator, is employed. This operator makes a cut through a triangular cross-section of the ring, thus producing two new triangular faces. The first cut of the ring produces one polyhedron. Each successive cut produces another polyhedron as illustrated in Figure 6.3c.

Using these operators it is possible to reach a situation where a tetrahedron cannot be cut away from any of the polyhedra created. Such a situation is illustrated in Figure 6.4a. The simple solution to this problem is to flip a diagonal on a side of a polyhedron as shown in the
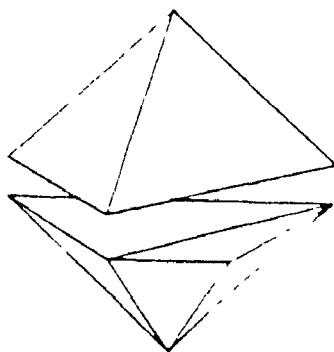
a) The vertex operator locates a trivalent convex vertex and removes the tetrahedron attached to it in one cut.
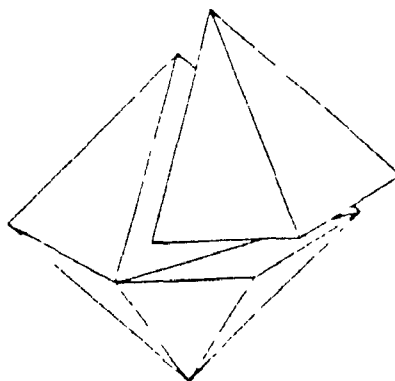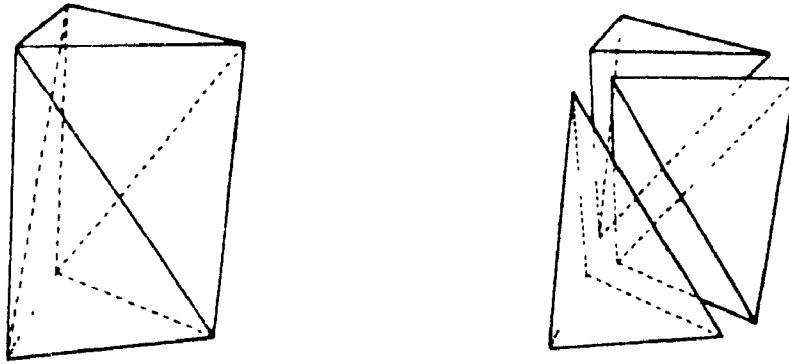

b) The edge operator locates a convex edge and removes the tetrahedron attached to it in two cuts.
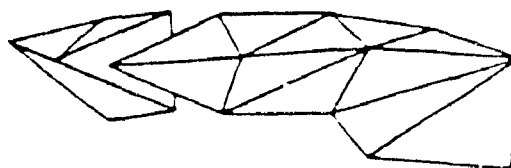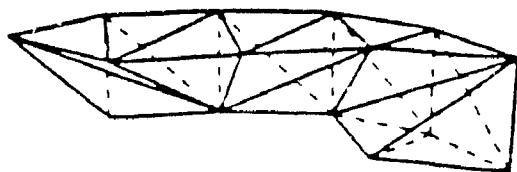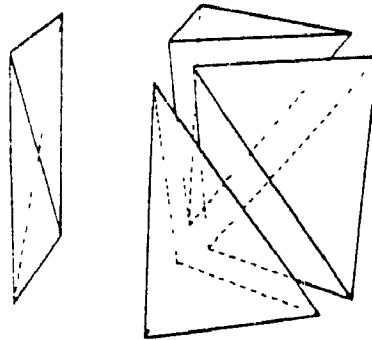

c) A topological cut is performed on a polyhedron, dividing it into two separate polyhedra.

FIGURE 6.3: THE VERTEX, EDGE and CUT TOPOLOGICAL OPERATORS
(After Boubez, 1986b)

a) No tetrahedron can be cut away from this polyhedron until one of its diagonals is flipped.

b) If the flipped diagonal is not on the outside surface of the mesh a 'flat' tetrahedron is created.
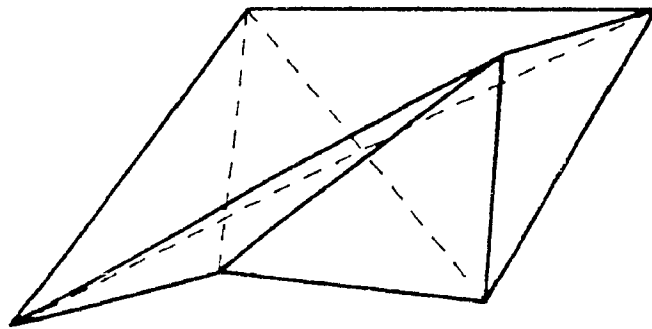
c) No diagonal can be flipped on this polyhedron and thus it cannot be meshed.

FIGURE 6.4: EXAMPLES OF DIFFICULT POLYHEDRA
a) flipping a diagonal. b) creating a flat tetrahedron and
c) encountering an unmeshable polyhedron. (After Boubez, 1986b)

figure. The two faces attached to the diagonal in question must be
planar if the geometry of the polyhedron is to be preserved upon
flipping. The polyhedron side must be an exterior side of the ring in
question and must not be a side that will later be part of a boundary
with another mesh. If this is not the case, the flip is topologically
unacceptable, since adjacent finite elements will have intersecting
edges and faces. In this case, a 'flat' tetrahedron is created, as shown
in Figure 6.4b. This flat tetrahedron operator, T2P, is an operator
unique to this mesh generator.

The presence of this flat tetrahedron preserves the correctness of
the mesh, but it is useless as a finite element. However, at the end of
the mesh generation process, after all cores and rings of all slices
have been meshed and assembled, the mesh is 'relaxed'. This is done by
moving every node in the mesh to a more suitable position. This more
suitable position is, in the case of the mesh generator, the geometric
centre of all nodes attached to the node in question. In this manner the
flat tetrahedron will be 'inflated'. It should be noted that only nodes
not defining the surface of a structure may be moved, otherwise the
shape of the structure would change.

The relaxation is done not only to inflate flat tetrahedra but also
to ensure that tetrahedra in the mesh have high aspect ratios. The
aspect ratio is a measure of how equilateral a tetrahedron is. A flat
tetrahedron has an aspect ratio of zero while a tetrahedron with all
internal solid angles equal has a ratio of unity. Tetrahedra with high
aspect ratios are desired in finite element analysis. This is because,
if the aspect ratio of a tetrahedron is small, the tetrahedron is narrow
(i.e. some of its vertices have low solid angles) and some of its edges
are longer than those of a more equilateral tetrahedron. The

displacement assumptions associated with these longer edges will not reflect the true displacement field as well as will those associated with shorter edges. This problem is equivalent to the problem associated with having larger elements in a mesh. Furthermore, tetrahedra with low aspect ratios contribute to errors in the computer solution in finite element analysis; this problem will be discussed in section 7.2.2.

The relaxation procedure may be visualized by imagining an assembly of springs constrained by an external surface. The relaxed mesh is equivalent to the equilibrium position of the spring assembly given the external shape constraints.

Unfortunately, it is possible to reach a situation where a diagonal cannot be flipped to produce a polyhedron capable of being meshed. This situation is illustrated in Figure 6.4c. In this case the meshing of the ring must be restarted. Usually, by giving the edge operator a new starting edge number, a successful mesh is created. However it is possible that no starting edge can be found to generate a successful mesh.

6.4 IMPROVEMENTS TO THE MESH GENERATOR

6.4.1 Introduction

Previously the mesh generator consisted of a series of separate programs. One program performed input and triangulation of the two-dimensional contours input in a very specific form. Another program built the slice core while a third built the slice ring. A fourth program meshed the structure while a fifth assembled slices and relaxed the structure. Input and output from each program had to be verified manually to ensure the meshing procedure produced a topologically correct mesh. The final output was a list of vertex coordinates of each

tetrahedron, in a form readable by the display program SMF but not suitable for input to the finite-element program. Meshing a structure was fairly cumbersome, especially when many slices were involved.

A number of procedural problems with the generator were corrected and all programs required for the mesh generation process were unified under one master program so that the mesh generator can now be run with no user interaction. The input routines were generalized to handle input from any file containing the point definitions of consecutive two-dimensional contours. The output routines were modified so that a file was generated that contained a list of node numbers and their coordinates, and a list of elements defined by their node numbers. This file was used by the finite-element program. Graphical displays were improved to better monitor the progress of the generator and the improved display program SMF helped to identify a number of meshing procedural problems.

Figure 6.5 is a flow chart of the automated master program TR4F. The triangulation subroutine TR42D is called once and is responsible for triangulating all two-dimensional contours making up the object under study. The master program then enters a loop where each slice (adjacent pair of two dimensional contours) is processed. Subroutine TETRA is responsible for joining overlapping two-dimensional cores and shredding the resulting prisms into tetrahedra. Subroutine RING performs the surface triangulation of the inner and outer edges of ring. Once the cores and rings of all slices have been formed, the program enters a loop where subroutine STRUCT then meshes the ring of each slice.

Subroutine GLOBAL is called after all slices have been processed. It assembles the meshed slices and performs the mesh relaxation. This relaxation must be carried out while ensuring the aspect ratio of all
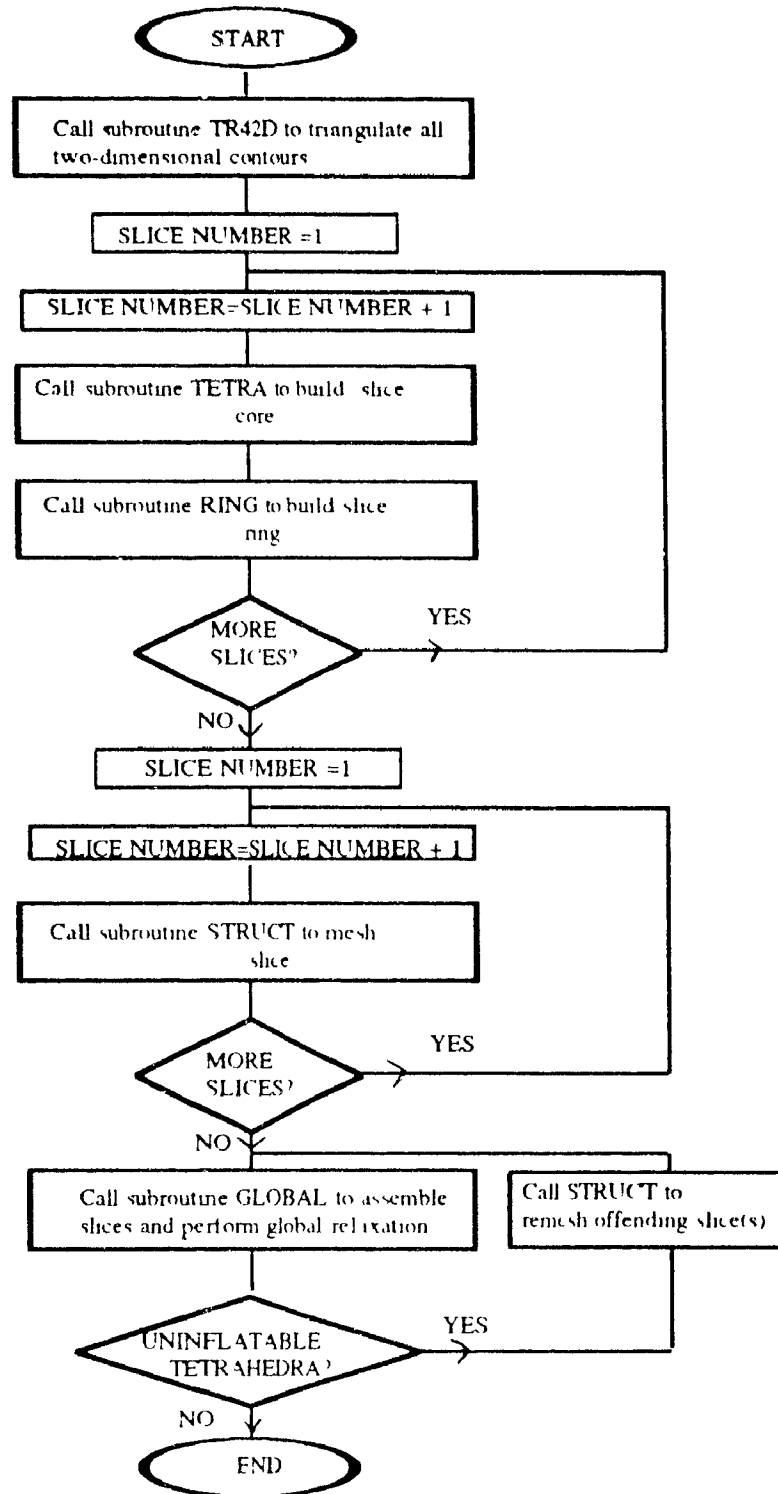
FIGURE 6.5: LOGIC OF THE MESH GENERATION PROGRAM TR4F

tetrahedra remain above a certain value. While testing the generator, it was found that some flat tetrahedra could not be inflated to an acceptable aspect ratio (as will be explained in section 6.4.6). If this occurs then the slice containing the offending tetrahedron is remeshed and the relaxation is redone. Finally, when a successful relaxation occurs the mesh is written to a file.

There were a number of serious procedural problems that only surfaced when meshing more complicated structures. The following sections describe a sample of them.

6.4.2 Slice Triangulation - TR42D

One of the problems encountered in this subroutine was that contours were read without being oriented (numbered) in the proper direction. They were assumed to be numbered in the same direction. This caused problems when subroutine RING tried to triangulate the outside surface of a slice. That surface is discretized by triangulating between consecutive two-dimensional contours (rather than between inner and outer contours as was the case for the triangulation of the two-dimensional ring.) If the nodes were not numbered in the same direction on adjacent contours, the triangulation algorithm tried to join a node on one side of the object on one contour with a node on the opposite side of the object on the next contour. This violated the geometry of the mesh. All contours are now forced to be counterclockwise as they are read in.

6.4.3 Building the Core - TETRA

The program previously could not handle the case where no matching two-dimensional elements were found (i.e. no core existed) and thus

code was added to handle this case.

6.4.4 Building the Ring - RING

One of the most serious problems with the generator was that the orientation of element faces was not consistent. Orientation of element faces determines how the nodes of tetrahedra are numbered. Proper node numbering is crucial in finite-element analysis. Calculations of the volumes of elements are meaningless if the numbering of nodes in an element is not consistent throughout a mesh. Proper assembly of these element matrices is impossible. The convention described in the original mesh generator documentation specified that all four faces in every tetrahedron must be oriented so that, using the right-hand rule, the vectors normal to the faces pointed outward from the tetrahedron.

One of the areas where the orientation problem manifested itself was in subroutine RING which is responsible for forming the outer ring of the object. To do this the list of faces making up tetrahedra in the core was examined. In this list of faces making up the core, faces on the outer edge of the core will be listed once while inner core tetrahedron faces will be listed twice (since adjacent tetrahedra share faces). By searching for faces occurring only once in the list, the inner face of the ring can be defined. Before using these faces to build the ring they must first have their orientations flipped so that, instead of having their normals pointing away from the core, they have them pointing away from the ring. This was not being done and was thus corrected. This was important because later in the subroutine all faces of the ring were being oriented using these inner ring faces as a reference.

This orientation procedure itself was being performed incorrectly.

The top and bottom faces of the ring should have been oriented by noting the orientations of adjoining inner ring faces attached to them and orienting accordingly. External faces could then be oriented by noting the orientation of adjoining top or bottom faces. However, due to a programming error the bottom faces were being oriented in the wrong direction. The orientation algorithm was corrected.

Another problem encountered in the generator was that the marking of different classes of faces was incorrect. Nodes of faces on the exterior of the object had to be marked as fixed in order not to be displaced during relaxation. Due to a programming error, nodes were assigned the wrong markers and thus the relaxation was proceeding incorrectly.

6.4.5 Meshing the Ring - STRUCT

The most complicated and time-consuming subroutine is STRUCT which performs the actual meshing of the ring. A large number of problems were encountered in this routine. Many different checks had to be made in the generator to make sure that edges and faces did not cross as the structure was being meshed. Due to the difficulty in performing these checks in three dimensions, geometrically inconsistent tetrahedra were sometimes being produced. No independent verification of the mesh was being performed. To ensure geometric consistency, as every tetrahedron was cut, a new check was made to ensure that its volume was positive and that all four faces were oriented correctly. This not only eliminated incorrectly oriented tetrahedra but also tetrahedra that had very small, near-zero volumes. This meant that zero-volume tetrahedra could only be generated by using the flat-tetrahedron topological operator T2P. Unnecessary zero-volume tetrahedra were thus avoided.

Another serious procedural problem was that writing of tetrahedra to file was being incorrectly performed. For instance, in the original algorithm, a check was made before every topological cut to see if the number of polyhedra left in the ring was four times the number of vertices left. This would indicate that all remaining polyhedra are simple tetrahedra and that the meshing is complete. This check was being made but only one of the remaining tetrahedra was being written to file, thus producing an incomplete mesh.

A problem occurred while flipping diagonals. When doing this, care has to be taken to ensure that the diagonal was not generated outside an enclosing quadrilateral. This occurs if two narrow faces join at an angle as illustrated in Figure 6.6.

Previously, when performing a cut with either the vertex operator T1 or the edge operator T2, a check was made to ensure that the aspect ratio of the tetrahedron formed was above a certain limit. This check was made if more than two of the faces of the tetrahedron were faces on the external boundary of the structure. This was done for quality-related reasons since no nodes of these tetrahedra could be relaxed.

It was found necessary, however, to force *all* tetrahedra in the mesh to have an aspect-ratio lower limit. If tetrahedra with very low aspect ratios are allowed in the mesh-generation process, polyhedra that have very low solid angles result. The mesh generator builds itself into a corner because these low solid angle polyhedra tend to be impossible to mesh.

6.4.6 Assembling the Slices and Relaxing the Mesh - GLOBAL

Previously the relaxation algorithm had been tested on small meshes where zero-volume tetrahedra were inflated without problem. The original

original
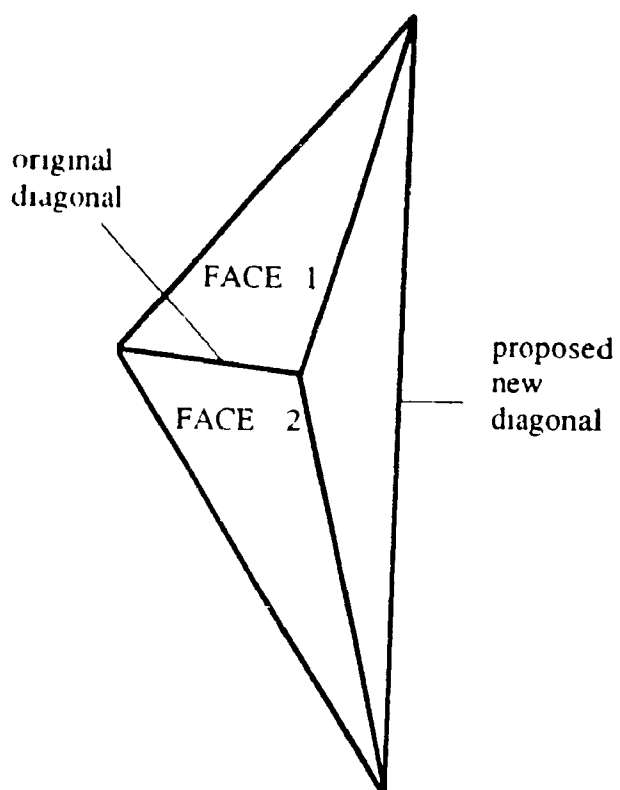diagonal

FACE 1

proposed
new
diagonal

FACE 2

FIGURE 6.6: AN EXAMPLE OF A DIAGONAL BEING GENERATED OUTSIDE
AN ENCLOSING QUADRILATERAL.

relaxation algorithm attempted only to move nodes to the geometric centre of surrounding nodes. This was done using an iterative scheme. An attempt was made on each iteration to move every node in the mesh to the geometric centre of surrounding nodes. This attempt was successful if the move did not violate the kernel of the node in question. (The kernel is defined as the volume within which a node can move such that adjoining edges do not cross each other.) If the kernel was violated, an attempt was made then to move the node halfway to the geometric centre. If for this attempted move the kernel was still violated, the distance to be moved was successively halved until the proposed distance fell below a certain tolerance. This relaxation procedure was repeated every iteration until the maximum acceptable move of all nodes in the mesh fell below a certain lower limit.

To relax more complicated multi-sliced meshes a number of changes were made. If no move as described above could be accomplished while trying to inflate a flat tetrahedron this presented a problem, as inflation was essential. (No move was possible when the geometric centre lay on the side of the tetrahedron opposite to the node in question.) This problem was corrected by moving the node away from the geometric centre, in the opposite direction, as illustrated in Figure 6.7. Unfortunately, it sometimes happens that any nodal movement violates its associated kernel. If flat tetrahedra cannot be inflated, the offending slice is remeshed, the new mesh is reassembled and the relaxation is redone.

Care had to be taken when reshaping any tetrahedron, flat or not, that in moving a node no tetrahedron was reflattened, or alternatively that all tetrahedra retained a certain minimum aspect ratio. If a proposed move caused the aspect ratio of a tetrahedron to fall below an
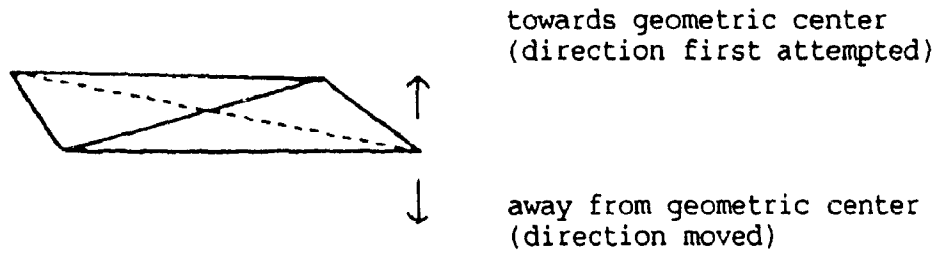
towards geometric center
(direction first attempted)

away from geometric center
(direction moved)

FIGURE 6.7: INFLATION OF A FLAT TETRAHEDRON
A flat tetrahedron cannot be inflated by moving a
node to the geometric center of all nodes surrounding
it because opposing diagonals would cross. The node is moved
in a direction opposite to that originally attempted.

acceptable lower limit, the move was not made.

Finally, a volume calculation and orientation check is made on each tetrahedron in the mesh after relaxation. Additionally, the volume of all tetrahedra is totalled and checked against the object volume. These checks ensure that the final mesh is correctly oriented and complete.

CHAPTER 7

PRELIMINARY MODEL TESTS AND RESULTS

7.1 INTRODUCTION

The only structure in the middle ear analysed so far is the lateral bundle of the posterior incudal ligament. A preliminary static analysis of this structure has been done. This chapter describes how this analysis was carried out. The results of this analysis give an indication of how well the tools developed and tested during the course of this research are suited for the modelling of the middle-ear ossicles and soft tissues.

7.2 DETERMINATION OF APPROPRIATE MESH RESOLUTION

7.2.1 Introduction

The accuracy and efficiency of any finite-element analysis relies on the appropriateness of the mesh resolution used when discretizing the structure of interest. In general, as the mesh resolution used to model a continuum increases, the displacement solutions will converge toward the true displacements. However, as the size of the elements in a mesh decreases (and the number of elements increases), the number of degrees of freedom increases. This increases the size of the global stiffness and load matrices and thus the time and resources required for computer analysis. An optimal resolution is the lowest resolution possible such that the displacement trial functions model the domain to the required accuracy.

To determine a reasonable resolution in an analysis, the convergence of nodal displacements in a structure, in response to a

given loading condition, as a function of mesh resolution must be determined. A number of tests should be made of meshes of successively finer resolutions until the differences in displacements are considered insignificant.

7.2.2 Error Analysis

Before determining the optimal mesh resolution for a finite-element analysis it is important to understand possible sources of error in the analysis.

One possible source of error is in the evaluation of element force and stiffness matrices using numerical integration. This is unimportant in the present analysis because for the true tetrahedral element used, integration of the element stiffness matrices is exact (see section 4.3.4, equation 4.24). In addition, only concentrated forces will be applied in the analyses presented in this chapter and thus no integrations are required to produce load matrices either. (For the collapsed-brick tetrahedral element, numerical integration is required for the element stiffness matrix. However, because linear elements are used this integration produces exact results, and this explains why analysis using this element produces the same results as analysis using the true tetrahedral element.)

Two sources of error may occur due to the use of meshes with non-equilateral (non-unity aspect-ratio) tetrahedra. The first was mentioned in Chapter 6, i.e. the linear displacements assumed by the shorter edges in the equilateral tetrahedron can better model the true displacements of a structure than can those assumed by the longer edges found in the low-aspect-ratio tetrahedron. Thus, given two meshes with the same average edge length, the mesh with the higher average aspect

ratio will be better able to model the true displacements of the structure.

The second source of error resulting from meshes with nonequilateral tetrahedra arises in the setting up of the finite-element equations and their solutions. This is because a computer with a finite number of digits to work with is being used. The errors arise because in the global stiffness matrices **K** for these meshes entries K_{ij} of tetrahedra with widely differing aspect ratios will be of widely varying values.

If the magnitudes of elements in the global stiffness matrix **K** differ greatly, an entry in **K** with a large magnitude will be represented with much more percentage accuracy than will an entry with a small magnitude, when performing adding or subtracting operations. Also, if diagonals of **K** differ greatly in magnitude then in the Gauss-Jordan elimination procedure used to solve the global stiffness equation (4.27), errors will arise. This is because in this elimination procedure, a multiple of an entry in one row is subtracted from a unmultiplied entry of another. Large multipliers occur if rows with widely varying diagonals (which determine the multiplication factor) are subtracted. Rounding off or truncating in this subtraction could cause large errors. A well-conditioned global stiffness matrix **K** (one where all entries are of similar magnitude) is desired in finite-element analysis. It should be noted that this error is magnified if meshes with nonhomogeneous material properties are analysed. If two elements have considerably different aspect ratios *and* different material properties the differing values of entries in their element stiffness matrices may lead to an even more ill-conditioned global stiffness matrix.

A number of methods exist to estimate the error in a solution due

to the finite precision on the computer. Because of these errors an approximate solution displacement matrix $\tilde{U}$ is being calculated and not the true solution matrix U. The difference between the actual load matrix and the product of the stiffness matrix and the resulting approximate displacement matrix may be calculated and is the residual, ΔR:

$$\Delta R = R - K\tilde{U} . \qquad (7.1)$$

The actual error in the displacement, r $(= U - \tilde{U})$ can be found by replacing R by KU, and is

$$r = K^{-1} \Delta R. \qquad (7.2)$$

Another method of estimating error is to determine the condition number of the matrix K. Because of computer error, the actual equation being solved is

$$R = (K + \delta K)(U + \delta U) \qquad (7.3)$$

Considering this equation, it may be shown (Bathe, 1982, pp. 485-486) that in the final solution the displacements will be accurate to s significant digits where

$$s \geq t - \log_{10}(\text{cond}(K)) \qquad (7.4)$$

where t is the number of digits of precision of the computer. The condition number is $\text{cond}(K) = \lambda_n^u / \lambda_n^1$ where λ_n^u is an upper bound for the

eigenvalues of the global stiffness matrix K and λ_n^1 is a lower bound.

Considering (7.1) and (7.2), it is possible that the residual ΔR may be small while the error in the solution, r, is large. A small residual is thus a necessary but not sufficient requirement for an accurate solution. Generally the condition number is much more important than the residual in analysing error (Cook 1981, Bathe 1982).

7.2.3 Tests

Preliminary tests were carried out to determine the resolution required for modelling. The tests involved shredding a regular block into a set of meshes of differing resolutions. This block had similar dimensions to the posterior incudal ligament, but because it was of regular geometry an analytical solution for a given load condition could be calculated. The test involved imposing boundary conditions on the block similar to those occurring for the posterior incudal ligament in the middle ear. The convergence of the finite-element solution towards the analytical solution, as a function of mesh resolution, was observed.

The procedure for the test was as follows. A block of dimensions $337\mu m$ x $1000\mu m$ x $421\mu m$ was used. (These are the very approximate average dimensions of the lateral bundle of the posterior incudal ligament.) Using the mesh generator this block was shredded into five different meshes containing 95 (BLOCK1), 144(BLOCK2), 560 (BLOCK3), 740 (BLOCK4) and 1203 (BLOCK5) elements. These meshes are illustrated in Figure 7.1. Figure 7.2 illustrates histograms of the aspect ratios for all meshes before relaxation and for the three highest resolution meshes after relaxation. The relaxation procedure could not increase the average aspect ratio of BLOCK1 (.276) or of BLOCK2 (.242) because no internal nodes are present in these meshes. However, it increased the average
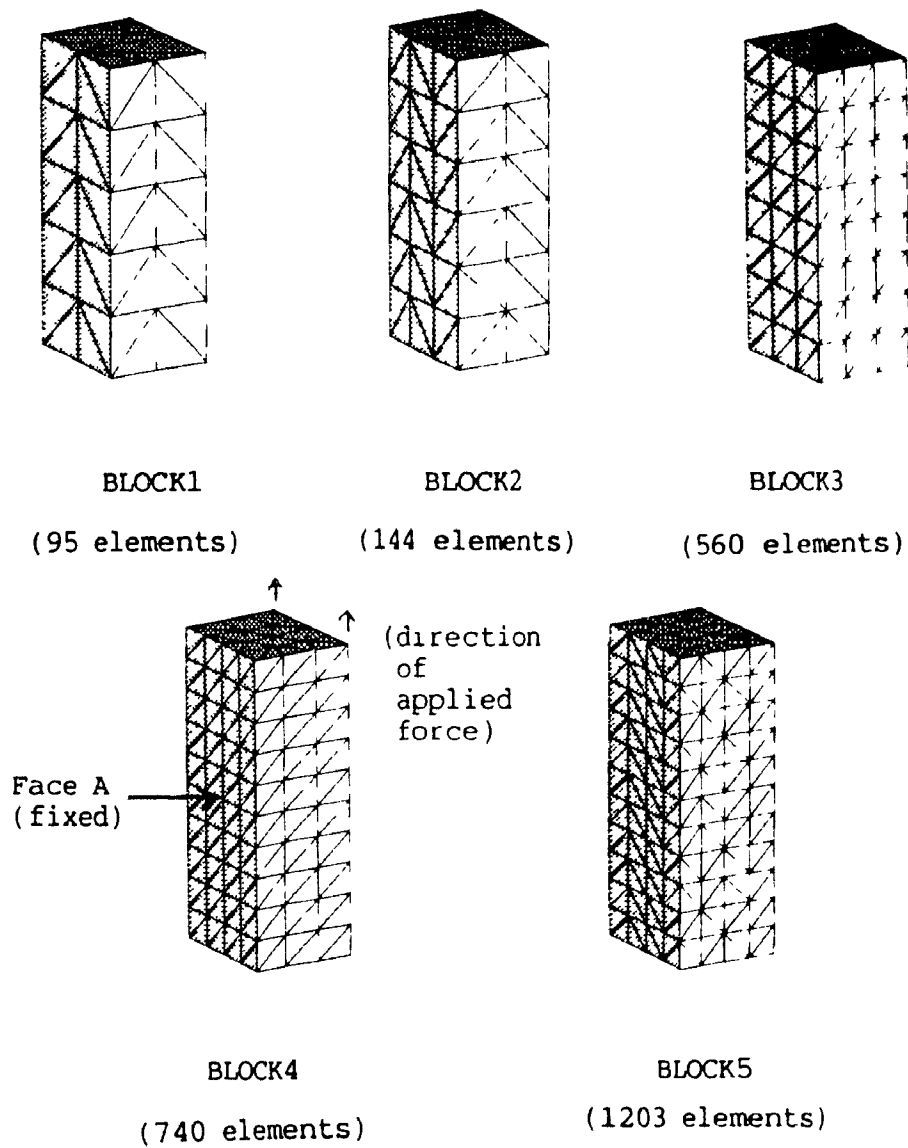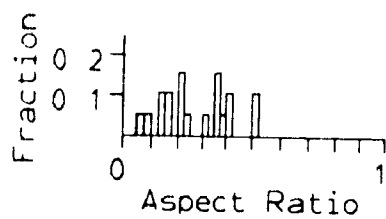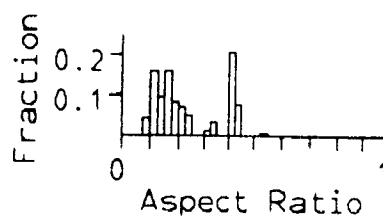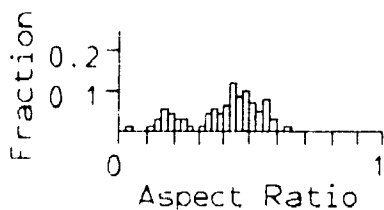
BLOCK1

(95 elements)

BLOCK2

(144 elements)

BLOCK3

(560 elements)

(direction
of
applied
force)

Face A
(fixed)

BLOCK4

(740 elements)

BLOCK5

(1203 elements)

FIGURE 7.1: FIVE MESHES OF THE TEST BLOCK
An upwards shear force is applied to all nodes of face B
(not seen in the figure). All nodes of the face opposite to
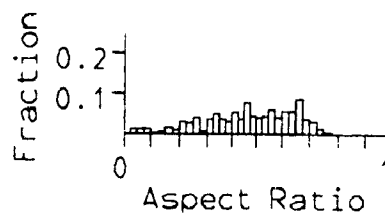face B, face A (seen), are constrained to be fixed.

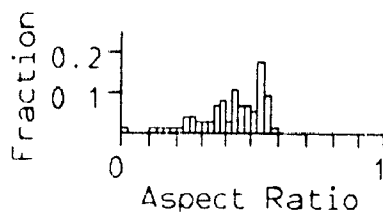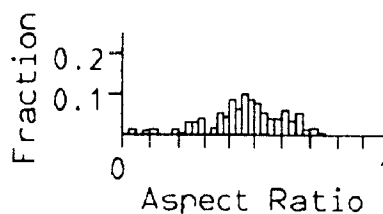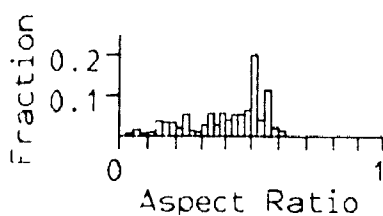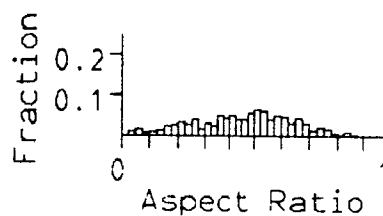**FIGURE 7.2:** ASPECT RATIO HISTOGRAMS FOR FIVE MESH
RESOLUTIONS OF THE TEST BLOCK
BLOCK1 and BLOCK2 could not be relaxed as all nodes of these
meshes are surface nodes. Only one histogram is shown for each
of these meshes. Histograms for both the original and relaxed
state of meshes BLOCK3, BLOCK4 and BLOCK5 are shown.

aspect ratio of BLOCK3 from .397 to .466, of BLOCK4 from .420 to .458 and of BLOCK5 from .404 to .450. The shift is largely due to the relaxation of the inner core tetrahedra, increasing their approximate average aspect ratio from 0.5 to a higher value.

A program FEMODEL was written to apply appropriate boundary conditions to the block. All nodes on one face of the block (face A, seen in the figure) were fixed (constrained to zero displacement) to simulate the fixation of the posterior incudal ligament to the middle-ear wall. An upwards shear force (perpendicular to the plane of the two dimensional contours) was applied to all nodes on the face opposite to face A of the block (face B, not seen in the figure). This shear force was applied to approximate the action of the incus on this ligament. This force was distributed over face B as follows. For each triangular facet of face B the total force to be applied to face B was multiplied by the ratio of the triangular facet area to the total area of face B to give the force to be assigned to that facet. Each node on face B was then given one third of the force assigned to each of the facets attached to it. These concentrated forces were used to directly build the load matrix R.

The geometric and force modelling assumptions for this test are gross oversimplifications of the true situation in the ear. However, they give an initial estimate of the mesh resolution required to model the ligament.

The maximum displacement of the block (Δ) in response to a shear force (P) applied to face B can be calculated by considering the effect of both flexural deformation (Δ_f) and shearing deformation (Δ_s) (Popov, 1976). It is

$$\Delta/P = (\Delta_f + \Delta_{.}) / P$$

$$= \frac{4L^3}{Ebh^3} + \frac{12L(1+\nu)}{5bhE} \qquad (7.5)$$

where E=modulus of elasticity = 2×10^7 N/m^2

ν =Poisson's ratio = 0.3

b=width of block = 421μm

h=height of block = 1000μm

L=length of block = 337μm.

Thus the maximum deformation in the direction of the shear force, per unit applied shear force, should be 143 μm/N. The force application condition in this test is essentially equivalent to fixing a rigid plate to the face of application and applying the shear force to that plate, i.e. nodes on that face do not move relative to each other. However because the force is applied to the finite-element mesh in such a manner that the nodes may move with respect to each other, the nodes on the upper edge of the block should exhibit displacements greater than those calculated analytically and the displacements should decrease for successively lower nodes.

7.2.4 Results

Figure 7.3 illustrates the components in the direction of the applied force of the displacements of all nodes of face B for all five mesh resolutions. These displacements converge close to the analytical solution as expected, indicating that the mesh-generation scheme and the finite-element analysis procedure are suitable for this simple analysis. The displacements do not converge monotonically. BLOCK2 is slightly stiffer than BLOCK1 even though BLOCK2 has a higher mesh resolution.
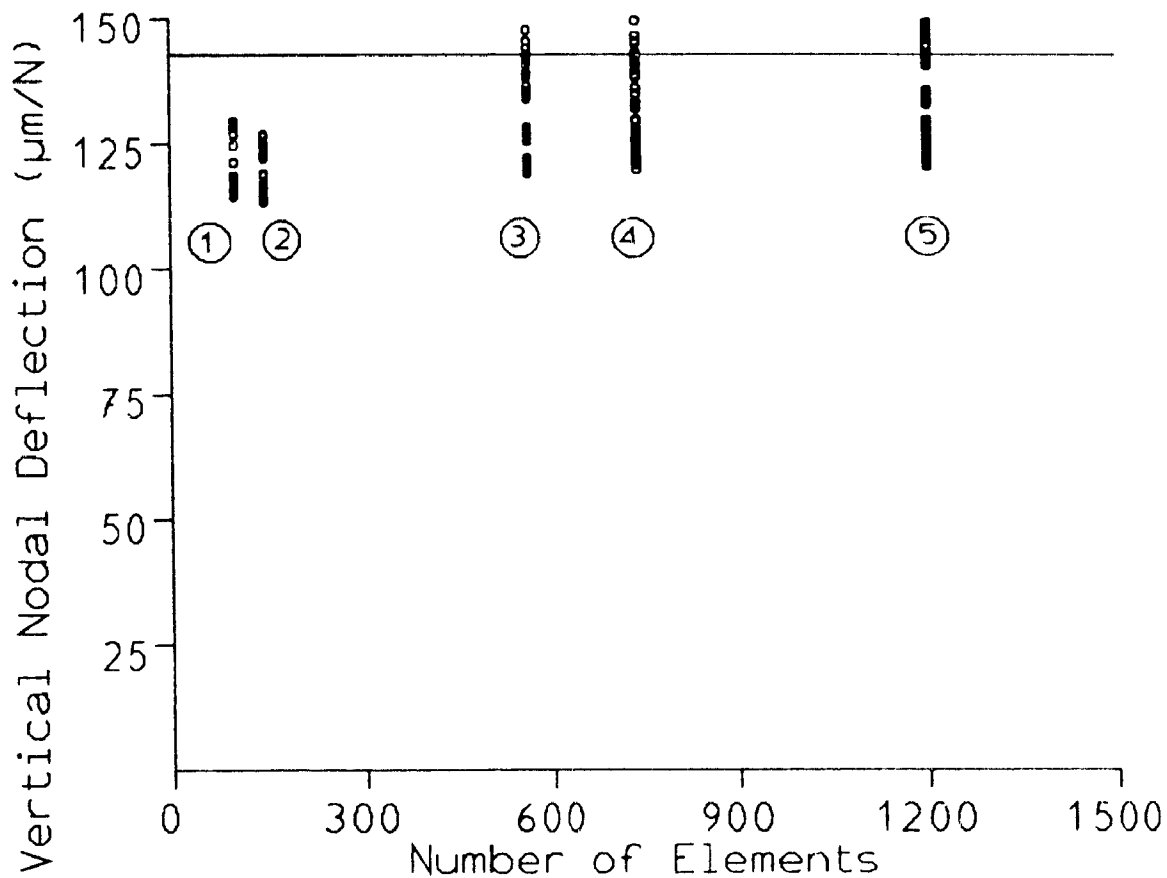
FIGURE 7.3: DISPLACEMENTS OF ALL NODES OF FACE B OF THE
TEST BLOCK FOR ALL FIVE MESH RESOLUTIONS
The displacements plotted are the components of the actual
displacements in the direction of the applied force. The solid
horizontal line at 143 μm/N indicates the analytical solution.

However, BLOCK2 has a lower average aspect ratio and this possibly explains why it is less able to model the true structural displacements.

The residual values for all meshes were found to be practically zero. More importantly, the number of digits of precision for the block meshes was calculated, using equation 7.4, to be 14.0(BMESH1), 13.6(BMESH2), 13.1(BMESH3), 13.1(BMESH4) and 12.5(BMESH5), based on the 16-digit precision of the computer used. This degree of error is insignificant in this analysis.

## 7.3 STATIC ANALYSIS OF THE POSTERIOR INCUDAL LIGAMENT

7.3.1 Tests

Once an idea of the accuracy of results for various mesh resolutions was obtained, a static analysis was done on two meshes of the lateral bundle of the posterior incudal ligament, PILLAT1 (483 elements) and PILLAT2 (992 elements). Figure 7.4 and Figure 7.5 illustrate these meshes. Figure 7.6 shows histograms of the aspect ratios of elements in these meshes before and after relaxation. The average aspect ratio of PILLAT1 increased from .238 to .246 while that for PILLAT2 remained the same (.329). The relatively low average aspect ratio of these meshes as compared to the block meshes results from the fact that many of the slices in the meshes of this ligament have no core. Tetrahedra of coreless slices generally have low aspect ratios.
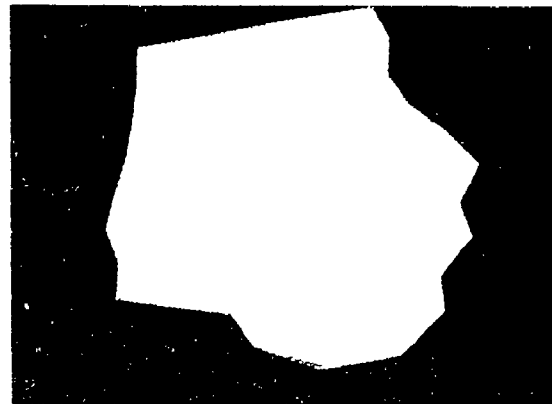
The program FEMODEL applied requested boundary conditions to these meshes. Boundary nodes of these meshes could be identified easily because all two-dimensional contours of the ligament had been digitized in segments as described in section 5.4.2. All nodes on contour segments corresponding to the ligament/middle-ear wall boundary were constrained
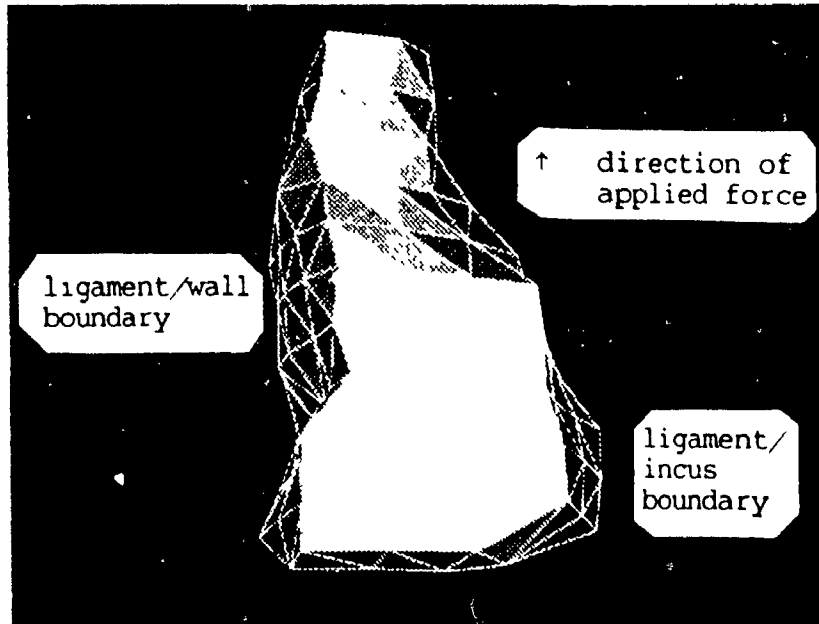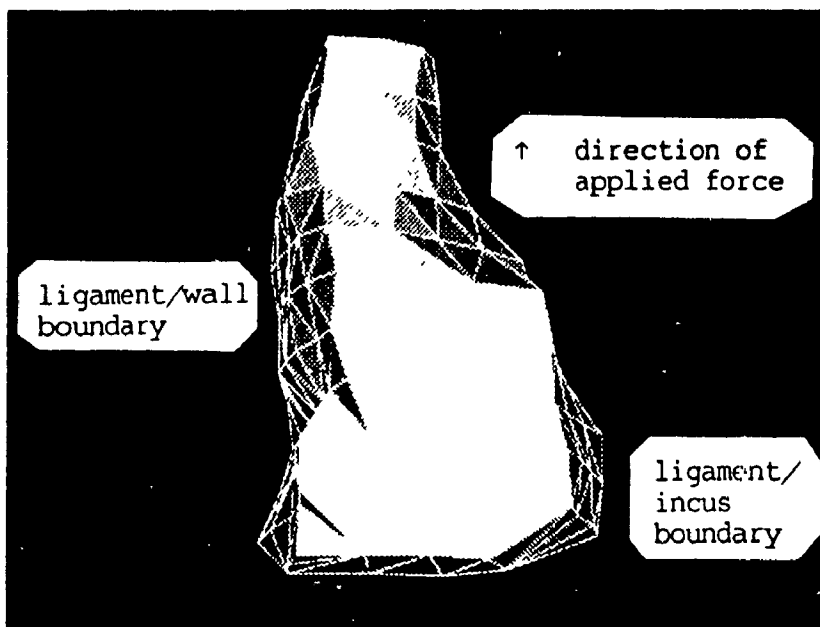
(a)
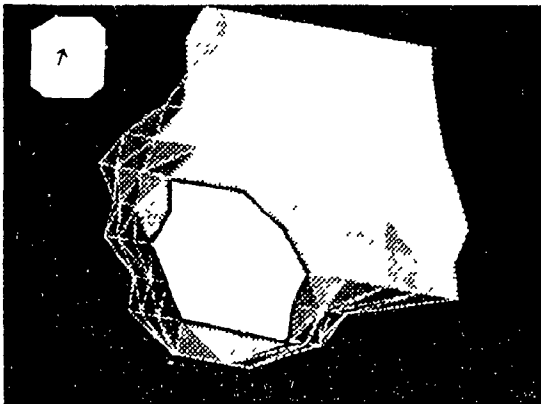
(b)   (c)

FIGURE 7.4: A MESH OF THE LATERAL BUNDLE OF THE
POSTERIOR INCUDAL LIGAMENT (PILLAT1, 483 elements).
Parts of the ligament/middle-ear wall boundary and the
ligament/incus boundary are visible in (a). An upwards force
is applied to all nodes of the ligament/incus boundary, shown
outlined in (b). All nodes of the ligament/middle-ear wall
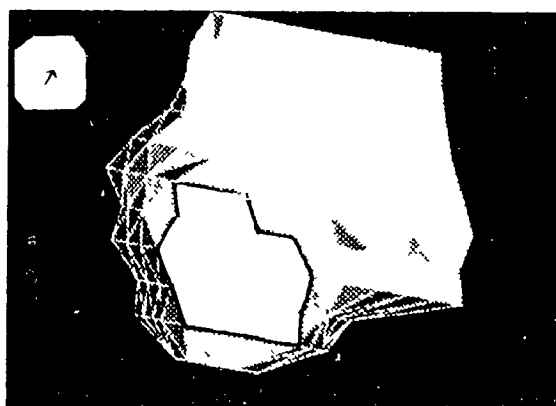boundary, shown in (c), are constrained to be fixed.
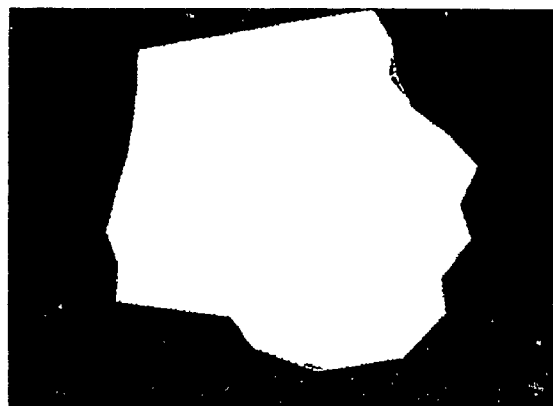
(a)

(b)

(c)

FIGURE 7.5: A MESH OF THE LATERAL BUNDLE OF THE
POSTERIOR INCUDAL LIGAMENT (PILLAT2, 992 elements).
Parts of the ligament/middle-ear wall boundary and the
ligament/incus boundary are visible in (a). An upwards for~e
is appl)ed to all nodes of the ligament/incus boundary, shown
outlined in (b). All nodes of the ligament/middle-ear wall
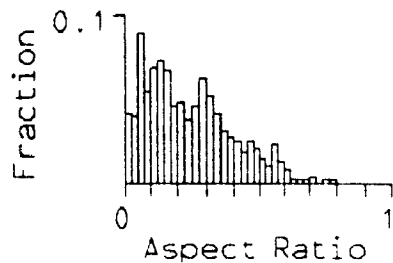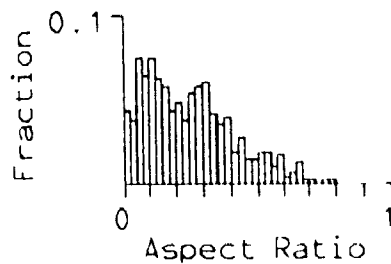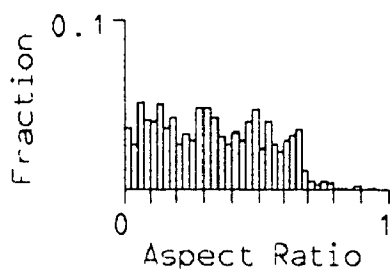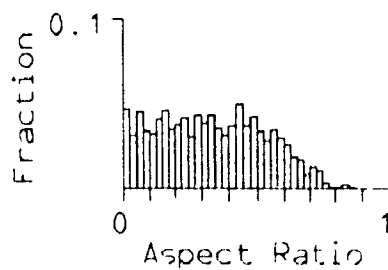boundary, shown in (c), are constrained to be fixed.

FIGURE 7.6: ASPECT RATIO HISTOGRAMS FOR TWO MESH RESOLUTIONS
OF THE LATERAL BUNDLE OF THE POSTERIOR INCUDAL LIGAMENT
Histograms for both the original and relaxed
state of meshes PILLAT1 and PILLAT2 are shown.

to be fixed. All nodes on contour segments corresponding to the ligament/incus boundary had a force applied to them. This force was applied in a direction perpendicular to the plane of the two-dimensional contours (as was the case for the block) and was of the same magnitude as the force applied to the block. The force was distributed over the ligament/incus boundary in the same way as it was applied to the block face. (For each triangular facet of the ligament/incus boundary the total force to be applied to the boundary was multiplied by the ratio of the triangular facet area to the total area of the boundary to give the force to be assigned to that facet. Each node on the boundary was then given one third of the force assigned to each of the facets attached to it.) It should be noted, however, that the facets corresponding to the ligament/incus boundary are not necessarily parallel to the applied force as was the case for the block.

These loading conditions are obviously not the true conditions in the middle ear. In reality, the incus will apply a complicated force to the ligament. Also, in the middle ear the ligament/incus boundary nodes will not be allowed to move freely as in this test case, because they will be constrained by the rigid incus. Boundary conditions will be better modelled in the integrated model of the ossicles and soft tissues.

7.3.2 Results

Figure 7.7 illustrates the components in the direction of the applied force of the displacements of all nodes of the ligament/incus boundary for both ligament meshes. Figure 7.8 illustrates the displacement vectors of all nodes of the ligament/incus boundary for both meshes. Although nothing can be concluded about the convergence

FIGURE 7.7: DISPLACEMENTS OF ALL NODES OF THE LIGAMENT/INCUS
BOUNDARY FOR TWO MESH RESOLUTIONS
of the lateral bundle of the posterior incudal ligament.
The displacements plotted are the components of the actual
displacements in the direction of the applied force.

a) The incus/ligament boundary is oriented as in Figure 7.4b.

(b) The ligament/incus boundary is oriented as in Figure 7.4a.

PILLAT1

a) The incus 'ligament boundary is oriented as in Figure 7.5b.

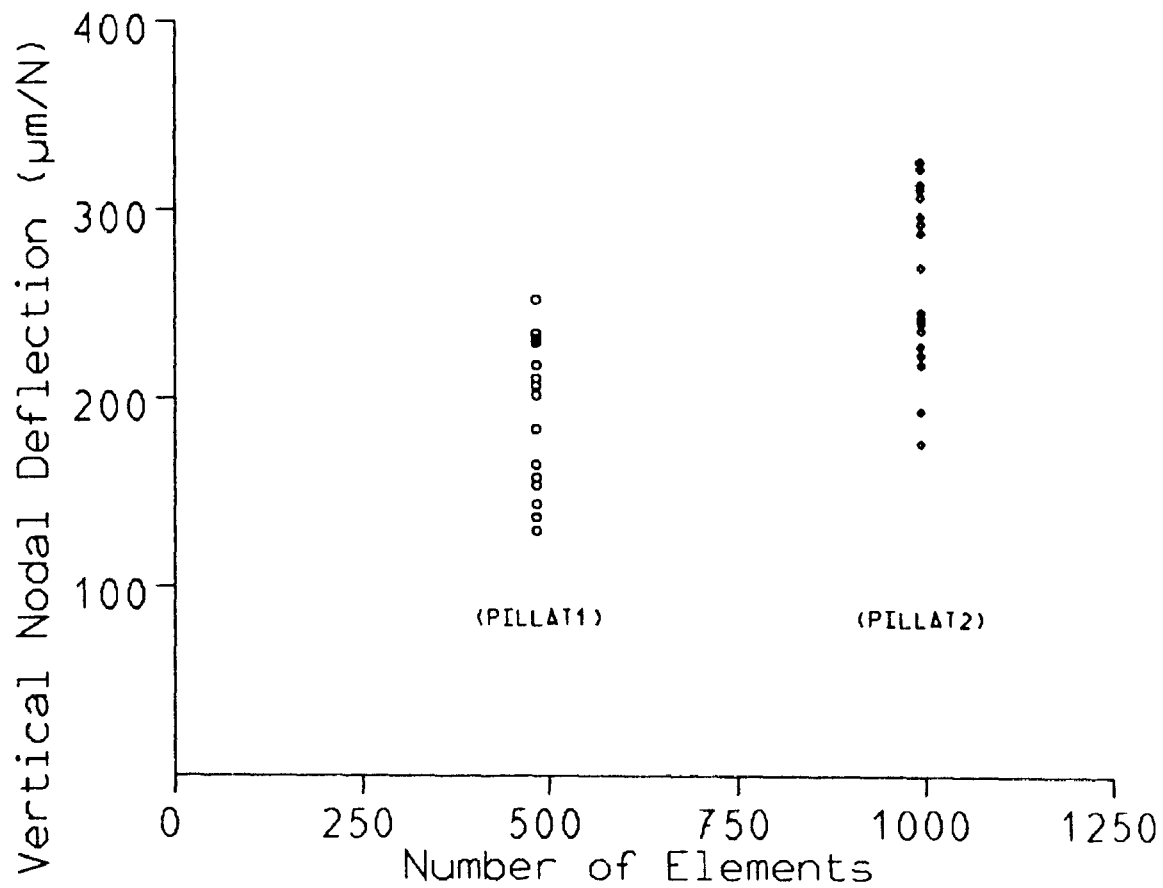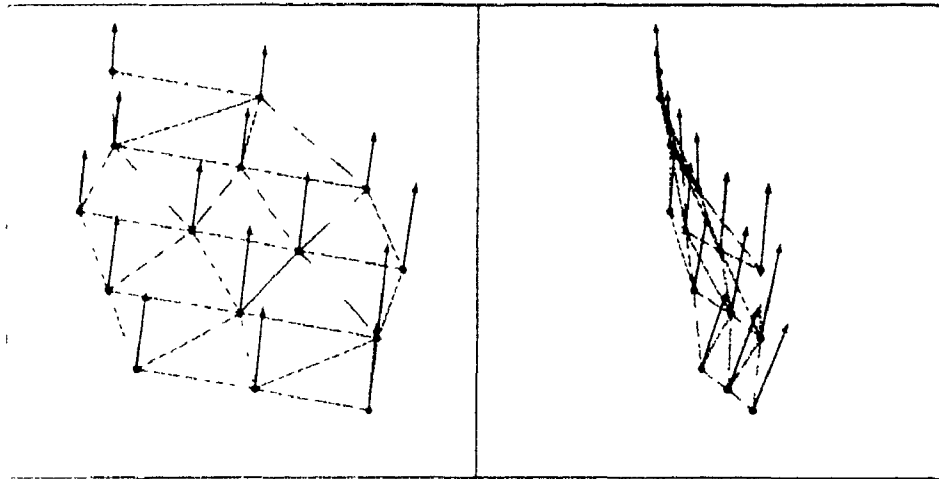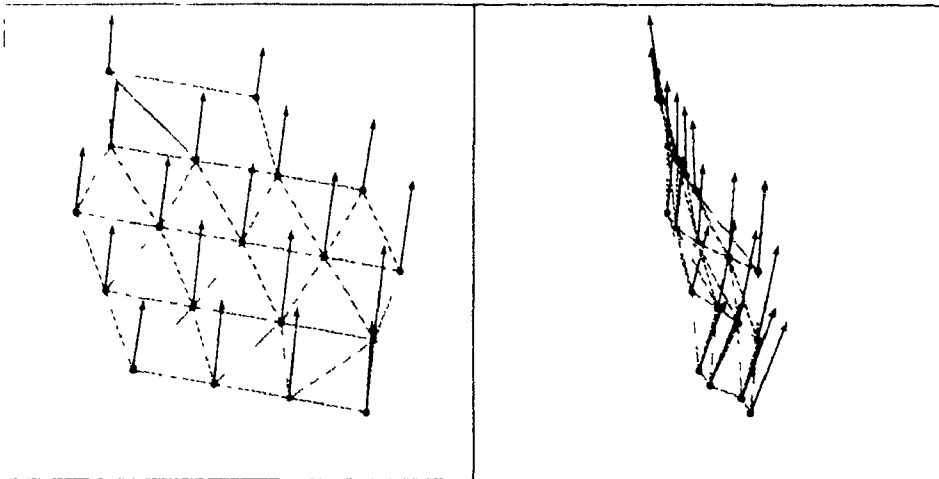(b) The ligament/incus boundary is oriented as in Figure 7.5a.

PILLAT2

FIGURE 7.8: DISPLACEMENT VECTORS OF ALL NODES OF
THE LIGAMENT/INCUS BOUNDARY
for both mesh resolutions of the lateral
bundle of the posterior incudal ligament.

behaviour of these meshes because only two meshes have been analysed, the finer mesh (PILLAT2) does exhibit larger nodal displacements than does the courser mesh (PILLAT1), as expected. The total volume of the ligament (2.55×10^{-10} m^3) is larger than that of the test block (1.42×10^{-10} m^3). However, the total area of the constrained facets of the ligament (PILLAT1 = 1.57×10^{-7} m^2, PILLAT2= 1.51×10^{-7} m^2) is smaller than the total area of the constrained block facets (4.21×10^{-7} m^2) by a factor of .373 for PILLAT1 and .359 for PILLAT2. In addition the ligament facets are not necessarily parallel to the applied force. Because the same magnitude and direction of force is applied to the ligament as to the block, the force per node of the ligament is therefore greater. Thus the ligament mesh displacements, which are up to more than twice as large as those calculated for the block, are of the right order of magnitude.

The residual values for all meshes were found to be practically zero. The number of digits of precision for the ligament meshes was calculated, using equation 7.4, to be 12.5(PILLAT1) and 11.9(PILLAT2) based on the 16-digit precision of the computer used. This degree of error is insignificant in this analysis.

7.4 CONCLUSION

More analysis of the lateral bundle of the posterior incudal ligament using meshes of finer resolution is required to determine the value towards which the mesh nodal displacements are converging. To do this, further work is required to make it easier to generate meshes. The modelling scheme used in this analysis is able to model complex structures in the middle ear providing a successful mesh can be produced. More study of, and work on the mesh generator is required to

determine whether circumstances leading to unmeshable polyhedra can be avoided. The next and final chapter summarizes possible methods of improving the mesh generator and mentions possible improvements that could be made to the modelling scheme in general. As well, it describes work required to complete the modelling of the complex mechanical action of the middle ear.

CHAPTER 8

CONCLUSIONS AND FUTURE DEVELOPMENTS

8.1 INTRODUCTION

The research described in this thesis involved developing the tools necessary for the finite-element modelling of the middle ear. This chapter summarizes conclusions drawn while developing and testing these tools and briefly describes work remaining in developing both a static and dynamic middle-ear finite-element model.

8.2 MESH GENERATION

8.2.1 Introduction

Further work is required to make it easier to generate meshes of structures of interest. Methods of improving the efficiency of the mesh generator are discussed in this section.

8.2.2 Two-Dimensional Triangulation

The algorithm used to triangulate two-dimensional contours sometimes runs into problems. For instance, the outer ring of the contour in Figure 8.1a could not be successfully triangulated using the triangulation routine discussed in section 6.3.1. This is because, when making an ordered list of nodes for the inner core boundary, the triangulation routine cannot determine in which direction to go when it reaches the neck of the inner core. (This is because more than two edges extend from the node at the neck.) If no successful triangulation can be performed as in this case the mesh generator triangulates the contour as in Figure 8.1b. The resulting slice, shown in Figure 8.2a, which uses
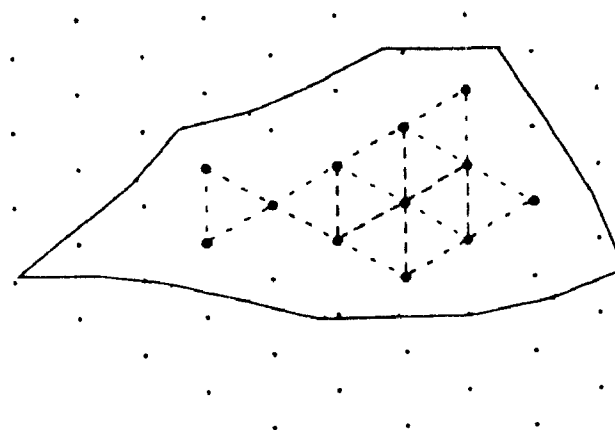
(a)
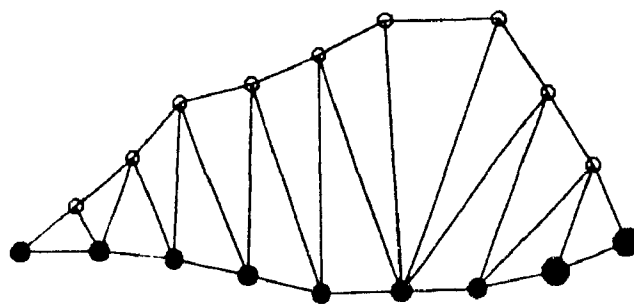
(b)

FIGURE 8.1: TWO-DIMENSIONAL TRIANGULATION OF A CONTOUR
Figure 8.1a illustrates a two-dimensional contour whose
core prevents a successful triangulation of the
two-dimensional ring. Figure 8.1b illustrates the
triangulation subsequently peiformed on the contour.

Top view   Bottom view

(a)

Top view   Bottom view
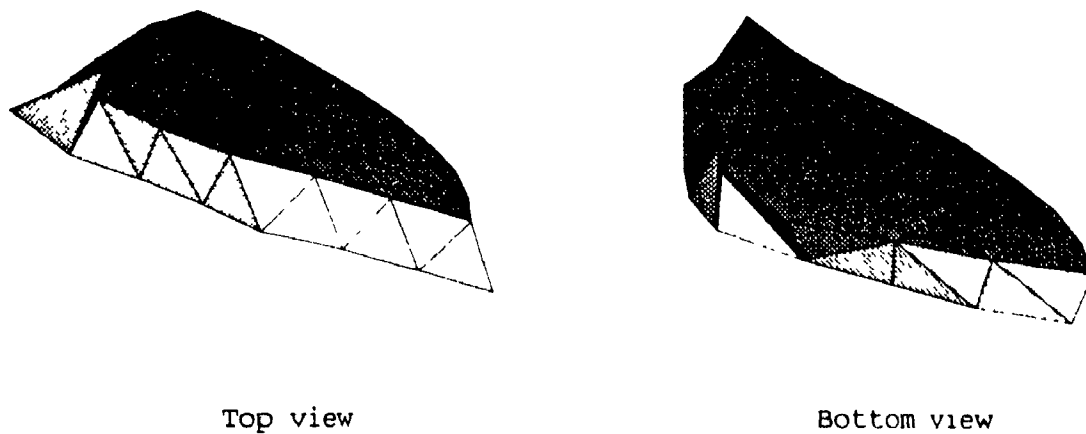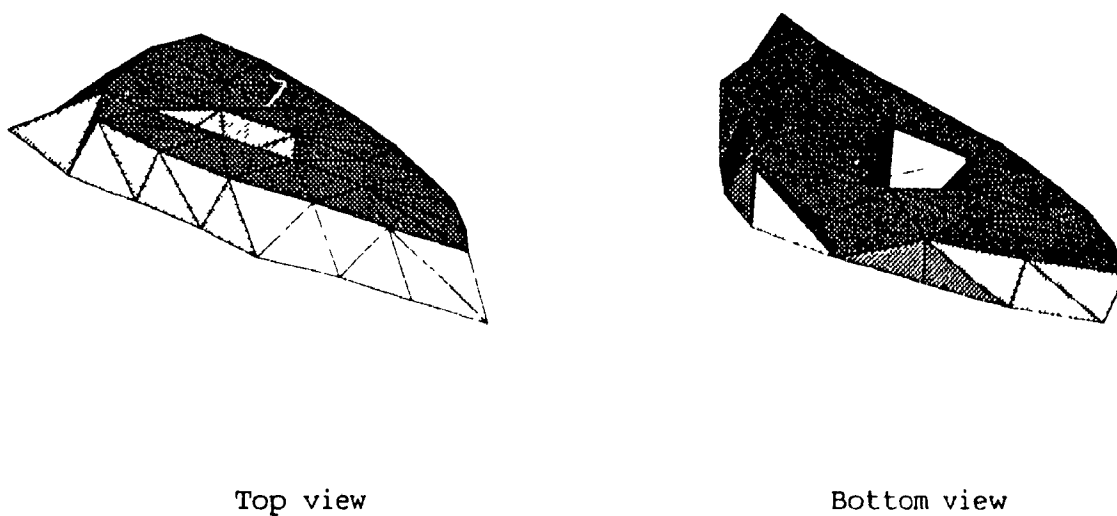
(b)

FIGURE 8.2: A THREE-DIMENSIONAL SLICE OF THE
LATERAL BUNDLE OF THE POSTERIOR INCUDAL LIGAMENT
Figure 8.2a illustrates a slice constructed using the two-
dimensional contour of Figure 8.1, triangulated as in Figure
8.1b, as its bottom contour. The mesh generator could not mesh
this slice. Figure 8.2b illustrates a slice constructed using
the same two-dimensional contours of Figure 8.2a. The
two-dimensional grid was slightly shifted and shrunk and
the resulting slice was successfully meshed.

this contour as its bottom contour is impossible to mesh. A better two-dimensional triangulation routine is required that can handle this sort of problem. A more robust two-dimensional algorithm has already been developed for triangulating eardrum meshes (Funnell et al., 1987) and can be adapted for the mesh generator.

At present this two-dimensional triangulation problem can be corrected in a few cases by shifting and/or shrinking the grid of a two-dimensional contour so that a successful triangulation may be performed. This results in a meshable slice as shown in Figure 8.2b. The three-dimensional core prisms produced for this slice are not right-angled prisms but this does not necessarily present a problem for the mesh generator.

8.2.3 Aspect Ratio

As mentioned in section 6.4.5, a minimum aspect ratio limit was found to be required in the mesh generation process. For instance, a minimum aspect ratio limit of 0.2 was used to generate both ligament meshes. More work is required to determine a systematic method of determining an optimal aspect ratio lower limit, i.e., one that is low enough not to restrict too many possible topological cuts, but high enough to avoid unmeshable polyhedra as mentioned above. A different algorithm was tried to determine if unmeshable polyhedra could be avoided by generating, at each cut, the tetrahedron with the highest aspect ratio possible. Before a cut was made using the edge operator, all possible edges where this cut could be made were noted, and then the cut producing the best shaped tetrahedron was actually made. Thus the resulting mesh, if successful, would have a high average aspect ratio. Unfortunately, this algorithm was not always capable of successfully

meshing slices (even when use of the original algorithm could). Possibly this algorithm should also force all cuts performed using the vertex operator (in addition to the edge operator) to also have as high an aspect ratio as possible. More study is required to determine what is the best strategy to be used to generate a mesh. Possibly this best algorithm would be a compromise between the original algorithm and the one attempted above.

One of the factors limiting the efficiency and possible accuracy of the finite-element analysis performed is the relatively low average aspect ratio of the meshes used. As the resolution of a mesh increases, an increasing percentage of the mesh is made up of core tetrahedra. Using the present algorithm, these core tetrahedra are formed by constructing right-angled prisms from overlapping two-dimensional cores. When these cores are shredded, a large number of tetrahedra with solid right angles are formed. This sort of tetrahedron has an aspect ratio of approximately 0.5 and thus significantly weights the aspect ratio average of a mesh. Surrounding tetrahedra of the ring have an average aspect ratio lower than this and thus the prospect of a good overall aspect ratio is poor.

Ideally the core tetrahedra should have as high an aspect ratio as possible. This could be accomplished by modifying the mesh generation algorithm such that regular grids on adjacent two-dimensional contours are alternately shifted horizontally with respect to each other. The amount of shift should be calculated so that the tetrahedra formed from the resulting prisms all have internal solid angles as equal as possible. In this manner the average aspect ratio of the core would be as high as possible. This modification is not critical to the successful operation of the generator but it would help to increase its efficiency.

The accuracy of the finite-element analysis performed depends more on the worst-shaped tetrahedron in the mesh.

8.2.4 Bandwidth Minimization

The global stiffness matrix **K** for a structure with many degrees of freedom can be quite large and require much computer storage. Fortunately this matrix is symmetric in structural finite-element analysis. Thus, only the lower diagonal portion of this matrix need be stored. This matrix also turns out to be banded which means for entries of column j

$$k_{ij} = 0 \text{ for } i > j + hb_k \tag{8.1}$$

where hb_k is the half bandwidth of **K** and $2hb_k + 1$ is the bandwidth of **K**. Only $hb_k + 1$ elements of column j need be stored. The bandwidth is determined by the differences between the global node numbers of nodes within elements and can be minimized by an appropriate global node-numbering scheme (Funnell & Laszlo, 1978). At present the mesh generator numbers global nodes in order of increasing Z coordinate value, then Y coordinate value and then X coordinate value. This is not optimal if the dimension in the Z direction is much greater than that in the X dimension. A node renumbering scheme that numbers the nodes in order of increasing structural dimension should be applied to finite-element meshes so that global node number difference within an element can be kept as small as possible.

8.2.5 Extended graphics

It is currently very difficult to analyse exactly what is happening

as an object is being meshed. At present, analysis of unsuccessful meshing attempts involves inspecting meshed slice files produced by the generator visually using the display program SMF and then inspecting a text recording file to see how the meshing occurred. This is rather tedious. What is required is a display program that could display a slice (after the mesh generation process is complete) as it had been meshed. The user could then inspect how the generator had meshed a slice and interactively determine any problems that might have occurred.

8.3 COMPUTING POWER

One of the major difficulties in the analysis performed is the large amount of computer resources required, both for mesh generation and finite-element analysis. Both the mesh-generation procedure and the finite-element analysis require considerable computer processing time and memory. This analysis will be increasingly effective as more powerful computers become available.

Parallel computers break up a task and perform subtasks in parallel. This sort of computer would be capable of performing mesh generation and finite-element analysis more quickly than traditional computers that perform an entire task serially. An analysis of just how the mesh generation and finite-element algorithms could be separated into subtasks is required. One task that could be separated into subtasks is the meshing of slices in the mesh generator. Different slices of a structure could be meshed at the same time.

8.4 ASSUMPTIONS

Finite-element analysis has been described as an art form (MacNeal, 1987). To properly analyse a structure using finite elements,

an understanding of all assumptions and approximations made along the way is required.

The model developed at present is a linear, homogeneous, isotropic model of a ligament whose geometry is only approximately represented. These approximations are due to artifacts produced when preparing the histological slides and due to the lack of an absolute alignment reference in this data. Errors in tracing and errors produced when triangulating contours of outlines of structures of interest also contribute to the geometrical approximations. As the modelling procedure is refined, some of these assumptions and approximations can be reduced but it is critical that their effects be analysed and understood.

8.5 MIDDLE-EAR MODELLING

The intended direction of future work on the middle-ear model is as follows. Once the lateral bundle of the posterior incudal ligament has been analysed, the other structures required for the static model of the middle ear must be analysed in a similar fashion. Once these meshes have been produced, meshes of all structures will be integrated into one mesh representing the middle-ear ossicles and soft tissues.

Initially a static analysis will be performed by loading various points of the manubrium. Next an analysis of undamped natural frequencies will be done to indicate what frequencies will probably be of interest in a dynamic model. Next, both the damped and undamped frequency response will be analysed.

As the theoretical work on the middle ear proceeds, experimental work will be done by collaborators S.M. Khanna (Department of Otolaryngology, Columbia University, New York) and W.F. Decraemer (Laboratory of Experimental Physics, University of Antwerp, Antwerpen,

Belgium) to validate the model. These experiments may involve stimulating directly various points on the manubrium to bypass the effect of acoustical stimulation of the eardrum. Also the stapes may be fixed or freed from the oval window to eliminate the effects of the cochlea. Detailed measurements and analysis of vibration modes of the manubrium can be made.

As this research proceeds results should help in refining the eardrum model. Dynamics of the ossicular axis of rotation will be of great help in determining the loading of the eardrum. The ossicle and soft-tissue model will eventually be integrated with the eardrum model.

The pattern of eardrum excitation is important in determining the loading of the combined eardrum-middle ear model. Modelling of the sound pressure variations at the eardrum is needed. An acoustical finite-element analysis of the ear canal will be performed in this lab in order to determine these variations.

The finite-element models of the ear canal, eardrum and middle ear should add significantly to the understanding of the ear external to the cochlea.

REFERENCES

Basek, M. (1970). "Treatment of Ménière's disease with ultrasound", Laryngoscope 80:(768-776).

Bathe, K.J. (1974 revised). SAP IV - A Structural Analysis Program for Static and Dynamic Response of Linear Systems. Report no. EERC 73-11, College of Engineering. University of California, (Berkeley, California).

Bathe, K.J. (1982). Finite Element Procedures in Engineering Analysis. Prentice-Hall, (New Jersey).

Beranek, L.L. (1954). Acoustics. McGraw-Hill, (New York).

Békésy, G.v. (1941). "On the measurement of the amplitude of vibration of the ossicles with a capacitive probe", (in German), Akust. Zeitschr. 6:(1-16).

Boubez, T.I. (1985). "Three-dimensional finite-element mesh generation using serial sections", Proc. 11th Can. Med. & Biol. Eng. Conf. (39-40).

Boubez, T.I., Funnell, W.R.J., Lowther, D.A., Pinchuk, A.R. & Silvester, P.P. (1986a). "Mesh generation for computational analysis. Part II-- geometric and topological considerations for three-dimensional mesh generation", Comp.-Aided Eng. J. 3(5):(190-195).

Boubez, T.I. (1986b). "Three-dimensional finite-element mesh geneiation using serial sections", M. Eng. thesis, McGill University, (Montréal, Canada).

Brebbia, C.A. ed. (1985). Finite Element Systems - A Handbook. 3rd rev. ed., Springer-Verlag, (Berlin).

Brenkman, C.J., Grote, J.J. & Rutten W.L.C. (1987). "Acoustic transfei characteristics in human middle ears studied by a SQUID magnetometer method", J. Acoust. Soc. Am. 82(5):(1646-1654).

Chawla, S.D., Glass, L., Freiwald, S. & Procter J.W. (1982). "An interactive computer graphic system for 3-D steieoscopic reconstruction from serial sections -- analysis of metastatic growth", Comput. in Biol. & Med. 12(3):(223 - 232).

Cook, R.D. (1981). Concepts and Applications of Finite Element Analysis. John Wiley and Sons, (New York).

Dahmann, H. (1929). "On the physiology of hearing: experimental studies on the mechanics of the ossicular chain, as well as on the behaviours of tones and air pressure I", Zeitschr. f. Hals-Nasen-Ohrenheilk. 24:(462-497).

Dahmann, H. (1930). "On the physiology of hearing: experimental studies on the mechanics of the ossicular chain, as well as on the behaviours of tones and air pressure II", Zeitschr. f. Hals-Nasen-Ohrenheilk. 27:(329-368).

Deaver J.B. (1926). Surgical Anatomy of the Human Body. Vol. 2, 2nd ed., Blakiston, (Philadelphia).

Decraemer, W.F., Khanna, S.M. & Funnell, W.R.J. (1989). "Interferometric measurement of the amplitude and phase of tympanic membrane vibrations in cat", Hearing Research 38(1):(1-18).

Ewing, D.J.F., Hawkes, A.J., & Griffiths, J.R. (1970). "Rules governing the number of nodes and elements in a finite element mesh", Int. J. Numer. Meth. Eng., 2:(597-601).

Fumagelli, Z. (1949). "Morphological research on the sound-transmission apparatus", Arch. Ital. Otol. Rinol. e Laringol. 60 Suppl. 1. 323 pp.

Funnell, W.R.J. (1972). "The acoustical impedance of the guinea-pig middle ear and the effects of the middle-ear muscles", M. Eng. thesis, McGill University, (Montréal, Canada).

Funnell, W.R.J. (1975). "A theoretical study of eardrum vibrations using the finite-element method", Ph.D. thesis, McGill University, (Montréal, Canada).

Funnell, W.R.J., & Laszlo, C.A. (1978). "Modeling of the cat eardrum as a thin shell using the finite-element method", J. Acoust. Soc. Am. 63(5):(1461-1467).

Funnell, W.R.J., & Phelan, K.E. (1981). "Finite-element modelling of the middle-ear ossicles", J. Acoust. Soc. Am. 69 Suppl.1:(s14).

Funnell, W.R.J., & Laszlo, C.A. (1982). "A critical review of experimental observations on ear-drum structure and function", ORL 44: (181-205).

Funnell, W.R.J. (1983). "On the undamped natural frequencies and mode shapes of a finite-element model of the cat eardrum", J. Acoust. Soc. Am. 73(5):(1657-1661).

Funnell, W.R.J. (1984a). "On the choice of a cost function for the reconstruction of surfaces by triangulation between contours", Comput. and Structures 18:(23-26).

Funnell, W.R.J., (1984b). "On the calculation of surface areas of objects reconstructed from serial sections", J. Neurosci. Meth. 11(3):(205-210).

Funnell, W.R.J., Decraemer, W., & Khanna, S.M. (1987). "On the damped frequency response of a finite-element model of the cat eardrum", J. Acoust. Soc. Am. 81(6):(1851-1859).

Grandin, H. (1986). Fundamentals of the Finite Element Method. Macmillan Publishing Company, (New York).

Guinan, J.J. & Peake, W.T. (1967). "Middle-ear characteristics of anesthetized cats", J. Acoust. Soc. Am. 41(5):(1237-1261).

Gundersen, T. & Högmoen, K. (1976). "Holographic vibration analysis of the ossicular chain", Acta Otolaryngol. 82:(16-25).

Gyo, K., Aritomo, H. & Goode, R.L. (**1987**). "Measurement of the ossicular vibration ratio in human temporal bone by the use of a video measuring system", Acta Oto-Laryngol. **103**:(87-95).

Helmholtz, H.F.L. (**1869**). "The mechanics of the middle ear ossicles and of the eardrum", (in German) , Pflügers Archiv. fur Physiol. **1**:(1-60). German title: "Die mechanik der gehorknochelchen und des trommelfells", trans. by AH Bucks & N Smith, W Woods & Co., (New York), (**1873**), 69 pp. Trans. by J Hilton, publications of the New Sydenham Soc., (London) **62**:(97 - 155), (**1874**).

Khanna, S.M. (**1970**). "A holographic study of tympanic membrane vibrations in cats", Ph.D. thesis, City University of New York, (New York).

Khanna, S.M. & Tonndorf, J. (**1972**). "Tympanic membrane vibrations in cats studied by time-averaged holography", J. Acoust. Soc. Am. **51**(6):(1904-1920).

Kobayashi, M. (**1954a**). "On the ligaments and articulations of tympanic ossicles of cat", in Japanese, Pract. Otol. (Zibi Rhinsho) **47**(7):(485 -491).

Kobayashi, M. (**1954b**). "On the ligaments and articulations of the tympanic ossicles of man", in Japanese, Pract. Otol. (Zibi Rinsho) **47**(9):(587-593).

Lindsay, P.H. & Norman, D.A. (**1977**). Human Information Processing: An Introduction to Psychology. 2nd ed., Academic Press, (New York).

Lynch, T.J. (1981). "Signal processing by the cat middle ear: admittance and transmission, measurements and models", Ph.D. thesis, Massachusetts Institute of Technology, (Cambridge, Massachusetts).

Lynch, T.J, Nedzelnitsky, V. & Peake, W.T. (1982). "Input impedance of the cochlea in cat", J. Acoust. Soc. Am. 72(1):(108-130).

MacNeal, R.H. (1987). "Zen and the art of finite element design", Finite Elements in Analysis and Design. 3:(85-91).

Mäntylä, M., & Kagawa, Y. (1983). "Topological analysis of polygon meshes", Comp. Aided Design, 15(4):(228-234).

Møller, A.R. (1961). "Network model of the middle ear", J. Acoust. Soc. Am. 33(2):(168-176).

Nedzelnitsky, V. (1980). "Sound pressure in the basal turn of the cat cochlea", J. Acoust. Soc. Am. 68(6):(1676-1689).

Onchi, Y. (1961). "Mechanism of the middle ear", J. Acoust. Soc. Am. 33(6):(794-805).

Peake, W.T. & Guinan, J.J (1967). "A circuit model for the cat's middle ear", MIT LAb. Electron. Quart. Progress Report 84:(320-326).

Popov, E.P. (1976). Mechanics of Materials. 2nd ed., Prentice-Hall, (New Jersey).

Rabbitt, R.D., & Holmes, M.H. (**1986**). "A fibrous dynamic continuum model of the tympanic membrane", J. Acoust. Soc. Am. **80**(6):(1716-1728).

Reddy, J.N. (**1984**). Energy and Variational Methods in Applied Mechanics. John Wiley and Sons. (New York).

Shaw, E.A.G. (**1977**). "Eardrum representation in middle-ear acoustical networks", J. Acoust. Soc. Am. **62**(s1):(s12).

Shaw, E.A.G. & Stinson, M.R. (**1983**). "The human external and middle ear: model and concepts", in Mechanics and Hearing, E. de Boer and M.A. Viergever eds., pp. 3-10.

Shaw, E.A.G. & Stinson, M.R. (**1986**). "Eardrum dynamics, middle ear transmission and the human hearing threshold curve", Proc. 12th Int. Cong. Acoust. Toronto, paper b6-6:2 pp.

Stuhlman, O. Jr. (**1937**). "The nonlinear transmission characteristics of the auditory ossicles", J. Acoust. Soc. Am. **9**(2):(119-128).

Tweed, J.J. (**1985**). "Development of a model of stapes motion during contraction of the stapedius muscle", M.Sc. thesis, ISVR SouthHampton University.

Vlaming, M.S.M.G. (**1987**). "Middle ear mechanics studied by laser doppler interferometry", Ph.D thesis, Technische Universiteit Delft, (Delft, The Netherlands).

Wever, E.G. & Lawrence, M. (**1954**). Physiological Acoustics. Princeton

University Press, (Princeton,New Jersey).

Woo, T.C. & Thomasma, T. (1984). "An algorithm for generating solid elements in objects with holes", Comput. and Structures, **18**:(333-342).

Wordenweber, B., (1984). "Finite element mesh generation", Comp. Aided Design **16**(5):(285-291).

Zwislocki, J. (**1962**). "Analysis of the middle ear function. Part I:Input impedance", J. Acoust. Soc. Am. **34**(9):(Part 2:1514-1523).